Astronomy Letters, Vol. 30, No. 1, 2004, pp. 1–13. Translated from Pis'ma v Astronomicheskiĭ Zhurnal, Vol. 30, No. 1, 2004, pp. 3–16.

The Phenomenon of the Galaxy NGC 6286: A Forming Polar Ring or a Superwind?

L. V. Shalyapina[1*], A. V. Moiseev[2], V. A. Yakovleva[1], V. A. Hagen-Thorn[1], and A. N. Burenkov[2]

[1] *Astronomical Institute, St. Petersburg State University, Bibliotechnaya pl. 2, Petrodvorets, 198904 Russia*

[2] *Special Astrophysical Observatory, Russian Academy of Sciences, Nizhnii Arkhyz, 357147 Karachai-Cherkessian Republic, Russia*

Received March 20, 2003; in final form, May 26, 2003

Abstract—We present our observations of the pair of interacting galaxies NGC 6285/86 carried out with the 6-m Special Astrophysical Observatory (SAO) telescope using 1D and 2D spectroscopy. The observations of NGC 6286 with a long-slit spectrograph (UAGS) near the Hα line revealed the rotation of the gaseous disk around an axis offset by 5″–7″ from the photometric center and a luminous gas at a distance up to 9 kpc in a direction perpendicular to the galactic plane. Using a multipupil fiber spectrograph (MPFS), we constructed the velocity fields of the stellar and gaseous components in the central region of this galaxy, which proved to be similar. The close radial velocities of the pair and the wide ($5' \times 5'$) field of view of the scanning Fabry–Perot interferometer (IFP) allowed us to simultaneously obtain images in the Hα and [N II] λ6583 lines and in the continuum, as well as to construct the radial velocity fields and to map the distribution of the [N II] λ6583/Hα ratio for both galaxies. Based on all these data, we studied the gas kinematics in the galaxies, constructed their rotation curves, and estimated their masses ($2 \times 10^{11} M_\odot$ for NGC 6286 and $1.2 \times 10^{10} M_\odot$ for NGC 6285). We found no evidence of gas rotation around the major axis of NGC 6286, which argues against the assumption that this galaxy has a forming polar ring. The IFP observations revealed an emission nebula around this galaxy with a structure characteristic of superwind galaxies. The large [N II] λ6583/Hα ratio, which suggests the collisional excitation of its emission, and the high infrared luminosity are additional arguments for the hypothesis of a superwind in the galaxy NGC 6286. A close encounter between the two galaxies was probably responsible for the starburst and the bipolar outflow of hot gas from the central region of the disk. © *2004 MAIK "Nauka/Interperiodica"*.

Key words: *polar-ring galaxies, NGC 6285/86, superwind, kinematics.*

INTRODUCTION

NGC 6285/86 (Arp 293) is a pair of interacting galaxies (Fig. 1) with similar luminosities and radial velocities.[1] They are $\sim 1\farcm5$ apart, which corresponds to $\sim$40 kpc for a distance $D = 91$ Mpc (at $H_0 = 65$ km s^{-1} Mpc^{-1} and $V_{\rm gal}^{\rm sys} = 5925$ km s^{-1}; see below). A faint bridge can be seen between the galaxies in deep CCD images. Whitmore *et al.* (1990) included one of the galaxies from the pair, NGC 6286, in the catalog of polar-ring galaxies as a possible candidate (C 51), because a diffuse structure (semi-ring) located to the southeast (SE) of the main body of the galaxy is clearly seen in the reproduction in the atlas by Arp (1966).

NGC 6286 is a spiral Sb-type (RC3) galaxy seen almost edge-on with a thick dust lane that runs at an angle to the stellar disk of the galaxy. Since, according to IRAS data, this galaxy has a high infrared luminosity, $\log(L_{\rm FIR}/L_\odot) = 11.28$ (Soifer *et al.* 1987), it was included in the studies of bright infrared galaxies (see, e.g., Baan 1989; Young *et al.* 1989). The infrared fluxes from NGC 6286 were measured at various wavelengths (Soifer *et al.* 1987, 1989). These fluxes were used to determine the dust temperature and mass (Young *et al.* 1989) and to estimate the star-formation rate, SFR $\sim 56 M_\odot$ yr^{-1} (Smith *et al.* 1998). Based on radio data, Sanders *et al.* (1986) estimated the H_2 mass for this galaxy, $\log M(H_2)/M_\odot = 9.97$.

The optical spectra of this galaxy have been described by several authors. Reshetnikov and Combes (1994) classified its nuclear spectrum as H II and pointed out a peculiarity in the radial velocity distribution of the gas along the minor axis of the galaxy. Veilleux *et al.* (1995) classified the nuclear spectra

* E-mail: lshal@astro.spbu.ru

[1] According to NED data.

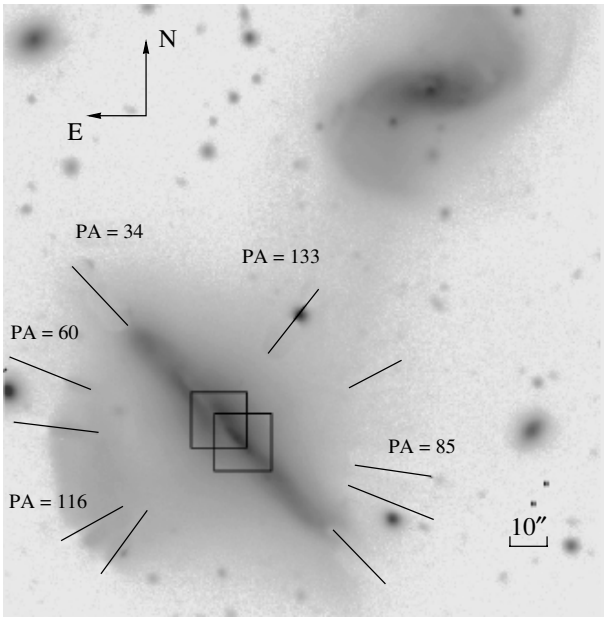

Fig. 1. An R-band image of the NGC 6285/86 pair obtained with the 6-m SAO telescope (for the assumed distance to the galaxies of $D = 91$ Mpc; $1''$ corresponds to 0.44 kpc).

of NGC 6286 and NGC 6285 as LINER and H II, respectively. Smith *et al.* (1996) used the Hα line to construct the rotation curve for NGC 6286 and estimated its mass ($M = 1.3 \times 10^{11} M_\odot$).

Reshetnikov *et al.* (1996) performed a detailed photometric study of NGC 6286 in the B, V, and R_c bands. Based on peculiarities of the radial velocity curve along its minor axis and on photometric data, they assumed that the diffuse structure (semi-ring) located at the SE edge of the galaxy is a forming polar ring.

To analyze the kinematics of the gaseous and stellar components of the galaxy NGC 6286 in more detail, we have undertaken its study using long-slit (1D) and 2D spectroscopy.

1. OBSERVATIONS AND DATA REDUCTION

The spectroscopic observations of NGC 6286 were made at the prime focus of the 6-m SAO telescope. The first observations were carried out with a long-slit spectrograph (UAGS) (Afanasiev *et al.* 1995) in 1997 and 1999. The observations with a multipupil fiber spectrograph (MPFS) (a description of the spectrograph can be found on the Internet at the SAO webpage[2]) were performed in 2001, and the data were obtained with a scanning Fabry–Perot interferometer (IFP) in 2002. A log of observations is given in table.

In the UAGS, the detectors were Electron 530× 580-pixel and Photometrics 1024 × 1024-pixel CCD arrays in 1997 and 1999, respectively. The UAGS slit size in the observations was $2'' \times 140''$. The observed spectral range included the Hα, [N II] λ6548, 6583, and [S II] λ6716, 6731 emission lines.

The UAGS spectroscopic data were reduced in the ESO–MIDAS environment using the LONG context. After the primary reductions, we performed a smoothing along the slit with windows of $0''.8$ for the central region and $2''$ starting from a distance of $15''$ from the center. The radial velocities were measured from the positions of the centers of the Gaussians fitted to the emission lines. The accuracy of these measurements was estimated from the night-sky [O I] λ6300 line to be ± 10 km s^{-1}. We also measured the relative intensities and full widths at half maximum (FWHMs) of the above emission lines. The observed FWHMs were corrected for the FWHM of the instrumental profile by using the standard relation $(\mathrm{FWHM})^2 = (\mathrm{FWHM})^2_{\mathrm{obs}} - (\mathrm{FWHM})^2_{\mathrm{instr}}$. According to the measurements of lines from a calibration lamp, the FWHM of the instrumental profile was 3.6 Å. The Hα, [N II] λ6583, and [S II] λ6716, λ6731 emission lines are most intense in the spectrum of this galaxy. These lines were used to construct the radial velocity curves for the ionized gas.

During our MPFS observations, we simultaneously took spectra from 240 spatial elements (in the form of square lenses) that formed an array of 16× 15 elements in the plane of the sky. The angular size of a single element was $1''$. The detector was a Techtronix 1024×1024-pixel CCD array. The observations were carried out in two spectral ranges. The green range included emission lines of the gaseous component (Hβ, [O III] λ 4959, 5007) and absorption lines of the stellar population of the galaxy (Mg I λ5175, Fe I λ5229, Fe I + Ca Iλ5270, and others). The red range contained the Hα, [N II] λ 6548, 6583, and [S II] λ 6716, 6730 emission lines.

We reduced the observations by using the software that was developed at the SAO by Afanasiev *et al.* (1995) (SAO) and that runs in the IDL environment. We constructed two-dimensional maps of the intensity and radial velocity (velocity field) from the emission lines and fitted the line profiles by Gaussians. The radial velocities were determined with an accuracy of 10–15 km s^{-1}. The radial velocity fields of the stellar component were constructed by means of a cross-correlation technique modified to work with 2D spectroscopic data and described in detail by Moiseev (2001). Spectra of the star HD 148293 and the

[2]http://www.sao.ru/gafan/devices/mpfs/mpfs_main.htm

Log of observations

Instrument, year	Exposure time, s	PA, field	Spectral range, Å	Reciprocal dispersion, Å/pixel	Seeing
UAGS	3 × 1800	34°	6200–7000	1.5	3″.2
Sep. 1997	3 × 1800	116	6200–7000	1.5	2.5
	3 × 1800	133	6200–7000	1.5	2.5
Aug.–Sep. 1999	3 × 1800	60	6200–7000	1.2	1.6
	3 × 1800	85	6200–7000	1.2	1.6
	3 × 1800	85	6200–7000	1.2	1.5
	3 × 1800	133	6200–7000	1.2	1.6
MPFS	3 × 1200	Center	4900–6200	1.35	2
Apr.–Sep. 2001	3 × 900	Center	5900–7200	1.2	2–2.5
IFP	32 × 300		Hα + [N II]	0.9	1.5
Apr.–Sep. 2002	32 × 180		[N II] λ6583	0.9	2.0

twilight sky were used as templates for cross correlation. The radial velocities were determined from the absorption lines with an accuracy of ∼10 km s^{-1}.

The IFP observations were carried out using the SCORPIO focal reducer. The reducer is described at the SAO webpage[3]; its parameters in interferometric observations were given by Moiseev (2002).

For our observations, we used an interferometer that worked in the 235th order at a wavelength of 6562.8 Å. In this case, the spacing between neighboring orders of interference, $\Delta\lambda = 28$ Å, corresponded to a ∼1270 km s^{-1} region free from order overlapping. Preliminary monochromatization was done by using narrow-band filters with FWHM = 19 Å centered at the selected spectral range, which included the Hα or [N II] λ6583 emission line of the galaxy. During the exposure, we sequentially took 32 interferograms of the object at various IFP plate spacings, so the size of the spectral channel was $\delta\lambda \approx 0.9$ Å(∼40 km s^{-1}). The width of the instrumental profile was FWHM ≈ 2.5 Å(∼110 km s^{-1}). The detector was the same CCD array as that used in the MPFS observations. Since the readout was performed in the 2 × 2-pixel binning mode, a 512 × 512-pixel image (the pixel size was 0″.56) was obtained in each spectral channel.

[3]http://www.sao.ru/∼moisav/scorpio/scorpio.html.

We reduced our interferometric observations using the software developed at the SAO (Moiseev 2002). After the primary procedures (the subtraction of night-sky lines and the reduction to the wavelength scale), the observational data constituted data cubes in which each point in a 512 × 512 field contained a 32-channel spectrum. Optimal data filtering, a Gaussian smoothing in spectral coordinate with FWHM equal to 1.5 channels and a two-dimensional Gaussian smoothing in spatial coordinates with FWHM ≈ 2–3 pixels (depending on the seeing), was made by using the ADHOC software package.[4] To construct the velocity fields and monochromatic images, we fitted the emission line profiles by Gaussians. The measurement errors of the radial velocities did not exceed 10 km s^{-1} for single lines.

However, the following factor hindered our measurements of the radial velocities and intensities of the emission lines during our observations near Hα: According to the long-slit observations, the range of radial velocities in the galactic disk is 450–500 km s^{-1} (see below). On the wavelength scale, this range accounted for about half of the FWHM of the narrow-band filter used to separate out the required spectral range (see Fig. 2a). Therefore, during the observations with the IFP670 filter centered on the shifted

[4]The ADHOC software package was developed by J. Boulesteix (Marseilles Observatory) and is freely available on the Internet.

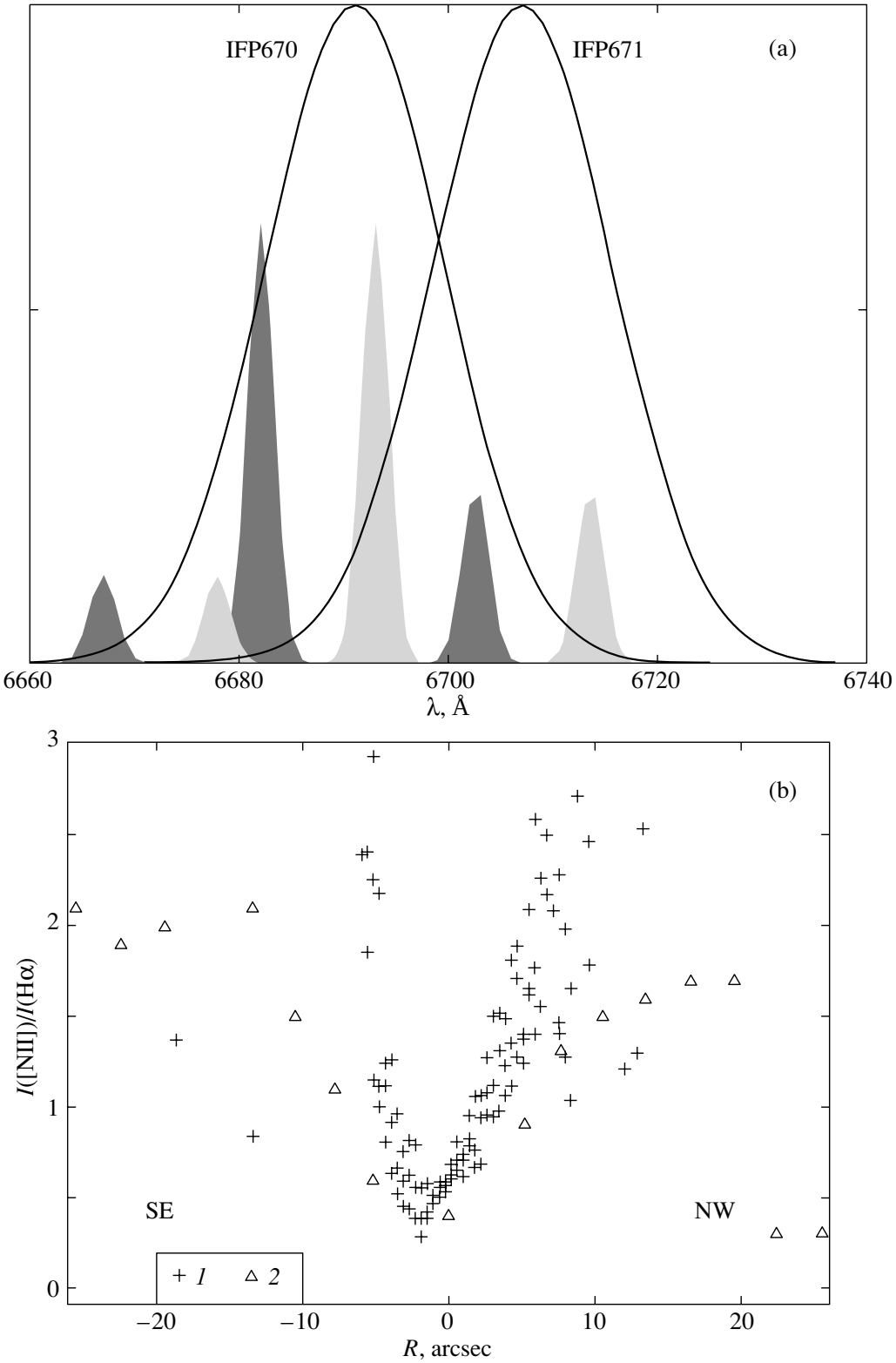

Fig. 2. (a) IFP observations. The spectra of the galaxy (the Hα λ6563 and [N II] λ6548, λ6583 lines) are shown schematically. The spectra that correspond to $V = 5450$ and 5950 km s^{-1} are colored black and gray, respectively. The solid lines represent the transmission curves of both filters (IFP670 and IFP671). (b) The distribution of the [N II] λ6583/Hα ratio, as constructed from (*1*) UAGS and (*2*) IFP data (at PA = 116°).

Hα line ($\lambda_c = 6691$ Å), the [N II] λ6583 line was also seen in the wing of the filter transmission curve in the central and SW regions of the galaxy. Thus, for the blueshifted regions, the observed intensity of the nitrogen line increased sharply, while the intensity of the Hα line decreased. Our standard procedure of correction for the filter transmission curve (a spectral flat field) does not allow the true intensities of the lines in the wing of the filter transmission curve to be restored (Moiseev 2002). In addition, in the central region of the galaxy (see Section 2.1), the Hα and [N II] line profiles virtually overlap, because the FWHMs of the emission lines increase. The two effects (the increases in relative [N II] intensity and line profile width) made it difficult to measure the radial velocities and intensities of Hα in the central and SW regions of the galactic disk.

To improve the radial velocities in the galactic disk, we carried out additional observations with a filter centered on the [N II] λ6583 line (IFP671 with $\lambda_c = 6707$ Å). In this case, the filter separated out only one spectral line (Fig. 2a).

Thus, we constructed the radial velocity fields and intensity distributions in the Hα and [N II] λ6583 lines from the observations with the IFP670 and IFP671 filters, respectively. A comparison of the measured line intensities based on the UAGS and IFP observations shows good agreement (Fig. 2b). We also imaged the galaxies in the continuum near the emission lines.

2. RESULTS

2.1. UAGS

We took long-slit spectra of NGC 6286 near Hα at the five position angles of the slit indicated in Fig. 1. The radial velocities were measured from the Hα, [N II] λ 6548, 6583 and [S II] λ 6716, 6730 emission lines. The data obtained from the forbidden lines are in close agreement, within the error limits. However, since [N II] λ6583 is more intense than the remaining lines, we will present the measurements of this line. Below, we give heliocentric velocities.

Figure 3a shows the radial velocity distribution along the major axis (PA = 34°). On the horizontal axis, $R = 0$ corresponds to the position of the peak continuum intensity, the photometric center. Along most of the velocity curve, the radial velocities measured from both lines (Hα, [N II]) are equal, except the region $-9'' \lesssim R \lesssim 7''$ where the data obtained from these lines systematically differ by $\sim$20 km s^{-1}.

The radial velocity to the SW of the photometric center is almost constant, decreasing slightly toward the edge. In the region $0 \lesssim R \lesssim 6''$, the radial velocity gradient is virtually constant. Farther out, in the NE direction, the velocity increases, but with a slightly smaller gradient. Note that the slit crosses the dust lane here. At distances from the photometric center larger than 22″, the curve flattens out, as confirmed by the data obtained later with the IFP.

Since the galaxy is seen nearly edge-on, the radial velocity curve along its major axis may be considered to be the curve of circular rotation (to within the radial projection of the noncircular velocities). Within the error limits, our data closely agree with the rotation curve from Smith *et al.* (1996) if we take the middle point of the radial velocity range, which is offset by about 5″.5 to the NE of the photometric center, as the coordinate origin and assume that the velocity at this point (5650 km s^{-1}) is the velocity of the system.

The noncoincidence of the photometric and dynamical centers also follows from our MPFS and IFP observations (see Sections 2.2 and 2.3) and is probably attributable to the presence of light-absorbing dust in the circumnuclear region. Note that there is a large uncertainty in establishing the position of the galactic nucleus. Since the dust lane runs at an angle to the disk plane (Fig. 1), the isophotal shape in the central region is distorted and asymmetric (Smith *et al.* 1996; Reshetnikov *et al.* 1996). As a result, the intensity peak is shifted to the SW of the nucleus, and this shift changes with wavelength due to selective dust absorption.

The middle parts of the radial velocity curves constructed at PA = 60° and 85° have rectilinear segments. As in the previous case, the centers of their symmetry do not coincide with the positions of the continuum intensity peaks, and the gradients decrease with increasing angle between the major axis of the galaxy and the spectrograph slit. The rectilinear segments are about 5″ long, which suggests rigid-body rotation of the gaseous galactic disk in this region. A surprising fact is that the emission lines are observed up to a distance of 4 kpc on both sides of the plane of the galactic disk.

The radial velocities at spectrograph slit positions close to the direction of the minor axis of the galaxy differ in behavior. At PA = 133°, the radial velocity is constant in the central region ($|R| \lesssim 5''$–$6''$), as must be the case for the circular rotation of the gaseous disk in the galactic plane. Farther out, as one recedes from the center on both sides, there is a large spread in radial velocities, with the intensity of the [N II] λ6583 line increasing, compared to the intensity of Hα. In this case, the spectrograph slit crossed the major axis of the galaxy at a point offset by $\sim$6″ to the NE of the photometric center.

Let us consider the features of the radial velocity curve at PA = 116° shown in Fig. 3b. As we see from the figure, the emission lines are traceable far

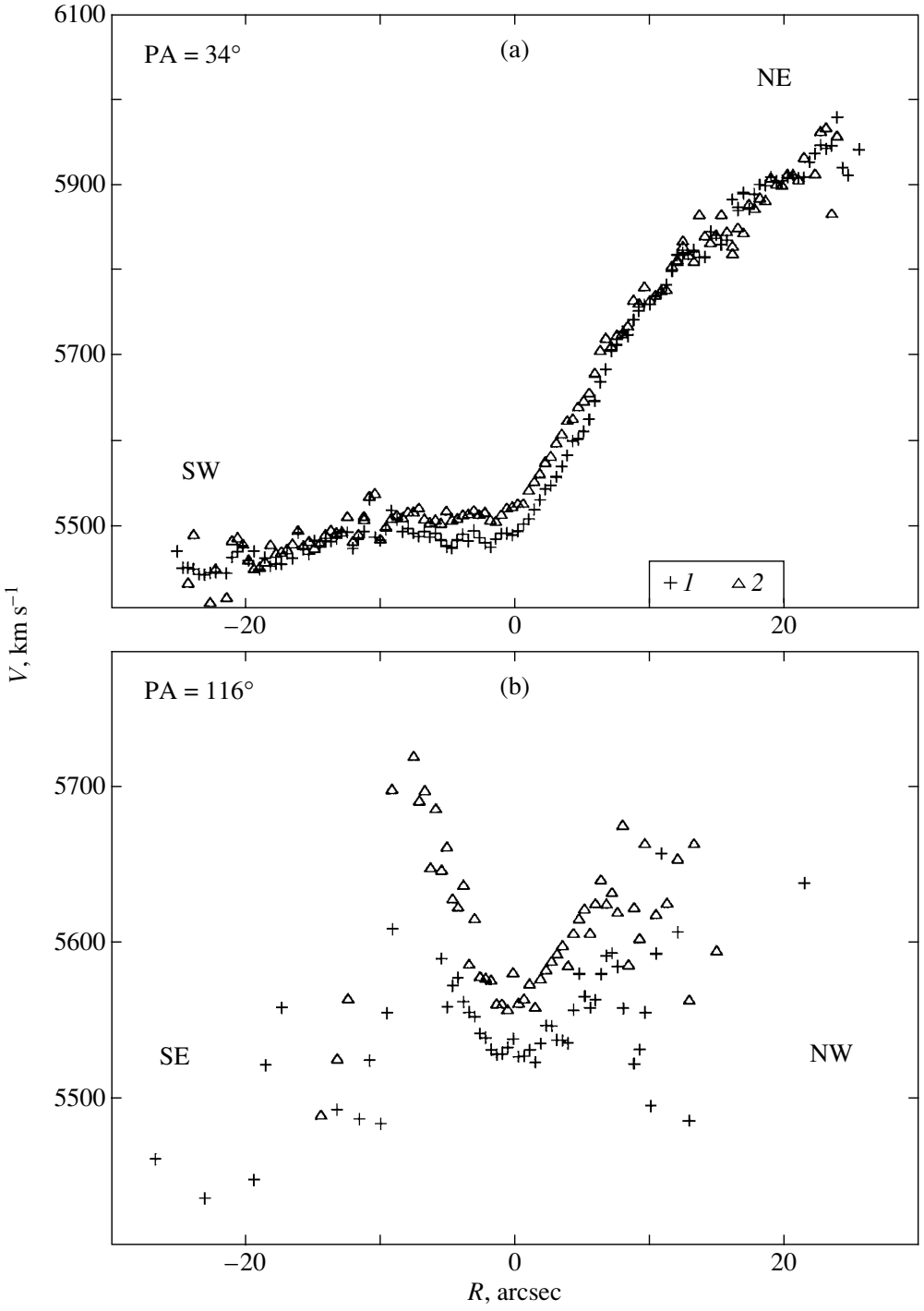

Fig. 3. Line-of-sight velocity curves: (a) PA = 34° along the major axis of the galaxy, (b) PA = 116°; *1*—Hα measurements, and *2*—[N II] λ6583 measurements. The peak continuum intensity was taken as zero on the horizontal axis.

from the disk plane, up to 9 kpc in the SE direction. In the central part of the curve, the radial velocities increase on both sides of the center. This behavior of the radial velocities can be explained by assuming that the directions of the slit and the rotation axis almost coincide and that the slit position is shifted by about 5″–7″ to the SW of the dynamical center. This assumption is justified in Section 2.3.

Apart from the radial velocities, we measured the relative intensities and full widths at half maximum (FWHMs) of the emission lines. As we noted above, a characteristic feature of the individual spectra is an

increase in the intensity of the [N II] line compared to the intensity of Hα as one recedes from the disk plane (Fig. 2b). The [N II]/Hα ratio is 0.35 at the photometric center and reaches 1.5 in the outer galactic regions. Below (see Section 2.3), we will consider the distribution of relative line intensities in more detail using IFP data.

The UAGS data suggest the existence of a luminous gas far from the plane of the galactic disk, but they do not allow the full picture of its motion to be constructed. In addition, they give no information about the stellar component of the galaxy. Such information was obtained when NGC 6286 was studied using 2D spectroscopy.

2.2. MPFS

The MPFS observations were performed for the central part of the galaxy. The positions of the spectrograph fields are shown in Fig. 1. The center of the field coincides with the photometric center in the green range and is shifted by 5″ to the NE in the red range. Near and to the SW of the photometric center, the radial velocities of the forbidden lines are higher than those of Hα and Hβ, as in the case of long-slit spectra. In general, however, the velocity fields constructed from the emission lines are similar, and we will consider the data obtained from Hβ to compare them with the velocity field of the stellar component. The results are shown in Fig. 4. We see that the motions of the stellar and gaseous components are similar and generally consistent with the assumption of circular rotation of the gas and stars, although the isovels are appreciably distorted in both fields. These distortions are most likely attributable to the presence of dust. Since the size of the field is small, we failed to accurately determine the position of the dynamical center. We may only note that it is shifted to the NE of the photometric center.

Based on the measured equivalent widths of absorption lines, we determined the Mgb and $\langle$Fe$\rangle$ chemical indices in the Lick system (Worthey *et al.* 1994) and constructed their radial distributions. The Mgb indices increase from 1.8 to 3, while the $\langle$Fe$\rangle$ indices have a small gradient and change from 1.5 to 2. The [Mgb/$\langle$Fe$\rangle$] ratio changes from 0.0 dex near the photometric center to +0.3 dex at a distance of 4″–5″ to the NE. Using model calculations (Worthey 1994), we determined the mean metallicity and age of the stellar population. Unfortunately, because of the strong emission in Hβ, we were unable to isolate the absorption line and made estimates using only metal absorption lines; hence we could not reliably separate the effects of the metallicity and age variations. Therefore, the metallicity near the photometric center of the galaxy is determined unambiguously, [Fe / H] = −1 dex, while the age can range from 12×10^9 to 17×10^9 years. At a distance of 4″–5″ to the NE (in a region closer to the galactic nucleus), the metallicity and age lie within the ranges 0.0–0.25 dex and $(1.5–2) \times 10^9$ yrs, respectively. These results provide circumstantial evidence that the galactic nucleus (where the metallicity must be higher and the age must be younger) does not coincide with the photometric center.

2.3. IFP

The IFP observations were performed in the Hα and [N II] λ6583 lines. Since the interferometer has a large field of view, the radial velocity fields as well as the distributions of line and continuum intensities, line FWHMs, and line ratios were constructed for both components of the interacting system NGC 6285/86 (Fig. 5). As we see from this figure, both the velocity fields and the emission-line images of each component are peculiar, but the most peculiar features are observed in NGC 6286. Let us consider the data for each galaxy in more detail.

NGC 6286. Intense emission is observed in the central part of the galactic disk, and a bright H II region can be identified ∼10″ to the SW of the photometric center. The [N II] λ6583/Hα ratio in the disk changes little; it is approximately equal to 0.35 in the SW part and is, on average, slightly higher in the NE part, being largest (0.6) near the dust lane. Since this ratio increases in the dust lane, we may assume that in this region we see the outer parts of the disk where the physical conditions differ from the conditions at the center. The small [N II] λ6583/Hα ratio suggests that photoionization is responsible for the formation of the emission-line spectrum.

A comparison of Figs. 5a, 5b, and 5c shows that the emission-line and continuum intensity distributions for NGC 6286 are different. In all cases, disk components crossed by the dust lane are traceable. The outer continuum isophotes are lenticular in shape, while two extended regions that are symmetric relative to the point shifted from the photometric center by about 5″–7″ to the NE in the continuum are observed in the emission lines. These regions are slightly asymmetric in extent relative to the disk plane; their SE parts are slightly larger than their NW parts. Remarkably, with the exception of a few separate knots, there is no gas emission inside the cones with an opening angle of about 60° the vertices of which are located at the above point. On both sides of the plane of the galactic disk, the intensity of the [N II] lines rapidly increases compared to Hα (Fig. 5f). Along the generatrices of the cones, the line ratio reaches its maximum, [NII]/H$\alpha \approx$ 2–2.5.

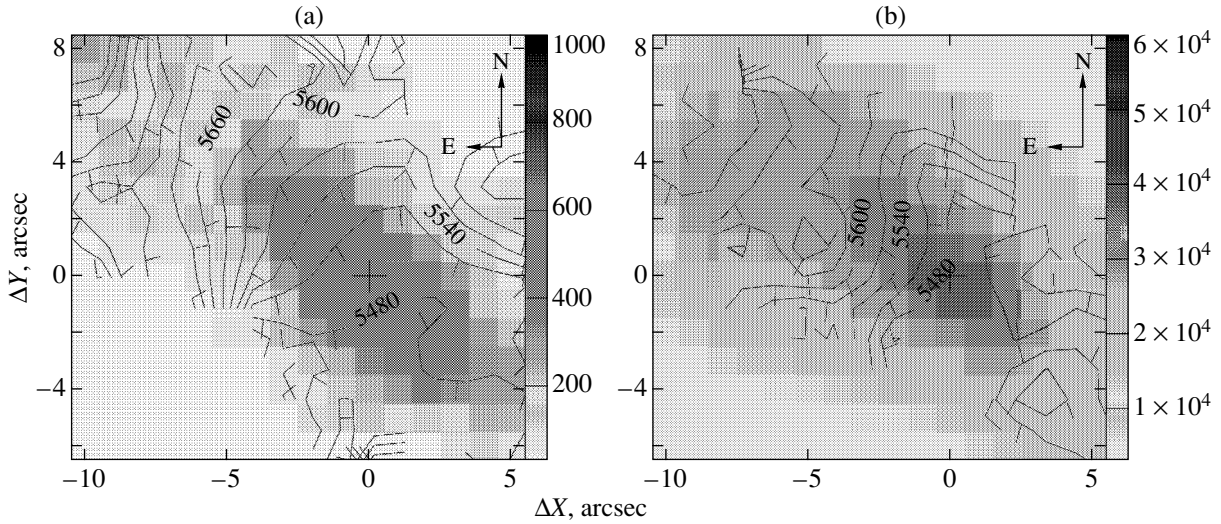

Fig. 4. MPFS data. The radial velocity fields of the gaseous component found from Hβ (a) and of stars (b) are superimposed on the Hβ and continuum intensity distributions (the flux gradation scale is in arbitrary units). The point with coordinates 0,0 corresponds to the continuum intensity peak.

Figure 5d shows the distribution of FWHMs for the [N II] λ6583 line. The FWHM changes from $\sim$200 to $\sim$320 km s^{-1} in the galactic disk and reaches its maximum, $\sim$400 km s^{-1}, along the generatrices of the cones.

The emission nebula that we detected in NGC 6286 (Figs. 5b, 5c) resembles in shape the nebulae observed in superwind galaxies, for example, NGC 1482 (Veilleux 2002). Not only the images of both galaxies in the Hα and [N II] lines but also the distribution maps of the [N II] λ6583/Hα ratio are similar.

The run of the isovels near the gaseous disk is indicative of its rotation around an axis perpendicular to the galactic plane. However, this axis does not pass through the photometric center in the continuum, but is shifted by $\sim5''$–$7''$ to the NE of it. Its position roughly coincides with the vertices of the cones in the emission-line images. The extent of the disk to the SW of the dynamical center is a factor of approximately 1.5 larger than its extent to the NE, which may be attributable to the disk asymmetry that resulted from gravitational interaction with the companion galaxy.

The behavior of the isovels in emission-line regions outside the galactic disk (Fig. 5e) is of considerable interest. The velocities are approximately constant along the straight lines that are parallel to the generatrices of the cones. For a clearer illustration of the peculiarities of the velocity field, Fig. 6a shows one-dimensional radial velocity distributions in directions that are perpendicular to the disk plane and that are offset from the dynamical center by 2 kpc to the NE (profile A) and SW (profile B). Both profiles pass through the most extended parts of the emission nebula. The radial velocity curves are symmetric relative to the disk plane and are mirror reflections relative to each other. The radial velocity amplitude in profile A that passes through the dust lane is smaller than that in profile B. The central parts of the profiles reflect the rotation of the gaseous disk; both profiles flatten out in the outer parts, with the mean velocities being approximately equal to 5720 and 5650 km s^{-1}, respectively. As we see from the velocity field, there is no evidence of gas motion around the major axis of the galaxy.

NGC 6285. The emission-line intensity distribution for the companion galaxy (Fig. 5b) exhibits the following features: a gaseous disk, intense emission in the nucleus, and a bright HII region $\sim7''$ to the west of the nucleus. The nucleus and the HII region lie on the opposite sides of the ringlike structure ($7''$ in diameter) that is clearly seen in the Hα and [N II] images. The SE side of the gaseous disk is elongated and bent toward the neighboring galaxy. In the unperturbed western part of the disk, the [N II] λ6583/Hα ratio is almost constant at $\sim$0.4, which suggests that photoionization is responsible for the formation of the emission. In the region where the disk is bent, the ratio changes randomly and, on average, is approximately equal to 1.3. Peculiar features in the radial velocity field can also be seen in this part of the disk (Fig. 5e).

In general, the velocity field of NGC 6285 is characteristic of an inclined gaseous disk with rigid-body rotation in its central part. However, the isovels are distorted both at the center and on the periphery, particularly in the SE part of the galaxy.

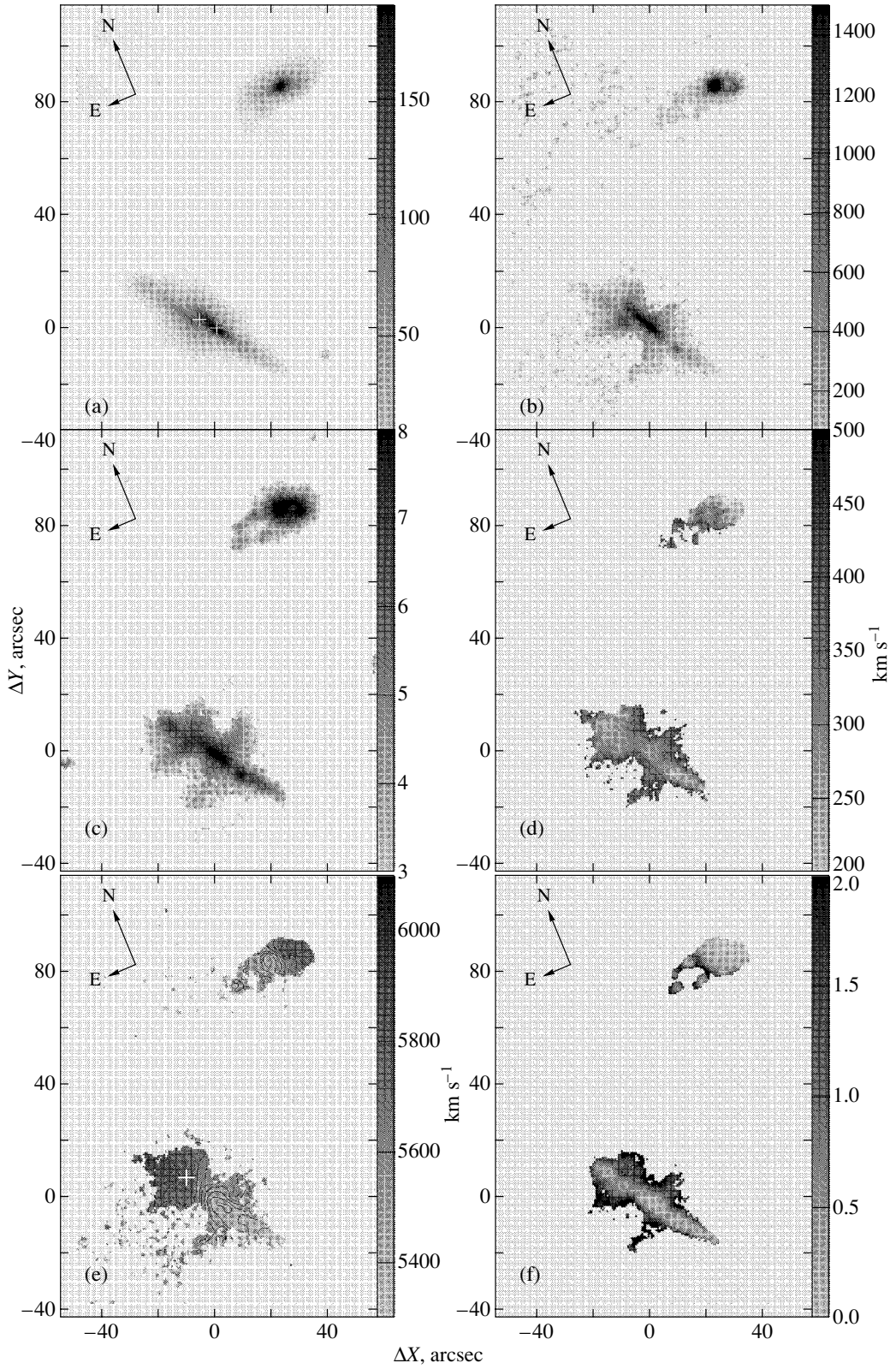

Fig. 5. IFP data: (a) the continuum intensity distribution: the crosses mark the positions of the photometric (coordinates 0, 0) and dynamical (−6, 3) centers; (b) and (c) the intensity distributions in the [N II] λ6583 and Hα lines (the flux gradation scale is in arbitrary units); (d) the distribution of FWHMs for the [N II] λ6583 line; (e) the velocity fields in this line: isovels are plotted in them at steps of 40 km s^{-1}, the cross marks the position of the dynamical center, and the velocity at this point is 5690 km s^{-1}; and (f) the [N II] λ6583/Hα ratio.

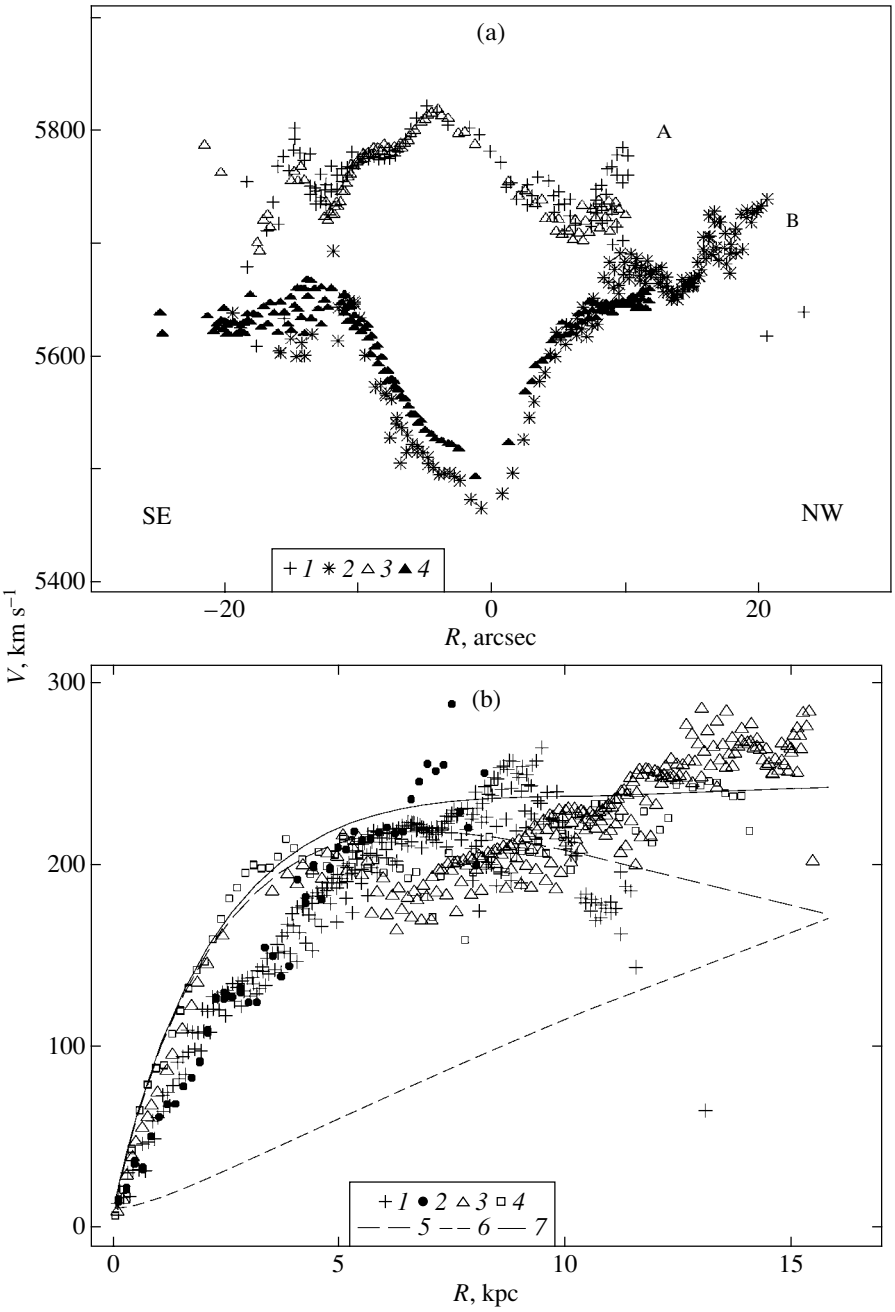

Fig. 6. (a) The radial velocity distributions in the emission-line regions A and B at slit positions parallel to the minor axis of the galaxy constructed from IFP observations: *1* and *2* represent the Hα data; *3* and *4* represent the [N II] λ6583 data. (b) The rotation curve for NGC 6286. The NE half of the radial velocity curve: *1* and *2* represent the IFP and UAGS data, respectively; the SW half: *3* and *4* represent the IFP and UAGS data, respectively; *5* is the model rotation curve for the disk, *6* is the halo model, and *7* is the ultimate model rotation curve for NGC 6286.

3. ANALYSIS OF OBSERVATIONAL DATA AND DISCUSSION

3.1. The Kinematics of Gas in the Galaxies of the Pair

NGC 6286. Since NGC 6286 is seen nearly edge-on ($i = 89°$; Smith *et al.* 1996), we constructed the rotation curve for this galaxy from our radial velocity measurements of the Hα and [N II] lines along its major axis by using both long-slit spectra and IFP data. The direction of the rotation axis and the position of the dynamical center were determined from the velocity field (Fig. 5e). Subsequently, we improved this position by achieving the closest coincidence in the region where the gradient of both halves of the radial velocity curve reached a maximum and where the

latter flattened out. As a result, we obtained $V_{\rm hel}^{\rm sys} = 5690 \pm 10$ km s^{-1} for the heliocentric velocity of the galaxy, which yields $V_{\rm gal}^{\rm sys} = 5925$ km s^{-1}.

Figure 6b shows the rotation curve on which the data for the two halves of the radial velocity curve are plotted by different symbols. Apart from the central region, $R \lesssim 1$ kpc, there is good agreement between the SW and NE parts of the curve only in some segments. Some differences between the two parts of the curve can be easily explained. For example, the decrease in velocity at $1.5 \leq R \leq 4.5$ kpc in the NE part of the curve stems from the fact that the dust lane passes through this region. Dust is known (Bosma *et al.* 1992) to decrease the velocity in the rotation curves of disk galaxies seen almost edge-on. The thickest part of the dust lane ends at a distance $R \sim 5$ kpc, and both branches of the rotation curve converge. Further out, we see a local minimum of the radial velocity on the SW branch at $5.5 \leq R \leq 7.5$ kpc. The giant H II region mentioned Section 2.3, which probably has proper motion, is located precisely in this place. Note that the waves in the radial velocity curves caused by various factors are a common phenomenon.

The initial part of the rotation curve, up to $R \sim 5$ kpc along the SW half, is well fitted by the model curve (Monnet and Simien 1977) that corresponds to the rotation of an exponential disk with a scale factor of $h = 3$ kpc (the curve plotted by long dashes in Fig. 6b). However, at a distance $R \geq 5$ kpc, the points lie above this curve. Therefore, we must assume the existence of a spherical isothermal halo to represent the observed curve over its entire length. Calculations show that this halo must have the following parameters: the central density is $\rho_0 = 0.017 M_\odot$ pc^{-3} and the core radius is $r_{\rm c} = 24$ kpc (Fig. 6b, short dashes). The ultimate theoretical rotation curve is represented by the solid line in Fig. 6b. This curve exhibits a rapid rise up to $R \sim 5$ kpc, which then slows down; the velocity reaches $V = 240$ km s^{-1} at $R \sim 8$ kpc, which yields an estimate of the mass within this radius, $1.1 \times 10^{11} M_\odot$. The total mass of the galaxy with the halo is $2 \times 10^{11} M_\odot$.

We particularly emphasize that we have found no spectroscopic evidence for the existence of a kinematically decoupled system that rotates in the polar plane with respect to the galactic disk. The radial velocity distributions shown in Figs. 5e and 6a indicate that in regions far from the disk plane, the velocities are close to the velocity of the galactic center; i.e., they correspond to those that might be expected in a spherically symmetric halo.

NGC 6285. As we noted above (Section 2.3), the velocity field of the companion galaxy NGC 6285 generally corresponds to the rotation of an inclined gaseous disk. We fitted our data by the model of gas rotation in circular orbits with the following parameters: the heliocentric radial velocity of the dynamical center is 5670 km s^{-1} ($V_{\rm gal}^{\rm sys} = 5905$ km s^{-1}) and the inclination of the disk plane to the plane of the sky is $i \sim 60^\circ$. The velocity turned out to reach its maximum, 180 km s^{-1}, at a distance of $\sim$2 kpc. The mass within the radius of 2 kpc is $10^{10} M_\odot$. Regions with high residual velocities (± 50 km s^{-1}) can be identified in the region of the ringlike structure between the nucleus and the bright H II region and on the SE side of the disk where the isovels are distorted. The high residual velocities are indicative of appreciable noncircular motions in these regions.

3.2. The Superwind in NGC 6286

Both the photometric and spectroscopic data suggest that NGC 6285/86 is a pair of interacting galaxies. The strong interaction between them is evidenced by the distortions of the structure of the galaxies—the asymmetry of their gaseous disks and the inclined dust lane in NGC 6286; the existence of a bridge between the galaxies and an extended luminous region to the SE of NGC 6286; and the peculiarities of the velocity fields. The most probable range of relative space velocities of the galaxies during their close encounter is 50–100 km s^{-1}. The probability that their relative space velocity is outside this range for the derived radial velocity difference between the galaxies of $\sim$20 km s^{-1} is low. We can then estimate the characteristic interaction time, $\sim 10^8$ yrs.

The interaction during a close passage of the galaxies could trigger a strong starburst in the central part of NGC 6286. This conclusion is confirmed, in particular, by FIR and IR data, according to which NGC 6286 is a galaxy with a high FIR luminosity: $\log(L_{\rm FIR}/L_\odot) = 11.28$. Such a luminosity $L_{\rm FIR}$ is suggestive of a high star-formation rate in it: 56–$65 M_\odot$ yr^{-1} (Smith *et al.* 1998; Poggianti and Wu 2000).

Such a high rate of star formation, which, in addition, takes place in a relatively small region in the central part of the galaxy, eventually leads to a much higher supernova rate than that in normal spiral galaxies. As a result, a phenomenon called a superwind arises (Heckman *et al.* 1990); this phenomenon consists in the strong heating of the interstellar medium and its outflow in a direction perpendicular to the galactic disk. X-ray emission from the outflowing hot gas (which has actually been detected from such well-known superwind galaxies as M 82 (Lehnert *et al.* 1999) and NGC 253 (Weaver *et al.* 2002)) and the presence of an optical emission

nebula serve as observational manifestations of this phenomenon. In this case, the edge-on orientation of the galaxy is most favorable for the detection of a superwind.

Let us consider the observational evidence suggesting the existence of a superwind in NGC 6286 in more detail. According to RASSFSC data, this galaxy is an X-ray source. We detected an optical emission nebula in the galaxy (Figs. 5b, 5c) the size of which reaches ~9 kpc in a direction perpendicular to the plane of the stellar disk. Note that the sizes of such nebulae in other superwind galaxies (*M* 82, NGC 1482, and others) lie within the range from several kpc to several tens of kpc (Heckman *et al.* 1990). As we noted above, no optical emission is observed inside the cones, because, according to the calculations by Strickland and Stevens (2000), the gas temperature in this region must be $\sim 10^7$ K.

A good illustration of a superwind in a galaxy is an enhanced [N II] λ6583/Hα emission-line ratio compared to an ordinary H II region. Thus, whereas this ratio is $\lesssim$0.5 in an H II region where photoionization dominates, it is much larger than 0.5 for a supersonic outflow of hot gas and the formation of shock fronts (the conditions under which collisional ionization dominates). We see from Fig. 5f that the derived ratios increase severalfold as one recedes from the disk plane. In this case, the emission-line ratio is highest in the regions that form the boundary of the conical ejections of hot gas from the galactic plane.

The line emission is strongest where the line of sight runs along the walls of the cone. The space velocity here is roughly perpendicular to the line of sight, and the radial velocities cannot give evidence of such motions. However, the increase in emission-line FWHMs to 400 km s^{-1} near the walls of the cone and their complex profiles, as was mentioned above, serve as their indirect confirmation.

Thus, we conclude that a superwind-type bipolar outflow of gas from the central region of the disk takes place in the galaxy NGC 6286.

We note in passing yet another fact that confirms the interaction between the galaxies. The [N II] λ6583/Hα ratio also increases in the SE part of the galaxy NGC 6285 that is closest to NGC 6286 (Fig. 5f). This increase may be attributable to the hot superwind gas that heats up and ionizes the interstellar medium in this part of the galaxy, which causes the intensity of the forbidden lines to increase.

Using the typical superwind outflow velocities (~500 km s^{-1}) from Veilleux (2002) and the observed sizes of the ionization region above and under the disk, we can estimate that the ejection began $\sim 10^7$ years ago. This estimate is consistent with the above estimate for the characteristic time of strong interaction.

CONCLUSIONS

In conclusion, we emphasize that our kinematic study of the gaseous component of the galaxy NGC 6286 has revealed no evidence of gas rotation around its major axis. Therefore, NGC 6286 is unlikely to be a galaxy with a forming polar ring, as assumed previously.

Based on the entire set of observational data, we have concluded that the peculiarities of NGC 6286 are attributable to the presence of a superwind that outflows from its central region. This is suggested by the following facts:

—the existence of an emission nebula stretching to a distance of ~9 kpc from the galactic plane whose shape corresponds to a bipolar outflow of hot gas; the presence of this outflow is confirmed by the presence of an X-ray source;

—the significant increase in [N II] λ6583/Hα ratio characteristic of superwind galaxies;

—the high infrared luminosity of the galaxy, which is indicative of a high star-formation rate (SFR 56–65$M_\odot$ yr^{-1}).

The starburst in the central region of the galaxy that gave rise to the superwind was probably triggered by a close encounter between the two galaxies.

ACKNOWLEDGMENTS

We are grateful to the Commission on the Subject of Large Telescopes (CSLT) for allocating observational time on the 6-m telescope and to E.V. Volkov for his participation in the discussion of our results. This work was supported in part by the Astronomy Federal Program (project no. 40.022.1.1.1001), the Russian Foundation for Basic Research (project no. 02-02-16033), and the Russian Ministry of Education (project no. E02-11.0-5).

REFERENCES

1. V. L. Afanasiev, A. N. Burenkov, V. V. Vlasyuk, and S. V. Drabek, Report Spec. Astrophys. Obs. Russ. Acad. Sci., 234 (1995).
2. V. L. Afanasiev, S. N. Dodonov, and V. L. Moiseev, *Stellar Dynamics: from Classic to Modern,* Ed. by L. P. Ossipkov and I. I. Nikiforov (St. Petersburg, 2001), p. 103.
3. H. Arp, Astrophys. J., Suppl. Ser. **14**, 1 (1966).
4. W. A. Baan, Astrophys. J. **338**, 804 (1989).
5. A. Bosma, Y. Byun, K. C. Freeman, and E. Athanassoula, Astrophys. J. **400**, L21 (1992)
6. T. M. Heckman, L. Armus, and G. K. Miley, Astrophys. J., Suppl. Ser. **74**, 833 (1990).
7. M. D. Lehnert, T. M. Heckman, and K. A. Weaver, Astrophys. J. **523**, 575 (1999).

8. A. V. Moiseev, Bull. SAO **51**, 11 (2001); astro-ph/0111219.
9. A. V. Moiseev, Bull. SAO **54**, 74 (2002); astro-ph/0211104.
10. G. Monnet and F. Simien, Astron. Astrophys. **56**, 173 (1977).
11. B. N. Poggianti and H. Wu, Astrophys. J. **529**, 157 (2000).
12. V. P. Reshetnikov and F. Combes, Astron. Astrophys. **291**, 57 (1994).
13. V. P. Reshetnikov, V. A. Hagen-Thorn, and V. A. Yakovleva, Astron. Astrophys. **314**, 729 (1996).
14. D. B. Sanders, N. Z. Scoville, J. S. Young, *et al.*, Astrophys. J. Lett. **305**, L45 (1986).
15. D. A. Smith, T. Herter, and M. P. Haynes, Astrophys. J., Suppl. Ser. **104**, 217 (1996).
16. D. A. Smith, T. Herter, and M. P. Haynes, Astrophys. J. **494**, 150 (1998).
17. B. T. Soifer, B. D. Sanders, B. F. Madore, *et al.*, Astrophys. J. **320**, 238 (1987).
18. B. T. Soifer, L. Boehmer, G. Neugebauer, and D. B. Sanders, Astron. J. **98**, 766 (1989).
19. D. K. Strickland and I. R. Stevens, Mon. Not. R. Astron. Soc. **314**, 511 (2000).
20. S. Veilleux, astro-ph/0201491 (2002).
21. S. Veilleux, D. C. Kim, D. B. Sanders, *et al.*, Astrophys. J., Suppl. Ser. **98**, 171 (1995).
22. B. C. Whitmore, R. A. Lucas, D. B. McElroy, *et al.*, Astron. J. **100**, 1489 (1990).
23. K. A. Weaver, T. M. Heckman, D. K. Strickland, and M. Dahlem, Astrophys. J. Lett. **576**, L19 (2002).
24. G. Worthey, Astrophys. J., Suppl. Ser. **95**, 107 (1994).
25. G. Worthey, S. M. Faber, J. J. Gonzalez, and D. Burstein, Astrophys. J., Suppl. Ser. **94**, 687 (1994).
26. J. S. Young, S. Xie, J. D. P. Kenney, and W. L. Rice, Astrophys. J., Suppl. Ser. **70**, 699 (1989).

Translated by V. Astakhov

Astronomy Letters, Vol. 30, No. 1, 2004, pp. 14–31. Translated from Pis'ma v Astronomicheskiĭ Zhurnal, Vol. 30, No. 1, 2004, pp. 17–36.

A Rotating Collapsar and Possible Interpretation of the LSD Neutrino Signal from SN 1987A

V. S. Imshennik[1]* and O. G. Ryazhskaya[2]

[1] *Institute for Theoretical and Experimental Physics, ul. Bol'shaya Cheremushkinskaya 25, Moscow, 117259 Russia*

[2] *Institute for Nuclear Research, Russian Academy of Sciences, pr. Shestidesyatiletiya Oktyabrya 7a, Moscow, 117312 Russia*

Received August 12, 2003

Abstract—We consider an improved rotational mechanism of the explosion of a collapsing supernova. We show that this mechanism leads to two-stage collapse with a phase difference of ∼5 h. Based on this model, we attempt a new interpretation of the events in underground neutrino detectors on February 23, 1987, related to the supernova SN 1987A. © *2004 MAIK "Nauka/Interperiodica".*

Key words: *supernovae and supernova remnants.*

INTRODUCTION

In effect, the idea of two-stage gravitational collapse has long been a subject of discussion, particularly in the case of the resumption (of the second stage) of the collapse in a neutron star with its transformation into a black hole (see, e.g., Imshennik and Nadyozhin 1988). However, if the rotation effects are taken into account, then such a two-stage collapse of an iron–oxygen–carbon (Fe–O–C) core acquires a different, more specific content that we have called the rotational mechanism of the explosion of a collapsing supernova (SN). The reason is that, in our opinion, the above rotation effects make it possible to solve the crucial problem of the transformation of the collapse into an explosion for high-mass and collapsing supernovae (all types of SN except the type-Ia thermonuclear SN). An extensive series of studies has been carried out since 1992 in connection with the famous SN 1987A (Imshennik and Nadyozhin 1992; Imshennik 1992; Aksenov and Imshennik 1994; Imshennik and Popov 1994; Aksenov *et al.* 1995; Imshennik 1995, 1996; Imshennik and Blinnikov 1996). Below, we consider the so-called improved rotational mechanism of explosion. The possibility of this mechanism was first mentioned by Imshennik and Popov (1994) in connection with the reception of two neutrino signals from SN 1987A (see Section 1) separated by a relatively long time interval of 4 h 44 min (≡4.7 h) (Dadykin *et al.* 1987; Aglietta *et al.* 1987) at $t_{UT} = 2$ h 52 min (February 23, 1987) and $t_{UT} = 7$ h 36 min (Hirata *et al.* 1987; Bionta *et al.* 1987). These observations of the neutrino signals were carefully analyzed by Dadykin *et al.* (1989). The above improvement of the explosion scenario for the rotating Fe–O–C core of a high-mass star stems not only from the necessity of explaining the observations of the neutrino signals from SN 1987A, but also from the intrinsic logic of the development of this scenario—it arose on the road to overcoming theoretical difficulties.

The neutrino spectra were obtained from theoretical estimates. These spectra are based on the hydrodynamic calculations of a quasi-one-dimensional model for the formation of a rotating collapsar (Imshennik and Nadyozhin 1977, 1992) and on the hypothesis of bulk neutrino radiation from a rotating collapsar (Imshennik and Nadyozhin 1972; Ivanova *et al.* 1969a) with the almost total dominance of electron neutrinos in the neutrino radiation (see Section 2). The derived spectra include the dimensionless chemical potential of electrons, φ, which is considered here as the only free parameter of these spectra.

In Section 3, we analyze the observations of the neutrino signal on the LSD detector at $t_{UT} =$ 2 h 52 min (February 23, 1987) by using the previously obtained neutrino spectra that additionally take into account the effects of self-absorption inside a rotating collapsar. We develop the hypothesis about the interaction of electron neutrinos with the nuclei of iron that is actually present in the LSD detector in large quantities. The products of these interaction reactions, mainly in the form of gamma-ray photons and electrons, are detected in a liquid scintillator with a photomultiplier. The detection efficiency is

*E-mail: imshennik@itep.ru

estimated by the Monte-Carlo method. We show that the observational data are consistent with the theory described in Sections 1 and 2 over a wide φ range.

1. THEORETICAL ANALYSIS OF THE TIME INTERVAL BETWEEN THE TWO STAGES OF COLLAPSE FOR SN 1987A

Thus, on the threshold of gravitational collapse, the Fe–O–C stellar core has a given (from calculations of the evolution of high-mass stars with a total mass on the main sequence $M_{\rm ms} \geq 10M\odot$) mass $M_{\rm t}$ and a total angular momentum J_0, which are, obviously, conserved during the collapse of this core into a rotating collapsar. Aksenov *et al.* (1995) numerically constructed a large family of such two-dimensional, axisymmetric collapsars as a function of the parameters $M_{\rm t}$ and J_0. Dong and Shapiro (1995) proved the high probability of collapsars falling into the region of dynamical instability that is specified by the standard criterion $\beta = \mathcal{E}_{\rm rot}/|\mathcal{E}_{\rm grav}| \geq 0.27$ (Tassoul 1978). The quantities $\mathcal{E}_{\rm rot}$ and $|\mathcal{E}_{\rm grav}|$ denote the total rotational and total gravitational energies, respectively. Note that during collapse with the conservation of total angular momentum J_0 and local specific angular momentum, the energy $\mathcal{E}_{\rm rot}$ greatly increases compared to $|\mathcal{E}_{\rm grav}|$, which, of course, is also an increasing quantity. This instability grows with a characteristic hydrodynamic time and typically leads to the breakup of the collapsar into pieces, in the simplest case, into a binary of neutron stars (NS); almost all of the angular momentum can transform orbital angular momentum, $J_{\rm orb} \leq J_0$. However, $\Delta J = J_0 - J_{\rm orb}$ becomes the spin angular momentum of the NS themselves essentially in the more massive component of this binary. In other words, the NS binary is formed through the hydrodynamic fragmentation of a rotating collapsar. Imshennik (1992) showed that, under the additional assumption of a circular orbit of the binary and for given $M_{\rm t}$ and $J_{\rm orb}$, all of the orbital parameters, including the orbital radius a_0 and velocity v_0 (in terms of the reduced binary mass $M_1M_2/M_{\rm t}$, according to the Kepler law) can be determined:

$$a_0 = \frac{J_{\rm orb}^2}{GM_{\rm t}^3}\cdot\frac{1}{\delta_0^2(1-\delta_0)^2},$$

$$v_0 = \frac{GM_{\rm t}^2}{J_{\rm orb}}\cdot\delta_0(1-\delta_0), \qquad \delta_0 = \frac{M_1}{M_{\rm t}}, \qquad (1)$$

where the free parameter $0 \leq \delta_0 \leq 1/2$ appears. Below, M_1 is assumed to be the mass of the less massive NS. Remarkably, the evolution of the binary is determined by only one factor—gravitational radiation. The latter is unique from an astrophysical point of view, because it pertains to the evolution of such binaries, but in the presence of a low-mass NS whose mass is much lower than the mass of the more massive NS at the very outset; this mass is also small in absolute terms—compared to $M\odot$ (see below). In the point-mass approximation, the gravitational radiation (Peters and Mathews 1963; Landau and Lifshitz 1973) and the conservative mass transfer are described by a simple differential equation (Imshennik and Popov 2002):

$$\frac{da}{dt} = -\frac{64G^3M_{\rm t}^3\delta(1-\delta)}{5c^5a^3} - 2a\frac{1-2\delta}{\delta(1-\delta)}\frac{d\delta}{dt}, \qquad (2)$$

where, according to the common property of NS (degenerate stars), there is mass transfer with a decrease in the mass of the low-mass NS ($d\delta/dt < 0$). The derivative $d\delta/dt$ can be explicitly calculated in the Roche approximation (the Roche lobe and potential), as was shown in detail in the paper mentioned above, which continues the classic works in this field pioneered by Paczynski and Sienkiewicz (1972). Equation (2) then describes the evolution under the action of two factors; the second factor is mass transfer that causes the radius a to increase, in contrast to the first factor that describes the approach of the components. However, the second factor comes into play only after the low-mass NS fills its Roche lobe. Before this time, the NS only approach each other at a constant parameter $\delta = \delta_0$ due to the gravitational radiation that carries away not only the energy of the NS binary, but also its orbital angular momentum. For $d\delta/dt = 0$, i.e., at $\delta = \delta_0$, Eq. (2) has a simple analytical solution from which $t_{\rm grav}$, the time of the closest approach of the components with a constant arbitrary parameter δ_0, can be obtained formally up to the radius $a = 0$ (Imshennik and Popov 1994):

$$t_{\rm grav} = 2.94\times10^{-4}\frac{j_0^8}{m_{\rm t}^{15}\delta_0^9(1-\delta_0)^9}\ {\rm s}, \qquad (3)$$

where $j_0 = J_{\rm orb}/8.81\times10^{49}$ erg s and $m_{\rm t} = M_{\rm t}/2M\odot$; this choice of scales for the dimensionless quantities j_0 and $m_{\rm t}$ corresponds to the typical conditions of a Fe–O–C stellar core on the threshold of its collapse (as applied to SN 1987A). It should be noted that the arbitrariness in specifying the initial rotation in the stellar core is severely restricted by the hypothesis that this rotation is rigid; this is related to the action of convection inherent in the structure of high-mass stars, particularly at the final stages of their thermonuclear evolution. For this reason, the rotational energy in the initial conditions is actually negligible compared to the gravitational energy, i.e., $\beta \ll 1$, and the stellar structure is virtually spherically symmetric.

Table 1 presents the values of δ_0 that follow from relation (3), as long as $m_{\rm t} = 0.9$ ($M_{\rm t} = 1.8M\odot$) and, most importantly, as applied to SN 1987A, $t_{\rm grav} =$

Table 1

$J_{\rm orb}$, erg s	8.81×10^{49}	6.17×10^{49}	3.17×10^{49}
j_0	1.00	0.700	0.360
$J_{\rm ac}$, erg s	1.72×10^{49}	1.45×10^{49}	1.25×10^{49}
$J_{\rm ac}/J_{\rm orb}$	0.195	0.235	0.394
$M_1, M\odot$	0.37	0.25	0.13
δ_0	0.206	0.139	0.0722
$\Delta t_{\rm gr}$, s	$\sim$0.04	$\sim$0.2	$\sim$10
$\Delta t_{\rm ac}$, s	$\sim$0.9	$\sim$1.0	$\sim$1.2

Note: $M_{\rm t}=1.8M\odot$, $J_0=8.81\times10^{49}$ erg s, $t_{\rm grav}=4.7$ h.

4.7 h $\equiv$ 16 920 s are given. In these calculations, we vary j_0, i.e., the fraction of the total angular momentum J_0 transformed into the orbital angular momentum $J_{\rm orb}$. According to the data in Table 1, j_0 varies between 1 and 1/3. The next row gives the orbital angular momentum $J_{\rm ac}$ at the time the low-mass NS fills its Roche lobe and the evolution of the binary with mass transfer begins. This evolutionary stage is called accretion for short; clearly, the solution of Eq. (2) with the second term $d\delta/dt\neq0$ on its right-hand side corresponds to this stage. We see that $J_{\rm ac}$ decreased significantly at the previous stage of NS approach under the effect of gravitational radiation alone: by a factor from $\sim$5 to $\sim$3, depending on j_0. Finally, the next rows give the sought-for values of the mass M_1 and δ_0 (its ratio to the total mass $M_{\rm t}$), which also decrease by a factor of almost 3. It is easy to see that the following strong inequality holds over the entire j_0 range: $M_1\ll M_2$ (at least, M_2 is larger than M_1 by a factor of 4 for the first column).

Thus, our identification of the time interval between the two neutrino signals for SN 1987A with the time of approach of the components of the putative NS binary due to gravitational radiation alone (based on relation (3)) fits into the theory of the rotational mechanism of supernovae explosions for the following reason: The minimum NS mass $M_1=0.13M\odot$ still exceeds the lower mass limit for stationary NS, $M_{1\rm min}=0.095M\odot$ (Blinnikov *et al.* 1990; Imshennik 1992; Aksenov *et al.* 1995), when the star explosively disintegrates with its transformation into an iron gas. The derived strong inequality $\delta_0\ll1$ qualitatively agrees with the first three-dimensional hydrodynamic calculations of the fragmentation of a rotating collapsar (Houser *et al.* 1994; Aksenov 1999), in which a $\sim0.1M\odot$ mass ejection actually emerges.[1]

Nevertheless, an analysis of the physical effects disregarded in relation (3) is required to justify the results presented in Table 1 more reliably. To this end, the last two rows of Table 1 give $\Delta t_{\rm gr}$ and $\Delta t_{\rm ac}$ that have the following meaning: The values of these quantities should be compared with the $t_{\rm grav}=$ 16 920 s specified above. Our estimates separately are smaller than the latter value at least by a factor of 2000 and are of no importance within the accuracy of the sought parameter δ_0. The physical meaning of $\Delta t_{\rm gr}$ is that, strictly speaking, from the time $t_{\rm grav}$ in relation (3), we should subtract the time interval when the radius of the NS binary $a=a_{\rm R0}$, where $a_{\rm R0}$, the critical radius for filling the Roche lobe for a low-mass NS, is (Paczynski 1971)

$$a_{\rm R0}=2.16R_{\rm NS1}\delta_0^{-0.33}, \qquad (4)$$

where $R_{\rm NS1}$ is the radius of a NS with mass M_1.[2] Thus, it follows from (4) that $a_{\rm R0}\gg R_{\rm NS1}$ at $\delta_0\ll1$. It is easy to show that $\Delta t_{\rm gr}=t_{\rm grav}(J_{\rm ac}/J_{\rm orb})^8$. The values of $\Delta t_{\rm gr}$ are given in Table 1; they are very small. Imshennik and Popov (1998) analyzed in detail the mixed type of evolution described by the complete equation (2) with mass transfer (!) until δ decreased to its critical value of $\delta_{\rm cr}=M_{1\rm min}/M_{\rm t}=0.053$, i.e., until the explosion time of the low-mass NS. By definition, mass transfer is possible if the condition for the immersion of a low-mass NS in its Roche lobe is satisfied, i.e., $a\le a_{\rm R}$, which includes the current critical radius for filling the Roche lobe,

$$a_{\rm R}=2.16R_{\rm NS}\delta^{-0.33}, \qquad (4')$$

obtained by a natural generalization of relation (4), depending on the parameter $\delta\le\delta_0$ and the radius $R_{\rm NS}$ of an NS with mass $M_1=\delta M_{\rm t}$. This inequality is actually satisfied throughout the mixed evolutionary stage of the NS binary, which can also

[1] Interestingly, if a rotating collapsar fragmented into pieces of equal mass ($\delta_0=1/2$) at the same values of $m_{\rm t}=1.8$ and $j_0=1.0$, the time of approach of the components ($t'_{\rm grav}\simeq$ 400 s), according to formula (3), would be many times shorter than the time specified by the observations of the neutrino signals ($t_{\rm grav}=16\,920$ s)!

[2] As the NS radius $R_{\rm NS}$, we may take interpolation formulas derived for numerical calculations of the radii of cold NS with the inclusion of low-mass NS, for examples, from Yaranowski and Krolak (1992). However, it should be remembered that, in our case, still very young and, hence, relatively hot NS whose radii are generally larger than the radii of cold NS are members of the binary. This implies that their Roche lobes are filled earlier and that their radii $a_{\rm R0}$ are larger, but the related changed corrections $\Delta t_{\rm gr}$ and $\Delta t_{\rm ac}$ are still negligible compared to the sought-for time $t_{\rm grav}$ from relation (3).

be proved from physical considerations (Imshennik and Popov 1996).

$\Delta t_{\rm ac}$ follow from these calculations, because the calculations yield a time dependence $\Delta t(\delta)$ within the range $\delta_0 \geq \delta \geq \delta_{\rm cr}$ with $\Delta t_{\rm ac} = \Delta t(\delta_{\rm cr})$. In contrast to $\Delta t_{\rm gr}$, this quantity should be added to $t_{\rm grav}$, because the two effects partly compensate each other. Therefore, their total effect, which is at a maximum in the last row of Table 1, is 8.8 s, which, we repeat, is negligible for the sought-for parameter δ_0. In short, quantitatively including the second evolutionary stage of the components of the NS binary turned out to be completely unnecessary.

Nevertheless, it remains to determine how important the assumptions about the total mass of the Fe–O–C stellar core, $M_{\rm t}$ (which was taken above to be $1.8M\odot$), about the total angular momentum J_0 (which was taken above to be 8.81×10^{49} erg s), and, finally, about a zero orbital eccentricity $e_0 = 0$ are. At a fixed $t_{\rm grav}$, obvious dependences follow from (3) for $\delta_0 \ll 1$: $(1-\delta_0)\delta_0 \simeq \delta_0 \propto j_0^{0.89} m_{\rm t}^{-1.7}$. In Table 1, the dependence $\delta_0 \propto j_0^{0.89}$, of course, holds. Since the decrease in initial J_0 as well as its increase are severely restricted by the condition of the dynamical rotational instability itself (Aksenov *et al.* 1995), the change in $M_1 \propto J_{\rm orb}^{0.89} \propto J_0^{0.89}$ is small. The same is also true for the dependence $M_1 \propto M_{\rm t}^{-1.7}$ that follows from the previous dependence of the dimensionless quantities, but for a different reason: the masses of Fe–O–C nuclei are limited to the standard range $1.2M\odot < M_{\rm t} < 2M\odot$, as predicted by the stellar evolution theory. Note that, in this case, $M_{\rm t} = 1.8M\odot$ in Table 1 is close to the upper limit of the range, so the possibility of its decrease in stellar cores before collapse definitely does not bring the corresponding values of δ_0 outside the inequality $\delta_0 > \delta_{\rm cr}$. We can reach the important conclusion that all the possible changes in parameters $M_{\rm t}$ and J_0 do not qualitatively change the results that were formulated above based on the data of Table 1.

Next, let us consider not a circular but an eccentric orbit that may well result from the hydrodynamic fragmentation of a collapsar, i.e., with an initial eccentricity $e_0 \neq 0$ $(0 \leq e_0 < 1)$. The problem of the evolution of an eccentric orbit for an NS binary was completely solved by Imshennik and Popov (1994). Although its solution (also analytical at an arbitrary value of e_0) is more complex than that in the limiting case of a circular orbit with $e_0 = 0$, the quantity $t_{\rm grav}$ of interest can be expressed elegantly (see the pioneering paper by Peters 1964) at the same values of $M_{\rm t}$ and J_0 as those in (3):

$$t_{\rm grav} = 2.94 \times 10^{-4} \frac{j_0^8 \tau(e_0)}{m_{\rm t}^{15} \delta_0^9 (1-\delta_0)^9} \ {\rm s}, \qquad (5)$$

where the new (compared to (3)) dimensionless function $\tau(e_0)$ is given in the form of an easily calculated integral with a certain factor (both are functions of the parameter e_0):

$$\tau(e_0) = \frac{48}{19} \frac{1}{e_0^{48/19} (1 + \frac{121}{304} e_0^2)^{3480/2299}} \qquad (6)$$
$$\times \int_0^{e_0} \frac{e^{29/19} (1 + \frac{121}{304} e^2)^{1181/2299}}{(1-e^2)^{3/2}} de.$$

This function $\tau(e_0) \geq 1$ differs only slightly from unity ($\tau(0) = 1$) as long as $e_0 \leq 0.5$ and increases steeply at $e_0 \to 1$, $\tau(e_0) \propto 1.81(1-e_0^2)^{-1/2}$. Our analysis shows that the limiting (singular) case of $e_0 = 1$ itself cannot be considered, because the necessary condition for the orbits being quasi-stationary is not satisfied. For this reason, this case has been excluded in the above e_0 range. The qualitative result obtained by Imshennik and Popov (1994) may be considered to be the establishment of such a rapid decrease in eccentricity e ($de/dt < 0$ for any e_0 and δ_0) due to gravitational radiation that $e = e_{\rm f} \leq 0.1$ by the time the low-mass NS fills its Roche lobe, i.e., the orbit is almost indistinguishable from a circular orbit. To be more precise, this inequality also depends on the parameters $m_{\rm t}$ and j_0 and on the radius $R_{\rm NS1}$ (Imshennik and Popov 1994):

$$e_{\rm f} < 0.044 \left(\frac{m_{\rm t}^3}{j_0^2} \right)^{19/12} \left(\frac{R_{\rm NS1}}{13.5 \ {\rm km}} \right)^{19/12}. \qquad (7)$$

As our analysis indicates, the influence of these parameters and the radius is quantitatively small, so the previous eccentricity estimate is definitely justified by formula (7). This circumstance seems quite fortunate, because the entire theory of mass transfer was constructed precisely for circular orbits. It would be instructive to estimate the influence of a finite initial eccentricity e_0 on δ_0. We take $j_0 = 1$ and $m_{\rm t} = 0.9$ in formula (5) and substitute $e_0 = 0.9$, so the function $\tau(e_0) = 3$; hence we obtain $\delta_0 = 0.241$ at $t_{\rm grav} = 4.7$ h, which should be compared with $\delta_0 = 0.206$ (the first column in Table 1). The following general conclusion can be reached: the influence of a finite initial eccentricity, $e_0 \neq 0$, is negligible and does not lead (like the influence of $m_{\rm t}$) to any violation of the condition $\delta_0 > \delta_{\rm cr}$. The latter inequality ensures the existence of a low-mass ejection ($\delta_0 \ll 1$) in the form of an NS.

One of the important results of the analytical model for the evolution of a close NS binary is the conclusion that, in the solution of Eq. (2) with mass transfer, the approach of the components very soon gives way to their recession from one another, and the dependence on the initial arbitrary parameter δ_0 of the

binary virtually disappears. We are talking here about the sought-for dependence of δ on time Δt during the mixed evolutionary stage under the action of both factors: gravitational radiation and mass transfer (accretion) (see Fig. 6 in the paper by Imshennik and Popov (1998) cited above). This circumstance is formally similar to what has been said above about the influence of the other initial parameter e_0 on the solution. Thus, during the evolution under consideration, the influence of both emerged arbitrary parameters, δ_0 and e_0, essentially vanishes, and the evolution of a close NS binary finishes irrespective of the choice of these parameters. However, a third arbitrary parameter, $\Delta J = J_0 - J_{\rm orb}$, appeared in the course of our theoretical analysis. This parameter may prove to be crucial: Will the evolution end with the merger or explosion of a low-mass NS that has overfilled its Roche lobe? As Imshennik and Popov (1998) showed, the concept of a (circular) orbit and the point approximation for the gravitational interaction of both NSs become meaningless at the very end of the evolution.[3] A numerical solution of the three-dimensional hydrodynamic problem is required. This solution is extremely complex if the effects of gravitational radiation, neutrino radiation, and the nonideal equation of state for these NS are included in the problem. Of course, this solution is of relevant interest, but we have to restrict our selves to reasonable (?) physical estimates before it can be implemented after the overcoming of fantastic difficulties. Until now, it has been assumed that the more massive component with mass $M_2 = (1 - \delta_0)M_{\rm t}$ does not collaps for the second time during the fragmentation of the rotating collapsar due to the residual total angular momentum ΔJ_0. The first neutrino signal was produced only by the primary collapse of the Fe–O–C stellar core that led to the formation of this collapsar before its fragmentation. However, even during the evolution, once the orbital radius $a = a_{\rm R0}$ was reached, the high-mass NS gradually (in a time $\Delta t_{\rm ac} \sim 1$ s) increased its mass up to $M_2 = (1 - \delta_{\rm cr})M_{\rm t}$. However, the centrifugal forces attributable to the angular momentum ΔJ could still reliably prevent its secondary collapse. Here, it is important to note that this angular momentum ΔJ can even exceed $J_{\rm ac}$: for example, for the second column of Table 1, $J_{\rm ac} = 1.45 \times 10^{49}$ erg s, while the corresponding $\Delta J = 2.64 \times 10^{49}$ erg s. Using relations (1), but for the final state of a binary with the orbital angular momentum $J_{\rm ac}$ given above, we can easily find that the parameters of this orbit are $a_{\rm f} = 2.22 \times 10^7$ cm and $v_{\rm f} = 3.28 \times 10^9$ cm s^{-1}, so the angular frequency of the binary is $\omega_{\rm f} = v_{\rm f}/a_{\rm f} = 1.48 \times 10^2$ s^{-1}. On the other hand, the angular frequency of a high-mass NS with the above value of $M_{2\rm f} = 1.70 M\odot$ is $\Omega_{\rm f} \sim 10^5$ s^{-1} for rigid rotation (overestimate) or $\Omega_{\rm f} \sim 10^3$ s^{-1} for a typical differential rotation law (underestimate).

In short, the strong inequality $\Omega_{\rm f} \gg \omega_{\rm f}$ holds. However, the corotation condition is valid in close binaries. According to this condition, the orbital angular momentum must be much larger than the spin angular momenta, because the frequencies of these rotations, $\omega_{\rm f}$ and $\Omega_{\rm f}$, are equalized by tidal forces.

Strictly speaking, this condition takes effect even at the very beginning of the mixed evolutionary stage, i.e., since the time the low-mass NS fills its Roche lobe. Thus, a corollary of the corotation condition is the transformation of spin angular momentum ΔJ into the orbital angular momentum of the binary. In this way, we also remove this main obstacle to the secondary collapse of a high-mass NS. The following legitimate question arises: Why did not the corotation condition prevent the appearance of a significant residual angular momentum ΔJ during the fragmentation of the rotating collapsar? A completely justified answer to this question will probably be given after the construction of a three-dimensional (!) hydrodynamic model with a consistent allowance for the same physical factors that we mentioned when discussing the end of the evolution of a NS binary, but we can make a qualitative estimate. To be more precise, we can draw attention to the characteristic times of the hydrodynamic fragmentation, which was called hydrodynamic not by chance. These characteristic times are only 10^{-3} s, while the characteristic times of the mixed evolution for a NS binary, as has been repeatedly said above, are much larger, $\sim$1 s. There is yet another factor in favor of the appearance of the residual angular momentum under consideration in a high-mass NS, as will be seen below.

Thus, a high-mass NS collapses in complete accordance with the standard model without rotation (Nadyozhin 1977a, 1977b, 1978). This collapse is accompanied by a standard neutrino signal, because during its evolution, the binary has virtually gotten rid of the bulk of its total angular momentum due to gravitational radiation. However, the remnant of the spin angular momentum was redistributed, according to the above assessment, to the orbital angular momentum, essentially transferring to the low-mass NS (see also below). It is important to recall that the integrated parameters of the standard neutrino signal

[3] Quantitatively, this last period of the evolution of a close NS binary is very short in terms of δ; more specifically, it arises at $\delta = \delta^* = 0.082$, which exceeds the above critical value of $\delta_{\rm cr} = 0.053$ only slightly. The parameter δ^* is virtually independent of the initial value of δ_0, but depends on other parameters, $M_{\rm t}$ and $J_{\rm orb}$ (Imshennik and Popov 1998).

are in satisfactory agreement with these parameters of the second neutrino signal from SN 1987A (Imshennik and Nadyozhin 1988; Blinnikov *et al.* 1988).

2. ESTIMATING THE (ELECTRON) NEUTRINO SPECTRA FOR SN 1987A

So far, we have been able to consistently analyze the collapse of a stellar Fe–O–C-core with initial rotation only in the one-dimensional, spherically symmetric statement of the problem by averaging the centrifugal force over the meridional angle (the only change of the problem then concerns the equation of motion from the complete system of four equations written in Lagrangian coordinates). The assumption that the local specific angular momentum j is conserved played a key role in this great simplification of the problem. In this case, the centrifugal force F_r was unambiguously expressed in terms of the initial rigid-rotation parameters $\omega_0 = \text{const}$ and $r_0(m)$ and the Eulerian radius $r = r(m,t)$, with $F_r \propto r^{-3}$. Obviously, the total angular momentum was then also automatically conserved in this case,

$$J_0 = \frac{2}{3}\int_0^{M_t} j dm = \frac{2}{3}\omega_0 \int_0^{M_t} r_0^2(m) dm,$$

with the factor $2/3$ being attributable precisely to the angular averaging of the centrifugal force:

$$F_r = \frac{2}{3}\frac{\omega^2 r^2}{r} = \frac{2}{3}\frac{\omega_0^2 r_0^4(m)}{r^3(m,t)}. \qquad (8)$$

The first numerical calculations of this kind were performed by Imshennik and Nadyozhin (1977). The equations of state, the processes of material neutronization, and the description of neutrino processes did not differ in any way from their representation in the standard model. These hydrodynamic models, which were called quasi-one-dimensional because of the described allowance for the rotation effects, were computed until the formation of a hydrostatic equilibrium configuration that was called above a rotating collapsar.

Another study of the quasi-one-dimensional model with detailed analysis and testing of the results was carried out later (Imshennik and Nadyozhin 1992). In this paper, we focus on the discussion of the neutrino radiation parameters that were limited in the papers by Imshennik and Nadyozhin (1977, 1992) only to data on a light curve with a total energy $\mathcal{E}_{\nu\tilde{\nu}} = 3.3 \times 10^{52}$ erg (by the end of the computation $t = 2.9$ s) and to parameters of the neutrinosphere. Apart from the marked difference between the neutrino light curves for the calculations of the standard model ($\omega_0 = 0$) and the quasi-one-dimensional model with $\omega_0 = 0.86\Omega_0$ ($\Omega_0 = (GM_t/R_0^3)^{1/2}$ is the velocity at which the centrifugal and gravitational forces are equal on the surface of the stellar core near the equator),[4] an enormous difference appears between the neutrino optical depths indicated by several numbers in these light curves (see Fig. 6 from Imshennik and Nadyozhin 1992). Whereas $\tau \geq 100$ for the standard model starting from the maximum of the light curve, τ is typically several units (except the middle part of the light curve where it rises to 32) in the model with rotation. This implies that the approximation of radiative heat conduction used in the calculations is near its validity boundary for the quasi-one-dimensional model. In addition, the region inside the neutrinosphere encloses less than half of M_t by mass (see Fig. 1 from the cited paper). By the end of the computation, this mass decreases by several more times ($\sim$5) (see Fig. 5 from the cited paper). We must also take into account the ambiguity in determining the neutrino optical depth itself (formally, four different determinations of it are possible!), in contrast to the photon optical depth. Nevertheless, an optically opaque region near the center of the collapsing stellar core since the time $t = 0.5$ s was introduced in the cited paper (see Fig. 1). The main objection to this introduction is as follows: The rotating collapsar in the initial two-dimensional axisymmetric configuration is a highly flattened structure (Aksenov *et al.* 1995) the polar radius of which is several times smaller than its equatorial radius. This flattening naturally entails a decrease in τ at least by the same number of times. In addition, it is clear that the rotating collapsar will be a hydrostatic equilibrium configuration only in an axisymmetric geometry. If the criterion for dynamical instability given above and obtained quantitatively, $\beta = 0.42 > 0.27 = \beta_{cr}$ (Imshennik and Nadyozhin 1992), is satisfied, instability relative to the third (azimuthal) coordinate will rapidly (on the characteristic hydrodynamic time scale) transform it into a dumbbell-like configuration. The central region of the collapsar with the lowest specific angular momenta will be located in the bar of this dumbbell, which is very thin compared to the end balls. Here, it should be emphasized that, strictly speaking, the rotating collapsar cannot be formed as an equilibrium structure if the criterion $\beta > \beta_{cr}$ is satisfied. It has the right to exist only for our idealization of axial symmetry and, of course, in

[4] Since the adopted initial angular velocity ω_0 is of great importance, we give its numerical value specified in the calculations of the quasi-one-dimensional model: $\Omega_0 = 1.78\ \text{s}^{-1}$ (at $M_t = 2M\odot$ (!), $R_0 = 4.38 \times 10^8$ cm), and the corresponding value of $\omega_0 = 0.86\Omega_0 = 1.53\ \text{s}^{-1}$ (the substitution of the coefficient 0.86 for 0.80 in the succeeding paper (Imshennik and Nadyozhin 1992) is among the corrections to the preceding paper (Imshennik and Nadyozhin 1977)

terms of the quasi-one-dimensional model. Thus, the former center of the collapsing stellar core will certainly be seen not only toward the poles, but also on the sides of the bar, into which it falls during the nonlinear growth of dumbbell barlike ($m = 2$) instability (Tassoul 1978; Aksenov 1996).

The above qualitative discussion gives us the right to advance the following hypothesis: the central region of the quasi-one-dimensional model with the formation of a rotating collapsar may be considered to be completely transparent for intrinsic neutrino radiation. Concurrently, it seems quite justifiable to retain the thermodynamic parameters in this region obtained in the calculations by Imshennik and Nadyozhin (1977, 1992) as moderately sensitive to this change of the status of neutrino radiation (from surface to bulk), because the optical depths are so small in these calculations. In any case, retaining such quantities as the central density and temperature (ρ_c and T_c) we can be sure of their consistency, because they satisfy three of the four equations of the quasi-one-dimensional model (together with a violation of the entropy equation). Concurrently, we retain the total energy of the neutrino radiation, $\mathcal{E}^*_{\nu\tilde{\nu}} = 2.7\mathcal{E}_{\nu\tilde{\nu}} = 8.9 \times 10^{52}$ erg. The numerical coefficient 2.7 is introduced by analogy with the standard model (Nadyozhin 1977a, 1977b, 1978), where the corresponding value of $\mathcal{E}_{\nu\tilde{\nu}} = 1.9 \times 10^{53}$ erg at time $t = 2.4$ s (see the table from Imshennik and Nadyozhin 1992) transforms into $\mathcal{E}^*_{\nu\tilde{\nu}} = 5.3 \times 10^{53}$ erg through justified estimates of the prolonged neutrino cooling stage of a hot NS (Imshennik and Nadyozhin 1988). The presented approach may be fraught with the overestimation of the bulk radiation parameters, particularly the total time of this process for an unstable rotating collapsar.[5] The interpretation of the observed time interval between the two neutrino signals from SN 1987A justified in the preceding section on the basis of the previously advanced rotational mechanism of the explosions of collapsing supernovae may serve as an indirect justification of the suggested approach.

Thus, we take the total energy carried away by neutrino radiation with allowance made for the cooling of the rotating collapsar (by the time $t_{\rm fin} \simeq 6$ s),

$$\mathcal{E}^*_{\nu\tilde{\nu}} = 8.9 \times 10^{52} \text{ erg}. \qquad (9)$$

At this time, the material is so cold that the neutrons degenerate (actually, this effect should have been taken into account at the end of the numerical calculation of the quasi-one-dimensional model, $t = 2.9$ s).

[5] We are grateful to D.K. Nadyozhin for a critical discussion in which he, in particular, drew special attention to the above circumstance.

Let us next consider the spectral properties of the neutrino radiation by assuming the bulk radiation mechanism due to the non-one-dimensional hydrodynamic collapse noted above. We restrict our analysis to the main reaction of the modified URCA-process $e^- + p \to n + \nu_e$, in which electron neutrinos ν_e are generated. If the material contains only free nucleons (see the estimates below), as was specified in the quasi-one-dimensional model, then, based on the Kirchhoff law and using the expression for the ν_e mean free path (Ivanova *et al.* 1969a; Imshennik and Nadyozhin 1972), we obtain the spectral specific radiation power:

$$\frac{q_\nu}{\rho} = \frac{4\pi B_\nu}{\rho} = \frac{1}{m_0}\frac{\ln 2}{(ft)_{np}}\frac{1}{1+\Theta} \qquad (10)$$
$$\times \left(\frac{\varepsilon_\nu}{m_e c^2}\right)^5 \frac{1}{1+\exp\left(\frac{\varepsilon_\nu}{kT} - \varphi\right)} \quad \text{g}^{-1}\,\text{s}^{-1},$$

where $\Theta = N_n/N_p$ is the degree of neutronization of the material, φ is the dimensionless chemical potential of the electron gas (see below), ε_ν is the neutrino energy in erg, and the spectral power is given per unit interval of this energy. Below, we will be interested in the dependence of (q_ν/ρ) on energy ε_ν, in which an allowance for the Pauli principle in the initial ν_e mean free path plays a crucial role: it is responsible for the exponential factor in (10). Note also that relation (10) gives the spectral power of the neutrino radiation B_ν per unit solid angle. By definition, the neutrino radiation in the reaction under consideration is isotropic in each (Lagrangian) particle of the material, so B_ν in (10) is also isotropic. The energy dependence of (q_ν/ρ) follows from (10):

$$\frac{q_\nu}{\rho} \propto \left(\frac{\varepsilon_\nu}{m_e c^2}\right)^5 \qquad (11)$$
$$\times \frac{1}{1+\exp\left(\frac{\varepsilon_\nu}{kT} - \varphi\right)} \propto \frac{x^5}{1+\exp(x-\varphi)} = \phi(x,\varphi)\,,$$

where $x = \varepsilon_\nu/kT$, $\varphi = \mu_e/kT$, and μ_e is the chemical potential of the electrons ($[\mu_e] =$ erg). The function $\phi = \phi(x,\varphi)$ with a specified parameter φ has only one maximum with $x_{\max} > \varphi$ and the following asymptotics: $\sim x^5$ (for $x \to 0$) and $\sim x^5 e^{-x}$ (for $x \to \infty$). The quantity $x_{\max} = x_{\max}(\varphi)$ can be easily calculated and is given in Table 2. Curiously, at $\varphi = 10$, the exact solution for $x_{\max} = \varphi = 10$, while in the remaining cases of specified φ, $x_{\max}$ is given with four significant figures. We probably could have also calculated the ν_e energy averaged over spectrum (11), but it will suffice to understand that it is close to $x_{\max}$, and exceeds it slightly. These important quantities in the ν_e spectrum appear to have the following main property: $x_{\max} \geq 5$ for $\varphi \leq 5$; $x_{\max} \simeq \varphi$ for $\varphi \geq 5$). The

inequality $x_{\max} \geq 5$ always holds for the lower limit of the maximum of the spectrum.

It would be appropriate to apply a correction for the self-absorption of neutrinos of sufficiently high energies in the layers surrounding the center of the rotating collapsar to the ν_e spectrum from (11). Let the mean optical depth of these layers be $\langle\tau_\nu\rangle = k$, where k is an arbitrary number that may be close to unity ($k \leq 1$) even if the non-one-dimensional effects are taken into account. Of course, it is smaller than the optical depths obtained by Imshennik and Nadyozhin (1992) (see above). The value of $\langle\tau_\nu\rangle$ can be determined by the following estimate together with its spectral value:

$$\langle\tau_\nu\rangle = R\frac{\int\limits_0^\infty B_\nu(1/l'_\nu)d\varepsilon_\nu}{\int\limits_0^\infty B_\nu d\varepsilon_\nu}, \qquad \tau_\nu = \frac{R}{l'_\nu}, \qquad (12)$$

where R is an effective radius (to simplify the estimation of (12), we disregard the weak dependence of the thermodynamic parameters in the surrounding layers on the current radius r). Thus, the mean $\langle\tau_\nu\rangle$ in (12) is weighted in radiation intensity B_ν from (10). Let us write the expression for the mean free path l'_ν, which will be needed below (recall that it is uniquely related to (10) for B_ν by the Kirchhoff law):

$$l'_\nu = \frac{m_0}{\sigma_0}\frac{1+\Theta}{\Theta}\frac{1}{\rho}\left(\frac{m_e c^2}{\varepsilon_\nu}\right)^2 \frac{1+\exp(\varepsilon_\nu/(kT)-\varphi)}{\exp(\varepsilon_\nu/(kT)-\varphi)}, \qquad (13)$$

whence we find an explicit expression for the mean $\langle\tau_\nu\rangle$:

$$\langle\tau_\nu\rangle = R\frac{\sigma_0}{m_0}\frac{\Theta}{1+\Theta}\rho\left(\frac{kT}{m_e c^2}\right)^2\Psi(\varphi). \qquad (14)$$

The dimensionless function $\Psi(\varphi)$ is given by

$$\Psi(\varphi) = \left[7\int\limits_0^\infty \frac{x^6}{1+\exp(x-\varphi)}dx\right] \times \left[\int\limits_0^\infty \frac{x^5}{1+\exp(x-\varphi)}dx\right]^{-1}. \qquad (15)$$

This expression can be easily tabulated by numerical integration. Table 2 gives the values of $\Psi(\varphi)$. In conclusion, we can easily determine the dimensionless energy $y = \varepsilon_\nu/(kT)$ that with l'_ν from (13) separates the spectrum into two parts: $\tau_\nu < k$ if $x < y$ and $\tau_\nu > k$ if $x > y$. To this end, we equate the spectral depth τ_ν to the mean $\langle\tau_\nu\rangle$ from (14). Substituting Eq. (13) for l'_ν and Eq. (14) for $\langle\tau_\nu\rangle$ into the equality $\tau_\nu = \langle\tau_\nu\rangle$ yields a transcendental equation for the sought-for quantity y:

$$y^2 = \Psi(\varphi)[\exp(\varphi - y) + 1]. \qquad (16)$$

Table 2

φ	0	2.5	5.0	7.5	10.0	20
$x_{\max}(\varphi)$	5.033	5.303	6.327	8.008	10.00	18.97
$\Psi(\varphi)$	42.30	44.29	50.14	59.70	71.39	125.9
$y(\varphi)$	6.509	6.750	7.396	8.757	10.57	19.32

The numerical solution of Eq. (16) is also presented in Table 2. We see that y exceeds $x_{\max}$ only slightly for all values of φ, implying that the ν_e spectrum at $k \simeq 1$ is cut off immediately after its maximum. For $k < 1$, the cutoff boundary is shifted slightly to higher energies. Note that the true value of k can be determined in future hydrodynamic calculations, but its closeness to unity follows from the paper by Imshennik and Nadyozhin (1992).

Below, we apply these simple estimates to the thermodynamic parameters of the quasi-one-dimensional model for a rotating collapsar. Unfortunately, only some of the characteristic quantities, and only in the form of ρ_c and T_c, the central density and temperature, but not the parameter φ_c, the central chemical potential of the electrons from (10), are at our disposal.[6] To calculate the corresponding value of φ_c, we will do the following. We will use the electrical neutrality condition for the material, which is naturally satisfied in the hydrodynamic calculations of collapse. It is greatly simplified in the ultrarelativistic case for a Fermi–Dirac electron gas:

$$\frac{8\pi}{3}\left(\frac{kT}{ch}\right)^3(\varphi^3 + \pi^2\varphi) = \frac{\rho}{m_0(1+\Theta)}. \qquad (17)$$

We can determine φ of interest from this condition (in the form of a cubic equation) by using the given parameters ρ and T. We know these parameters at the stellar center, ρ_c and T_c, for the time $t = 2.9$ s at which the computation ends (Imshennik and Nadyozhin 1992; see the table there) and for the earlier time $t = 0.0$ s at which neutrino opacity sets in (Imshennik and Nadyozhin 1977). Two pairs of these parameters are presented in Table 3. However, as we see from condition (17), the parameter Θ should

[6] In both their publications of the calculations of the quasi-one-dimensional model, Imshennik and Nadyozhin (1977, 1992) focused on the rotation effects and the possibility of the transformation of collapse into an explosion and provided only minimum information concerning the integrated quantities of the light curve for neutrino radiation and its total energy.

Table 3

$\rho_c = 2.6 \times 10^{14}$ g cm^{-3}, $T_c = 6.2 \times 10^{10}$ K ($kT_c = 5.34$ MeV)				$\rho_c = 1.70 \times 10^{13}$ g cm^{-3}, $T_c = 5.89 \times 10^{10}$ K ($kT_c = 5.074$ MeV)	
Θ_c	12.6	100	1000	Θ_c	12.6
φ_c	25.7	13.0	5.63	φ_c	10.6

also be specified to solve the cubic equation. In Table 3, it is varied for the first pair of ρ_c and T_c over a wide range; the lowest value from the previous case will suffice for the second pair. In reality, the hydrodynamic calculations yield values of the material neutronization parameter Θ that do not exceed 100. Therefore, we conclude from the data of Table 3 that $\varphi_c \simeq 10$ may serve as a rough estimate. The corresponding energies, the mean energy and the energy at the maximum of the spectrum, in (11) are then found to be equal (see Table 2):

$$\langle \varepsilon_\nu \rangle \simeq \varepsilon_{\nu\max} \simeq kT_c\varphi_c \simeq (53.4\text{–}50.7)\ \text{MeV} \simeq 50\ \text{MeV}. \quad (18)$$

Estimate (18) should be improved further, but the unusual hardness of the neutrino spectrum compared to the standard model of collapse without rotation is beyond question. We emphasize that the steep fall attributable to the ν_e self-absorption considered above (see Table 2) takes place immediately after the maximum of the spectrum.

Next, let us first estimate the total number of ν_e required for the almost complete neutronization of the material of a rotating collapsar ($\Theta \le 100$) independent of the mean energy of the ν_e spectrum:

$$N_\nu = 1.8 M_\odot \frac{1}{m_0}\left(\frac{Z_{\rm Fe}}{A_{\rm Fe}}\right) = 1.0 \times 10^{57}.$$

On the other hand, according to the previous estimate of N_ν, the total energy $\mathcal{E}_\nu$ of these neutrinos with $\langle \varepsilon_\nu \rangle = 50$ MeV is

$$\mathcal{E}_\nu = N_\nu \langle \varepsilon_\nu \rangle = 8.0 \times 10^{52}\ \text{erg},$$

a value that is only slightly lower than $\mathcal{E}_{\nu\tilde\nu}$ from (9). To be more precise, about 10% of the energy remains for antineutrinos, $\tilde\nu_e$:

$$\mathcal{E}_{\tilde\nu} = \mathcal{E}_{\nu\tilde\nu} - \mathcal{E}_\nu = 0.9 \times 10^{52}\ \text{erg}.$$

Note that the necessary condition $\mathcal{E}_{\nu\tilde\nu} > \mathcal{E}_\nu$ is still satisfied, with nothing remaining for muon and taon neutrinos ($\mathcal{E}_{\nu\mu\tilde\nu\mu} = \mathcal{E}_{\nu\tau\tilde\nu\tau} = 0$). Meanwhile, the large deficit of $\tilde\nu_e$ was clear from our estimate of the electron chemical potential. According to Imshennik and Nadyozhin (1972), the latter is related to the neutrino chemical potential by a simple relation for the thermodynamic equilibrium conditions of the $\nu_e(\tilde\nu_e)$ and $e^-(e^+)$ degenerate gases:

$$\psi = \varphi - \ln\Theta.$$

Thus, for $\varphi = 10$, we obtain $\psi = 4.6\text{–}7.7$, depending on $\Theta = 100\text{–}10$. This implies that the number of $\tilde\nu_e$ is strongly suppressed, being proportional to $\exp(-\psi)$, compared to the number of ν_e.

It may seem that we use the parameters T_c and ρ_c noncritically, with the density of the material (on the order of nuclear density!) playing a major role in the achievement of high characteristic values of $\varphi_c \simeq 10$. However, the density ρ_c was carefully analyzed by Imshennik and Nadyozhin (1992), including its dependence on the initial values of the rotation parameter ω_0, using the derived analytical formula that relates this density to the relative centrifugal force near the center of the rotating collapsar. This analysis inspired confidence that initial rigid rotation with a sufficiently large total angular momentum, $J_0 \simeq 10^{50}$ erg s, does not prevent the emergence of a high density, $\rho_c \simeq 10^{14}$ g cm^{-3}, at the center of the rotating collapsar.

One would think that a significant admixture of iron nuclei etc. may be retained in the material under these conditions of relatively cold collapse (for a comparison of the central temperatures of the calculation under consideration and the standard model, see Imshennik and Nadyozhin (1992)). This admixture, of course, would immediately made condition (17), from which the chemical potential φ was estimated, more complex. The iron mass fraction $X_{\rm Fe}$ can be estimated using the paper by Imshennik and Nadyozhin (1965), where a universally accepted equation of state for the material was derived. Thus, using formula (29) from the cited paper for the specified parameters from Table 3, we find that $X_{\rm Fe}/X_n \simeq 1.3 \times 10^{-2}$; i.e., for $X_n \simeq 1$, we actually obtain a negligible iron mass fraction, $X_{\rm Fe} \simeq 10^{-2}$. Note that a correction on the order of unity to condition (17) then arises, but it also implies an increase in the sought-for parameter φ.

In conclusion, we may mention one subtle effect called the redistribution of specific angular momentum. In the quasi-one-dimensional model, this redistribution, of course, is constant, but it can change in principle during the fragmentation of a rotating collapsar. This would even be necessary at $\delta_0 \simeq 0.5$; i.e., when the collapsar is divided into equal pieces. What physical factors could provide this redistribution? First, we may point out the impact of three-dimensional tidal forces on any shear viscosity (for estimates of the neutrino viscosity, see Imshennik and Nadyozhin (1992)) and, finally, on the magnetic field. Of course, these factors should be included in

Table 4

Model	$\mathcal{E}_1$, erg	$\mathcal{E}_2$, erg	$\mathcal{E}_3$, erg	$\bar{\varepsilon}_{\tilde{\nu}_e}$, MeV	$\bar{\varepsilon}_{\nu_e}$, MeV	$\bar{\varepsilon}_{\nu_{\mu,\tau}}$, MeV	T, s
I	$(3-14)\times 10^{53}$	$(0.5-2.3)\times 10^{53}$	10^{52}	12.6	10.5	–	20
II				10	8	25	5

Note. $\mathcal{E}_1$ is the total burst energy transformed into neutrinos of all types; $\mathcal{E}_2$ is the total energy carried away by ν_i, where $\nu_i = \nu_e, \tilde{\nu}_e, \nu_\mu, \tilde{\nu}_\mu, \nu_\tau, \tilde{\nu}_\tau$; $\mathcal{E}_3$ is the total energy carried away by ν_e during the neutronization of the star in a time $\sim 3\times 10^{-2}$ s; $\bar{\varepsilon}_{\tilde{\nu}_e}$, $\bar{\varepsilon}_{\nu_e}$, $\bar{\varepsilon}_{\nu_{\mu,\tau}}$ are the spectrum-averaged energies of $\tilde{\nu}_e$, ν_e, and $\nu_{\mu,\tau}$, respectively; T is the duration of the neutrino burst.

future hydrodynamic models. At present, however, we may dispense with them if we are dealing with fragmentation into two pieces with a large difference in their masses ($\delta_0 \ll 1$). The initial rigid-rotation law then provides a high orbital angular momentum of a low-mass ejection almost without any redistribution of specific angular momentum. In our opinion, this circumstance is another argument for fragmentation with low values of the parameter δ_0 (see Table 1) suggested in Section 2.

It would probably make sense to discuss the main conclusion of this section concerning the hard spectrum of electron neutrinos in the absence of other types of neutrinos from the viewpoint of possible future studies. We repeat that this conclusion requires a new series of quasi-hydrodynamic calculations of collapse in which, first, the bulk nature of the neutrino radiation in the generalized URCA process with corrections for self-absorption (Ivanova *et al.* 1969a) would be postulated, and, second, the more general kinetic equation for neutronization to which the complete system of kinetic equations reduces in nuclear statistical equilibrium (Imshennik and Nadyozhin 1982) would be used in the calculations of the degree of neutronization of the material instead of the rough approximation of kinetic equilibrium for the β-processes. We may take the risk of asserting that such calculations will generally lead to a decrease in the central temperature of the rotating collapsar, but with a simultaneous increase in its central density. According to relation (18), such changes in thermodynamic parameters will entail approximate conservation of or, most likely, a moderate decrease in the characteristic energies of the ν_e spectrum, which will probably be in better agreement with the LSD observations of the neutrino signal from SN 1987A than the very hard spectrum with $\langle\varepsilon_\nu\rangle \simeq \varepsilon_{\nu\max} \simeq$ 50 MeV in (18) considered above.

3. A MODEL FOR A ROTATING COLLAPSAR AND A POSSIBLE INTERPRETATION OF THE EXPERIMENTAL RESULTS OBTAINED WITH NEUTRINO DETECTORS AT THE EXPLOSION TIME OF SN 1987A ON FEBRUARY 23, 1987

Let us consider how the various detectors operated during the explosion of SN 1987A could record the neutrino signals in terms of the model for a rotating collapsar that reduces to the following:

(1) Two neutrino bursts separated by a time $t^{\mathrm{grav}} \sim$ 5 h must exist.

(2) The neutrino flux during the first burst consists of electron neutrinos (ν_e) with a total energy $\mathcal{E}_{\nu_e} = \mathcal{E}_{\nu_e} = 8.9\times 10^{52}$ erg; the neutrino energy spectrum $\phi(\mathcal{E}_{\nu_e}, \varphi)$ (11) is hard and asymmetric with mean energies in the range 25–50 MeV (Fig. 1); the duration of the neutrino radiation is $t_{\mathrm{fin}} \sim$2.9–6 s.

(3) The second neutrino burst corresponds to the theory of standard collapse.

To compare the detector responses to these two neutrino bursts, we first give basic parameters of the neutrino fluxes obtained in the standard model and consider the neutrino detection methods.

The experimental searches for neutrino signals from collapsing stars began with the paper by Zeldovich and Guseinov (1965), who showed that gravitational collapse is accompanied by an intense short pulse of neutrino radiation. The search for collapse by detecting such a signal was first suggested by Domogatsky and Zatsepin (1965). The role of neutrinos in stellar collapses was considered by Arnett (1966), Ivanova *et al.* (1969b), Imshennik and Nadyozhin (1982), Nadyozhin and Otroshchenko (1982) [model I], Bowers and Wilson (1982), Wilson *et al.* (1986) [model II] and Bruenn (1987).

Parameters of the neutrino fluxes during the collapse of nonmagnetic, nonrotating, spherically symmetric stars were obtained by the above authors and are given in Table 4.

It follows from the theory of standard collapse that the total energy carried away by neutrinos of all types (ν_e, $\tilde{\nu}_e$, ν_μ, $\tilde{\nu}_\mu$, ν_τ, $\tilde{\nu}_\tau$) corresponds to $\sim$0.1 of the

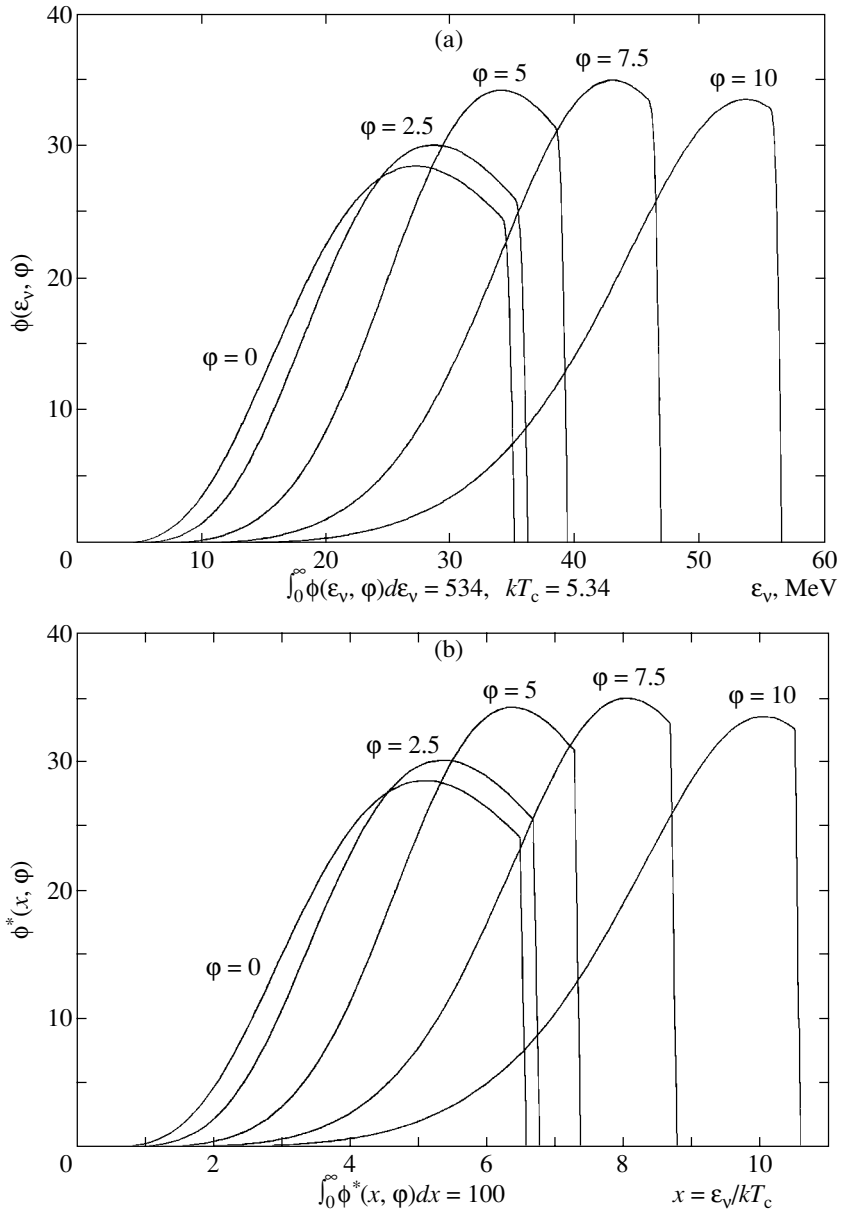

Fig. 1. Neutrino energy spectrum $\phi(\varepsilon_\nu, \varphi)$ (in arbitrary units) versus ε_ν in MeV (a) and $\phi^*(x, \varphi)$ (in arbitrary units) versus $x = \varepsilon_\nu/kT$ (b); $\varphi = \mu_e/kT$ is the dimensionless chemical potential of the electron gas.

stellar core mass and is equally divided between these six components.

Until now, Cherenkov (H_2O) and scintillation (C_nH_{2n}) detectors, which are capable of recording mainly $\tilde{\nu}_e$, have been used in searching for and detecting neutrino radiation. This choice is natural and is related to the large cross section for the interaction of $\tilde{\nu}_e$ with protons:

$$\tilde{\nu}_e + p \to e^+ + n, \qquad (19)$$

$$\sigma_{\tilde{\nu}_e p} \cong 9.3E_{e^+}^2 \times 10^{-44}\ \text{cm}^2, \quad E_{e^+} \gg 0.5\ \text{MeV}.$$

Moreover, reaction (19) has a distinctive signature, and, as was first shown by Chudakov *et al.* (1973), a proton may be used as a neutron catcher with the subsequent formation of deuterium (d) and the emission of a γ-ray photon with a time $\tau \approx 180$–200 μm:

$$n + p \to d + \gamma, \quad E_\gamma = 2.2\ \text{MeV}. \qquad (20)$$

Electron antineutrinos $\tilde{\nu}_e$ can be detected by searching for a pair of pulses separated by the capture time. The first and second pulses are attributable to the detection of e^+ and γ-ray photons, respectively.

The ν_e-scattering reactions have much smaller cross sections, but they allow the neutrino arrival direction to be determined in Cherenkov detectors:

$$\nu_e + e^- = \nu_e + e^-, \quad \sigma_{\nu_e e} = 9.4\varepsilon_{\nu_e} \times 10^{-45}\ \mathrm{cm}^2, \quad \varepsilon_{\nu_e} \geq 0.5\ \mathrm{MeV}, \tag{21a}$$

$$\tilde{\nu}_e + e^- = \tilde{\nu}_e + e^-, \quad \sigma_{\tilde{\nu}_e e} = 3.9\varepsilon_{\nu_e} \times 10^{-45}\ \mathrm{cm}^2, \quad \varepsilon_{\tilde{\nu}_e} \geq 0.5\ \mathrm{MeV}, \tag{21b}$$

$$\begin{cases} \nu_i + e^- = \nu_i + e^-, \quad \sigma_{\nu_i e} = 1.6\varepsilon_{\nu_i} \times 10^{-45}\ \mathrm{cm}^2, \quad \varepsilon_{\nu_i} \geq 0.5\ \mathrm{MeV}, \\ \tilde{\nu}_i + e^- = \tilde{\nu}_e + e^-, \quad \sigma_{\tilde{\nu}_i e} = 1.3\varepsilon_{\tilde{\nu}_i} \times 10^{-45}\ \mathrm{cm}^2, \quad \varepsilon_{\tilde{\nu}_i} \geq 0.5\ \mathrm{MeV}, \end{cases} \quad i = \mu, \tau. \tag{21c}$$

In scintillation detectors, neutrinos with energies above the threshold (E_{thr}) also interact with carbon:

$$\nu_i + {}^{12}\mathrm{C} \rightarrow {}^{12}\mathrm{C}^* + \nu_i, \quad E_{\mathrm{thr}} = 15.1\ \mathrm{MeV}, \quad i = e, \mu, \tau, \tag{22a}$$
$$\hookrightarrow {}^{12}\mathrm{C} + \gamma, \quad E_\gamma = 15.1\ \mathrm{MeV},$$

$$\nu_e + {}^{12}\mathrm{C} \rightarrow {}^{12}\mathrm{N} + e^-, \quad E_{\mathrm{thr}} = 17.34\ \mathrm{MeV}, \tag{22b}$$
$$\hookrightarrow {}^{12}\mathrm{C} + e^+ + \nu_e, \quad \tau = 15.9\ \mathrm{ms},$$

$$\tilde{\nu}_e + {}^{12}\mathrm{C} \rightarrow {}^{12}\mathrm{B} + e^+, \quad E_{\mathrm{thr}} = 14.4\ \mathrm{MeV}, \tag{22c}$$
$$\hookrightarrow {}^{12}\mathrm{C} + e^- + \tilde{\nu}_e, \quad \tau = 29.3\ \mathrm{ms},$$

where E_{thr} is the threshold energy of the reaction, and τ is the mean lifetime of the ^{12}B and ^{12}N isotopes.

The cross sections for reactions (22a)–(22c) were calculated by Donnely (1973), Fukugita *et al.* (1988), Mintz *et al.* (1989), Kolb *et al.* (1994), and Engel *et al.* (1996) and measured in the Los Alamos E225 (Athanassopoulos *et al.* 1990), LSND (Allen 1997), and KARMEN experiments (see, e.g., Mashuv 1998).

Reaction (22a), which yields a monochromatic line at 15.1 MeV, allows one to measure the fluxes of ν_μ and ν_τ with energies twice the ν_e energy (Ryazhskaya and Ryasny 1992) for standard collapse and the total neutrino flux with energy $\mathcal{E}_\nu > 15.1$ MeV for any model of collapse. Reactions (22b) and (22c) in the standard scenario yield a smaller number of events without oscillations. With oscillations, the number of events increases and becomes comparable to the effect produced by reaction (22a) at equal neutrinosphere temperatures for neutrinos and antineutrinos, $T_{\tilde{\nu}_e}$ (Aglietta *et al.* 2002).

The cross section for the interaction of neutrinos with ^{16}O nuclei in Cherenkov detectors $\sigma(\nu^{16}\mathrm{O})$ for $\varepsilon_\nu \leq 25$ MeV is low compared to the cross section $\sigma(\nu^{12}\mathrm{C})$ (Bugaev *et al.* 1979).

In Cherenkov and scintillation detectors, the emission from e^+, e^-, and photons is recorded by a photomultiplier. A neutrino burst is identified by the appearance of a series of pulses in the range of amplitudes from the detector energy threshold (E_{thr}) to 50 MeV in a time from several seconds to several tens of seconds, depending on the model of collapse.

Four detectors were operating during the explosion of SN 1987A: two scintillation (in USSR and Italy) and two Cherenkov (in USA and Japan). Parameters of the detectors are given in Table 5.

The effects from reactions (19) and (21a), (21c) expected in the model of standard stellar collapse in the Large Magellanic Cloud are shown in Table 6. We see that reaction (19) gives the largest contribution. It should be noted that all of the detectors except the LSD could record only e^+; i.e., there was no signature of the event by which reaction (19) could be unambiguously identified.

Features of the Construction of Scintillation Detectors

Since we explore the possibility of detecting electron neutrinos by the nuclei of the detector materials, we will briefly consider the features of the construction of scintillation detectors, because some of them have not been reported previously.

The Baksan Underground Scintillation Telescope (BUST) (Alexeyev *et al.* 1979) is a cube with sides 14 m square. There are two horizontal planes inside the cube. 400 scintillation counters $0.7 \times 0.7 \times 0.3\ \mathrm{m}^3$ in size are located on each of the cube's planes (six outer and two inner). Each counter is watched by one photomultiplier. The spacing between the horizontal planes separated by an absorber is about 3.6 m; the thickness of the absorber is $\sim$170 g cm^{-2}, $\sim$20 g cm^{-2} of which is made up of iron. The scintillator is made of white spirit (Voevodskii *et al.* 1970); the molecular composition is $\mathrm{C}_n\mathrm{H}_{2n}$, $\overline{n} = 10$. The detection threshold of energy release in the module is $\sim$10 MeV. The working volume of the detector consists of counters located on three horizontal planes: the two inner and one lower; the scintillator mass is 132 t. In analyzing the results of February 23, 1987, the authors also used data from some of the

Table 5

Detector	Depth of water equivalent, m	Working mass, t	Material	Detection threshold, MeV	Detection efficiency		Background pulse frequency m, s^{-1}**
					e^+ spectrum of reaction $\tilde{\nu}_e p \to e^+ n$ (19)	e^- spectrum of reaction $\nu_i e^- \to \nu_i e^-$ (21a, 21c)*	
BUST, USSR	850	130(200)	C_nH_{2n}	10	0.6	0.15 (0.54)	0.013 (0.033)
		160	Fe				
LSD, USSR–Italy	5200	90	C_nH_{2n}	5–7	0.9	0.4 (0.7)	0.01
		200	Fe				
KII, Japan–USA	2700	2140	H_2O	7–14	0.7	0.17 (0.54)	0.022
IMB, USA	1570	5000	H_2O	20–50	0.1	0.02 (0.18)	3.5×10^{-6}

* The detection efficiencies of the electron spectrum produced in the reactions $\nu_{\mu,\tau}(\tilde{\nu}_{\mu,\tau}) + e^- \to \nu_{\mu,\tau}(\tilde{\nu}_{\mu,\tau}) + e^-$ (21c) are given in parentheses.
** The background is given in the energy range E_{thr}–50 MeV; for the Cherenkov detectors, the background is given for the recording of internal events.

outer detectors, which increased working mass to 200 t.

The LSD detector (Badino *et al.* 1984; Dadykin 1979) operated under Mont Blanc at a depth of 5200 m.w.e. consists of nine modules located on three floors with an area of 6.4×7.4 m^2. The LSD height was 4.5 m. The module is an iron container with an area of 6.4×2.14 m^2, a height of 1.5 m, and a wall thickness of 2 cm, with eight cells separated by 2-cm-thick iron sheets in which $1 \times 1.5 \times 1$ m^3 scintillation counters are located. In fact, LSD is an iron scintillation detector. To reduce the influence of radioactivity from the surrounding rocks, the detector is shielded by steel plates. The total iron mass is about 200 t. The mass of the scintillator is made up of white spirit (Voevodskiĭ *et al.* 1970) is 90 t. Each counter is watched by three photomultipliers (FEU-49B). The high sensitivity and low background of the detector allow both e^+ and n particles in reaction (19) to be detected.

Table 6

Detector	K_{e^+} (19)	K_{e^-} (21a) + (21c)	K_{e^-} (21c)
LSD	1.5	0.043	0.024
BUST	2	0.052	0.036
KII	17	0.53	0.36
IMB	6	0.4	0.35

The parameters of the Kamiokande II and IMB detectors are well known (see Hirata *et al.* 1987; Bionta *et al.* 1987).

Experimental Data

To understand how the recorded events during the collapse of SN 1987A on February 23, 1987, fit into the scenario of a rotating collapsar, we present them in the chronological sequence of observation:

(1) February 23, 1987, 2:52:36.79 UT: LSD recorded a cluster of five pulses in real time; the estimated probability of this being mimicked by background radiation is low (less than once in three years). No such event had been observed in two years of LSD operation (1985–1987) (Aglietta *et al.* 1987; Dadykin *et al.* 1987, 1988). At present, we may add that the detector recorded no similar signal over its entire operation time until 1999. However, it is worth noting that the background conditions in 1988 were improved by an additional shield.

(2) February 23, 1987: information about the event measured by the LSD was transmitted to the group

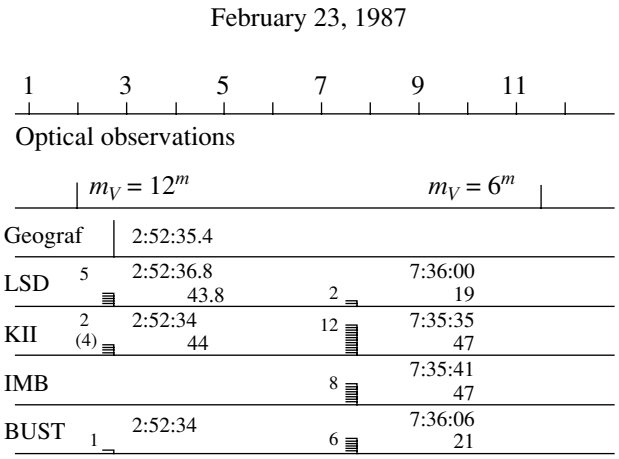

Fig. 2. Time sequence of the events recorded by various detectors on February 23, 1987.

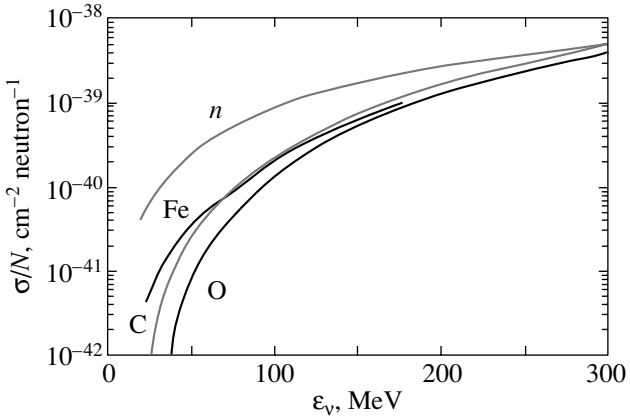

Fig. 3. Comparison of the reduced total cross sections with the neutrino cross section on a free neutron for the reaction $\nu_e + (A, Z) \rightarrow e^- + (A, Z+1)^*$ (Bugaev *et al.* 1979).

working with the GEOGRAV gravitational antenna (Rome).

(3) February 23, 1987, 10 : 40 UT: the first optical observation is made of SN 1987A in the Large Magellanic Cloud, ~50 kpc from Earth, and is reported only the next day (IAU Circ. 1987).

It is worth emphasizing that the LSD event was observed and reported to Amaldi's group before information about the supernovae explosion was obtained. The data from the other detectors were analyzed later. Figure 2 shows the time sequence of the events recorded by various detectors on February 23, 1987. We see that there are two groups of events concentrated near the LSD time (2:52:36) and the IMB and KII time (7:35:35). All the events have been extensively discussed for the last several years.

Interestingly, strong correlations between the pulses from gravitational antennas and underground detectors were observed from 2:00 UT until 8:00 UT (Amaldi *et al.* 1987; Pizzella 1989; Aglietta *et al.* 1989, 1991), but the analysis of this fact is not the subject of this paper. Here, we wish to analyze the event recorded under Mont Blanc in terms of the model of a rotating collapsar. The events measured by underground detectors near 7:36 UT are interpreted by most physicists as the detection of antineutrino radiation, while attempts to explain the LSD data at 2:52 UT in a similar way run into difficulties.

Table 7 presents the parameters of the LSD pulses. The third column gives energies of the measured pulses corresponding to the two muon calibrations made before and after February 23, 1987 (each in a time interval of three months) and separated by two months. We see that the energy is determined with an accuracy of 20–25%.

Difficulties in Interpreting the Effect Measured by LSD at 2:52 UT in the Case of Antineutrino Detection

As was shown by Dadykin *et al.* (1989), a total neutrino radiation energy of $\mathcal{E}_\nu = 6\mathcal{E}_{\tilde{\nu}_e} \approx 1.2 \times 10^{55}$ erg is required to explain the LSD effect in terms of the detection of antineutrino radiation if the conflicts with the results of other underground detectors have been eliminated. This energy is more than an order of magnitude higher than the binding energy of a neutron star with a baryon mass of about $2M_\odot$.

In addition, only one of the five measured pulses in the cluster was accompanied by a neutron-like pulse that was offset from the trigger signal in the detector by 278 μm and that had an energy of 1.4 MeV. Assuming the detection of five antineutrinos, one would expect the detection of five positrons accompanied, on

Table 7

Event no.	Time, UT ± 2 ms	Energy, MeV
1	2:52:36.79	7–6.2
2	2:52:40.65	8–5.8
3	2:52:41.01	11–7.8
4	2:52:42.70	7–7.0
5	2:52:43.80	9–6.8
1	7:36:00.54	8
2	7:36:18.88	9

Table 8

F*	$\sigma = 1.27 \times 10^{-40}$ cm^2	$E^{***}_{K,e^-} = 31.84$ MeV, $E_\gamma = 1.82$ MeV, $n\gamma$: $\sum_n E_\gamma = 1.72$ MeV
GT**	$\sigma = 6.41 \times 10^{-41}$ cm^2	$E_{K,e^-} = 30.84$ MeV, $E_\gamma = 1$ MeV, $E_\gamma = 1.82$ MeV, $n\gamma$: $\sum_n E_\gamma = 1.72$ MeV
GT	$\sigma = 1.05 \times 10^{-40}$ cm^2	$E_{K,e^-} = 27.84$ MeV, $E_\gamma = 4$ MeV, $E_\gamma = 1.82$ МэВ, $n\gamma$: $\sum_n E_\gamma = 1.72$ MeV
GT	$\sigma = 1.27 \times 10^{-40}$ cm^2	$E_{K,e^-} = 24.84$ MeV, $E_\gamma = 7$ MeV, $E_\gamma = 1.82$ MeV, $n\gamma$: $\sum_n E_\gamma = 1.72$ MeV

* The Fermi level.
** The Gamow–Taylor resonance.
*** The electron kinetic energy.

average, by two neutrons. In this case, the probability of measuring one pulse attributable to the neutron capture by hydrogen and offset from the positron signal by 1.5τ, where τ is the neutron lifetime, is less than 5%.

The above arguments make the explanation of the LSD effect in terms of antineutrino detection implausible.

A Possible Explanation of the LSD Effect in the Model of a Rotating Collapsar

As was mentioned above, the collapsar emits electron neutrinos (ν_e) with a total energy of $\mathcal{E}\nu_e{}^* \sim 8.9 \times 10^{52}$ erg, the spectrum shown in Fig. 1, and mean energies of 30–40 MeV for ~2.9–6 s. These neutrinos can be recorded by the detector nuclei via the reactions

$$\begin{cases} \nu_e + (A,Z) \to e^- + (A,Z+1) \\ \nu_e + (A,Z) \to e^- + (A,Z+1)^*, \end{cases} \quad (23a)$$

$$\nu_e + (A,Z) \to \nu'_e + (A,Z)^*. \quad (23b)$$

The detectors operated on February 23, 1987, contained either oxygen, mainly ^{16}O (KII and IMB), or carbon, mainly ^{12}C, and iron ^{56}Fe (LSD, BUST). It follows from the paper by Bugaev *et al.* (1979) that the reduced cross section $\sigma_{\nu_e n} = \sigma_{\nu_e A}/N$ for iron at $\varepsilon_\nu \le 40$ MeV exceeds $\sigma_{\nu_e n}$ for oxygen by more than a factor of 20 ($\sigma_{\nu_e n}(^{56}\mathrm{Fe}) > 20\sigma_{\nu_e n}(^{16}\mathrm{O})$) (see Fig. 3). Thus, for these energies, the number of $\nu_e A$ interactions in the LSD (200 t of Fe) will be larger than that in the KII (1900 t ^{16}O).

To answer the question of how the ν_eFe interactions are detected in the LSD, we turn to Table 8. As an illustration, this table presents the partial cross sections calculated for the following reaction for $\varepsilon_\nu = 40$ MeV (Gaponov *et al.* 2003):

$$\nu_e + {}^{56}_{26}\mathrm{Fe} \to {}^{56}_{27}\mathrm{Co} * + e^-. \quad (24)$$

The ground level of $^{56}_{26}$Fe–0^+, the ground level of $^{56}_{27}$Co–4^+. The difference between the binding energies is $E[^{56}_{27}\mathrm{Co}] - E[^{56}_{26}\mathrm{Fe}] = 4.056$ MeV.

The threshold energy for reaction (24) is 8.16 MeV. An electron can be produced with an energy from ~31.8 to 24.8 MeV, and its appearance is always accompanied by cascade γ-ray photons with a total energy of from 3.54 to 10.54 MeV. Recall that the critical energy (ε) in iron (the electron energy at which the ionization losses are equal to the radiative losses) is 21 MeV. Thus, an electron with an energy $E \ge \varepsilon$ in iron on a thickness of $d \ge 1$ t units (t is the radiation unit of length, 1 t units = 13.9 g cm^{-2} (1.78 cm)) produces a small electromagnetic cascade. Calculations indicate that, during the interaction of electron neutrinos with $\varepsilon_{\nu_e} = 40$ MeV in a 2–3-cm-thick iron layer located between two scintillation layers, many more γ-ray photons than electrons fall into the scintillator (Dedenko and Fedunin 2003). The mean energies of these particles are ~7–9 MeV. The detection efficiency of ν_eFe interactions (η) depends on the design of the detector and on the energy threshold: $\eta \sim 75\%$ for the inner part of the LSD (~90 t of Fe), $\eta \sim 35\%$ for its outer part (~110 t of Fe), and $\eta \le 15\%$ for the BUST. We see that in the scenario under consideration, the mean energies recorded by a scintillation detector with an iron interlayer are close to the energies measured by the LSD on February 23, 1987. The estimated effect of the detection of neutrino radiation in the first phase of the collapse of a rotating star by different detectors is presented in Table 9. We used the cross sections of reactions (23a) and (23b) for ^{56}Fe and ^{12}C and the cross sections of

Table 9

Detector	Detection threshold	Estimated number of $\nu_e A$ interactions				Estimated effect	Experiment
		N_1	N_2	N_3	N_4	$N_2\eta$	
LSD	5–7	3.2	5.7	3.5	4.9	3.2	5
KII	7–14	0.9	3.1	1.2	2.5	2.7	2*
BUST	10	2.8	5.2			~1	1**

* See De Rujula (1987a, 1987b).
** Alexeyev *et al.* (1987).

reaction (23a) for ^{16}O (Bugaev *et al.* 1978; Gaponov *et al.* 2003; Fukugita *et al.* 1988; Haxton 1987). The estimates were obtained for monochromatic neutrinos with $\varepsilon_{\nu_e} = 30$ MeV (N_1), $\varepsilon_{\nu_e} = 40$ MeV (N_2) and for the electron neutrino spectrum (Fig. 1) at $\varphi = 5$ (N_3) and $\varphi = 7.5$ (N_4).

We see that these estimates are consistent with the experimental data. If almost only electron neutrinos with a mean energy of ~35–40 MeV were emitted in the first collapse, then the experimental data correspond to the scenario for the rotational mechanism of a supernova explosion.

To be able to detect neutrino radiation from future stellar collapses (if the above scenario is realized), it is necessary to have detectors capable of recording not only $\tilde{\nu}_e$, but also ν_e with high efficiency. Two detectors of this type exist: the LVD (1.1 kt of scintillator, 1.1 kt of Fe) and the SNO (1 kt of D_2O). The Super K and Kamland detectors will be able to clearly see ν_e with $\varepsilon_{\nu_e} \geq 40$ MeV.

CONCLUSIONS

We have put forward and partly justified our interpretation of the signal recorded by the underground LSD detector at 2:52 UT on February 23, 1987, as the first detection of a neutrino burst from the collapse of SN 1987A. We proceeded from the previously suggested rotational mechanism of the explosions of collapsing supernovae and the idea of taking into account the interaction of electron neutrinos with the nuclei of iron whose presence in the LSD's construction enormously increases the sensitivity to the first phase of collapse. A careful study of the corresponding nuclear reactions for the deneutronization and excitation of iron nuclides when electron neutrinos of sufficiently high energies, mainly from 20 to 50 MeV, interact with them led us to this conclusion. From the viewpoint of the rotational mechanism, it may be asserted that a rotating iron stellar core collapses in two phases separated by a relatively long time interval; the first phase of collapse was most likely detected by the LSD. According to this mechanism, the first phase is peculiar in that a rotating collapsar is formed in it with the emission of a very hard electron neutrino spectrum attributable to the reaction $e^- + p \rightarrow n + \nu_e$ with an energy at the maximum of the spectrum up to 50 MeV in the almost complete absence of electron antineutrinos and other types of neutrinos (muon and taon). A more detailed study of this spectrum based on numerical calculations (quasi-one-dimensional model) not only allows us to confirm the above properties but also to justify why other neutrino detectors have not recorded the first neutrino signal. We additionally took into account other possible nuclear reactions of electron neutrinos with oxygen nuclides in the KII and IMB Cherenkov detectors.

In addition, according to the same mechanism, we can reliably interpret the time interval between the first and second neutrino signals. This time interval is mainly attributable to the well-known gravitational radiation generated during the fragmentation of the rotating collapsar into a binary of NS with greatly differing masses. The evolution of such a binary was theoretically analyzed in detail in Section 1. At this time, gravitational radiation carried away a significant fraction of the initial angular momentum of the iron core, which was undoubtedly conserved during the first phase of collapse. It may be asserted that allowance for the rotation effects of the collapsing iron core alone allows us to theoretically interpret the two successive neutrino signals from SN 1987A. Until now, the presence of a neutrino signal on the LSD detector has been ignored in the theory of this famous event, which is besides enigmatically correlated with the signals from two gravitational antennas: in Italy and the United States. We have not yet been able to reasonably interpret how the mentioned antennas responded to gravitational radiation during the fragmentation of the rotating collapsar into a NS binary, which was theoretically estimated to be very modest.

It remains to be added that the second neutrino signal recorded by the KII, IMB, and BUST was associated with the detection of electron antineutrinos predicted in the universally accepted standard model

for the secondary collapse of the high-mass NS in the putative binary once it had accreted the bulk of the mass from the low-mass NS and gotten rid of the remnants of its angular momentum. Theoretically, this signal corresponds to the standard hydrodynamic one-dimensional model of collapse without rotation with the formation of a neutrinosphere and with an equal energy distribution between all types of neutrinos. Electron neutrinos could not be recorded on the LSD detector at this time, because these neutrinos must have much lower mean energies, about 15 MeV. The cross section for their interaction with iron nuclides is too small.

Of crucial importance is the fact that a low-mass NS simultaneously ceases to exist once it has reached a critical mass of about $0.1M_\odot$ and has been destroyed by an explosion relatively far (several hundred km) from the high-mass NS. This transformation into an ejection of iron with the release of recombination energy ($\sim$5 MeV/nucleon) and in the presence of high kinetic energy ($\sim 0.3 \times 10^{51}$ erg) leads to an explosion with quite a sufficient total energy of about 10^{51} erg, and with a directed symmetry (the direction of the initial orbital motion of the ejection); i.e., it solves the fundamental problem of the transformation of iron-core collapse into a supernova explosion with an observed total energy of about 10^{51} erg.

ACKNOWLEDGMENTS

Undoubtedly, we would be unable to reliably interpret the five famous events recorded by the LSD without the great progress in calculating the cross sections for the interaction of neutrinos with iron nuclides, or to reliably justify the high detection efficiency of neutrino interactions in the LSD without calculating the development of low-energy electromagnetic cascades. We wish to thank Yu.V. Gaponov, S.V. Semonov, L.G. Dedenko, and E.Yu. Fedunin, who made these calculations available to us. The strong stimulating influence of G.T. Zatsepin, whom we wish to thank, on the development of the theory of collapse and supernova explosion and the experimental methods for detecting neutrino radiation from these natural phenomena, including SN 1987A, is hard to overestimate. We wish to thank L.B. Okun for his interest in the problem, D.K. Nadyozhin for his helpful critical discussions, D.V. Popov for his help in calculating the evolution of a NS binary, and V.A. Matveev for his invariable interest in this problem. We are grateful to all members of the LSD collaboration, especially to C. Castagnoli, G. Cini-Castagnoli, V.L. Dadykin, V.G. Ryasny, O. Saavedra, and W. Fulgione for their fruitful discussions; to V.B. Braginskii, G. Pizzella, and E. Coccia for their discussion of the possibility of recording gravitational radiation during SN 1987A, and to N.Yu. Agafonova, N.A. Vulikh, and V.V. Kuznetsov for their help in preparing the paper for publication. This work was supported by the Russian Foundation for Basic Research (project nos. 03-02-16414a and 03-02-16436) and grants from scientific schools (projects NSh-1787.2003.2 and NSh-1782.2003.2).

REFERENCES

1. M. Aglietta *et al.*, Nuovo Cimento C **12**, 75 (1989).
2. M. Aglietta *et al.*, Nuovo Cimento C **14**, 171 (1991a).
3. M. Aglietta *et al.*, Nuovo Cimento B **106**, 1257 (1991b).
4. M. Aglietta *et al.*, Europhys. Lett. **3**, 1321 (1987).
5. M. Aglietta *et al.*, Nucl. Phys. B (Proc. Suppl.) **110**, 410 (2002).
6. A. G. Aksenov, S. I. Blinnikov, and V. S. Imshennik, Astron. Zh. **72**, 717 (1995) [Astron. Rep. **39**, 638 (1995)].
7. A. G. Aksenov and V. S. Imshennik, Pis'ma Astron. Zh. **20**, 32 (1994) [Astron. Lett. **20**, 24 (1994)].
8. A. G. Aksenov, Pis'ma Astron. Zh. **25**, 163 (1999) [Astron. Lett. **25**, 127 (1999)].
9. A. G. Aksenov, Pis'ma Astron. Zh. **22**, 706 (1996) [Astron. Lett. **22**, 634 (1996)].
10. E. N. Alexeev *et al.*, Pis'ma Zh. Éksp. Teor. Fiz. **45**, 461 (1987) [JETP Lett. **45**, 589 (1987)].
11. E. N. Alexeev *et al., Proc. of the 16th ICRC.—Kyoto, Japan,* **10**, 282 (1979).
12. R. C. Allen, Phys. Rev. Lett. **64**, 1871 (1990).
13. E. Amaldi *et al.*, Europhys. Lett. **3**, 1325 (1987).
14. W. D. Arnett, Can. J. Phys. **44**, 2553 (1966).
15. C. Athanassopoulos *et al.*, Phys. Rev. C **55**, 2078 (1997).
16. J. Badino *et al.*, Nuovo Cimento **7**, 573 (1984).
17. R. M. Bionta *et al.*, Phys. Rev. Lett. **58**, 1494 (1987).
18. S. I. Blinnikov, V. S. Imshennik, D. K. Nadyozhin, *et al.,* Astron. Zh. **67**, 1181 (1990) [Sov. Astron. **34**, 595 (1990)].
19. S. I. Blinnikov, V. S. Imshennik, and D. K. Nadyozhin, Astrophys. Space Sci. **150**, 273 (1988).
20. R. Bowers and J. R. Wilson, Astrophys. J. **263**, 366 (1982).
21. S. Bruenn, Phys. Rev. Lett. **59**, 938 (1987).
22. E. V. Bugaev, G. S. Bisnovatyi-Kogan, *et al.*, Nucl. Phys. A **324**, 350 (1979).
23. A. E. Chudakov, O. G. Ryajskaya, and G. T. Zatsepin, *Proc. of 13th ICCR, Denver, 1973*, Vol. 3, p. 2007.
24. V. L. Dadykin, G. T. Zatsepin, and O. G. Ryazhskaya, Usp. Fiz. Nauk **158**, 140 (1989) [Sov. Phys. Usp. **32**, 459 (1989)].
25. V. L. Dadykin *et al.*, *Proc. of the 16th ICRC, Kyoto, Japan* **10**, 285 (1979).
26. V. L. Dadykin *et al.,* Pis'ma Astron. Zh. **14**, 107 (1988) [Sov. Astron. Lett. **14**, 44 (1988)].
27. V. L. Dadykin *et al.,* Pis'ma Zh. Éksp. Teor. Fiz. **45**, 464 (1987) [JETP Lett. **45**, 593 (1987)].
28. L. G. Dedenko and E. Yu. Fedunin, Private Communication (2003).

29. G. V. Domogatsky and G. T. Zatsepin, *Proc. of 9th ICCR, London, 1965,* Vol. 2, p. 1030.
30. Dong Lai and S. L. Shapiro, Astrophys. J. **442**, 259 (1995).
31. T. W. Donnely, Phys. Lett. B **43B**, 93 (1979).
32. J. Engel *et al.*, Phys. Rev. C **54**, 2740 (1996).
33. M. Fukugita, Y. Kohyama, and K. Kubodera, Phys. Lett. B **212**, 139 (1988).
34. Yu. V. Gaponov, O. G. Ryazhskaya, and S. V. Semenov, Yad. Fiz. (2003, in press).
35. W. C. Haxton, Phys. Rev. D **36**, 2283 (1987).
36. K. Hirata *et al.*, Phys. Rev. Lett. **58**, 1490 (1987).
37. J. L. Houser, J. M. Centerella, and S. C. Smith, Phys. Rev. Lett. **72**, 1314 (1994).
38. IAU Circ. No. 4316 (1987).
39. V. S. Imshennik, Pis'ma Astron. Zh. **18**, 489 (1992) [Sov. Astron. Lett. **18**, 194 (1992)].
40. V. S. Imshennik, Space Sci. Rev. **74**, 325 (1995).
41. V. S. Imshennik, *Eruptive Stars,* Ed. by A. G. Masevich (MID RF, Moscow, 1996), p. 7 [in Russian].
42. V. S. Imshennik and S.I. Blinnikov, *IAU Coll. 145: Supernovae and Supernova Remnants,* Ed. by R. McCray and Zhenru Wang (1996), p. 119.
43. V. S. Imshennik and D. K. Nadyozhin, Astron. Zh. **42**, 1154 (1965).
44. V. S. Imshennik and D. K. Nadyozhin, Zh. Éksp. Teor. Fiz. **63**, 1548 (1972).
45. V. S. Imshennik and D. K. Nadyozhin, Pis'ma Astron. Zh. **3**, 353 (1977) [Sov. Astron. Lett. **3**, 188 (1977)].
46. V. S. Imshennik and D. K. Nadyozhin, Usp. Fiz. Nauk **156**, 576 (1988).
47. V. S. Imshennik and D. V. Popov, Pis'ma Astron. Zh. **20**, 620 (1994) [Astron. Lett. **20**, 529 (1994)].
48. V. S. Imshennik and D. K. Nadyozhin, Pis'ma Astron. Zh. **18**, 195 (1992) [Sov. Astron. Lett.**18**, 79 (1992)].
49. V. S. Imshennik and D. K. Nadyozhin, Itogi Nauki Tekh., Ser. Astron. **21**, 63 (1982).
50. V. S. Imshennik and D. V. Popov, Preprint MPA 940 (1996).
51. V. S. Imshennik and D. V. Popov, Pis'ma Astron. Zh. **24**, 251 (1998) [Astron. Lett. **24**, 206 (1998)].
52. V. S. Imshennik and D. V. Popov, Pis'ma Astron. Zh. **28**, 529 (2002) [Astron. Lett. **28**, 465 (2002)].
53. L. N. Ivanova, V. S. Imshennik, and D. K. Nadyozhin, Nauchn. Inform. Astron. Soveta Akad. Nauk SSSR **13**, 3 (1969a).
54. L. N. Ivanova *et al., Proc. Int. Seminar on Physics of Neitrino and Neitrino Astrophysics* (FIAN SSSR, Moscow, 1969), Vol. 2, p. 180 [in Russian].
55. E. Kolb *et al.*, Phys. Rev. C **49**, 1122 (1994).
56. L. D. Landau and E. M. Lifshits, *Field Theory* (Nauka, Moscow, 1973) [in Russian].
57. R. Mashuv, Prog. Part. Nucl. Phys. **40**, 183 (1998).
58. S. L. Mintz *et al.*, Phys. Rev. C **40**, 2458 (1989).
59. D. K. Nadyozhin and N. V. Otroshchenko, Astron. Zh. **263**, 366 (1982).
60. D. K. Nadyozhin, Astrophys. Space Sci. **49**, 399 (1977a).
61. D. K. Nadyozhin, Astrophys. Space Sci. **51**, 283 (1977б).
62. D. K. Nadyozhin, Astrophys. Space Space Sci. **53**, 131 (1978).
63. B. Paczynski, Annu. Rev. Astron. Astrophys. **9**, 183 (1971).
64. B. Paczynski and R. Sienkiewicz, Acta Astron. **22**, 73 (1972).
65. R. C. Peters, Phys. Rev. **136**, B1224 (1964).
66. P. C. Peters and J. Mathews, Phys. Rev. **131**, 435 (1963).
67. G. Pizzella, Nuovo Cimento B **102**, 471 (1989).
68. A. De Rujula, *Proc. EPS Conf., Uppsala, 1987.*
69. A. De Rujula, Phys. Lett. B **193**, 514 (1987).
70. O. G. Ryazhskaya and V. G. Ryasnyĭ, Pis'ma Zh. Éksp. Teor. Fiz. **56**, 433 (1992) [JETP Lett. **56**, 417 (1992)].
71. O. G. Ryazhskaya and V. G. Ryasny, Nuovo Cimento A **106**, 257 (1993).
72. J. L. Tassoul, *Theory of Rotating Stars* (Princeton Univ. Press, 1978).
73. A. V. Voevodskiĭ, V. L. Dadykin, and O. G. Ryazhskaya, Prib. Tekh. Éksp. **1**, 85 (1970).
74. P. Yaranowski and A. Krolak, Astrophys. J. **394**, 586 (1992).
75. J. R. Wilson *et al.*, Ann. N.Y. Acad. Sci. **470**, 267 (1986).
76. Ya. B. Zel'dovich and O. Kh. Guseinov, Dokl. Akad. Nauk SSSR **162**, 791 (1965).

Translated by V. Astakhov

Astronomy Letters, Vol. 30, No. 1, 2004, pp. 32–40. Translated from Pis'ma v Astronomicheskiĭ Zhurnal, Vol. 30, No. 1, 2004, pp. 37–46.

Observations of Supernovae in the Period 1997–1999

D. Yu. Tsvetkov* **and N. N. Pavlyuk****

Sternberg Astronomical Institute, Universitetskii pr. 13, Moscow, 119992 Russia

Received June 5, 2003

Abstract—We present our photometric observations of the 15 supernovae (SN) discovered in the period 1997–1999; of these, six are type Ia SN, two are peculiar type Ia SN, three are type Ib/c SN, and four are type II SN. For 11 SN, we constructed reliable light curves and determined their maximum brightnesses and absolute magnitudes at maximum. Based on the shapes of the light curves, we improved the classification for three type II SN. We show that the two peculiar type Ia SN (similar to SN 1991T) studied, SN 1998es and SN 1999aa, have enhanced and normal luminosities at maximum, respectively.

Key words: *supernovae and supernova remnants*.

INTRODUCTION

At present, studies of supernovae (SN) are attracting increasing attention. Type Ia supernovae are widely used as "standard candles" to construct the distance scale and for cosmological studies; type II supernovae, notably SN II-P (with a plateau), can also be used to determine the distances independently of the classical multistep "ladder" of calibration objects. The particular attention being given to type Ib/c supernovae stems from their possible association with gamma-ray bursts.

Light curves are the main material for all these studies. Despite the significant increase in the number of photometric observations in various spectral ranges in recent years, many bright supernovae have not yet been studied adequately. Therefore, it is of relevant interest to observe as many supernovae as possible.

Systematic photometric observations of supernovae have been carried out at the Sternberg Astronomical Institute (SAI) for many years. Using CCD detectors since 1998 has allowed the number of observed supernovae to be significantly increased. The following SN were observed from July 1997 through May 1999: 1997cx, 1997dn, 1997do, 1997dq, 1997ef, 1997eg, 1997ei, 1998D, 1998aq, 1998dh, 1998ef, 1998es, 1999D, 1999X, and 1999aa. Main data on the supernovae and their parent galaxies are given in Table 1. In this table, $\Delta\alpha$ and $\Delta\delta$ are the distances from the galactic center to the SN, and m_{SN} is the magnitude estimate during its discovery; the data on the galaxies—the type, the heliocentric radial velocity, and the extinction in the Galaxy—were taken from the NED database (`http://nedwww.ipac.caltech.edu`).

OBSERVATIONS AND DATA REDUCTION

Photographic B-band observations of the supernovae were carried out with a 50-cm meniscus telescope at the Crimean Station of the SAI. We used HT-1AC plates with a BS-8 filter. The plates were measured on a microphotometer with a constant aperture; the galactic background was subtracted by averaging the measurements at eight points around the SN. The magnitudes of the comparison stars were obtained from CCD observations; they are given in Table 2.[1] The results of our photographic observations are presented in Table 3. The errors of the magnitudes are about $0^m.1$ for SN with a magnitude of $14–15^m$, about $0^m.2$ for SN with $16–17^m$, and up to $0^m.4$ for SN fainter than 18^m.

CCD observations of the supernovae were carried out with 125-cm and 60-cm telescopes at the Crimean Station of the SAI and with a 70-cm SAI reflector in Moscow using SBIG ST-7 and ST-6 CCD cameras. The sets of filters used accurately reproduced the Johnson standard B and V bands, but the instrumental r and i bands differed significantly from the Cousins standard R_c and I_c

*E-mail: `tsvetkov@sai.msu.su`
**E-mail: `pavlyuk@sai.msu.su`

[1] Tables 2–5 are published in electronic form only and are accessible via ftp cdsarc.u-strasbg.fr/pub/cats/J (130.79.128.5) or http://cdsweb.u-strasbg.fr/pub/cats/J.

1063-7737/04/3001-0032$26.00

Main data on the supernovae and their parent galaxies

SN Galaxy	Date of discovery Type of galaxy	$\alpha_{SN,2000}$ V_r, km s^{-1}	$\delta_{SN,2000}$ A_B	$\Delta\alpha$ $\Delta\delta$ m_{SN} Discovery of SN	Type of SN Determination of SN type
1997cx	July 12	$10^h05^m37^s.43$	$80°17'27''.6$	5″ W 15″ N 15^m	II
NGC 3057	SB(s)dm	1524	$0^m.101$	Schwartz (1997)	Jha *et al.* (1997a)
1997dn	October 29	$10^h54^m18^s.95$	$27°14'07''.3$	35″ W 20″ S $16^m.0$	II
NGC 3451	Sd	1334	$0^m.092$	Boles (1997)	Jha *et al.* (1997b)
1997do	October 31	$7^h26^m42^s.50$	$47°05'36''.0$	$2''.6$ W $3''.8$ S $15^m.8$	Ia
UGC 3845	SB(s)bc	3034	$0^m.270$	Qiu *et al.* (1997)	Qiu *et al.* (1997)
1997dq	November 2	$11^h40^m55^s.90$	$11°28'45''.7$	43″ W 29″ N $15^m.0$	Ib
NGC 3810	SA(rs)c	993	$0^m.191$	Aoki (1997a)	Jha *et al.* (1997c)
1997ef	November 25	$7^h57^m02^s.82$	$49°33'40''.2$	10″ E 20″ S $16^m.7$	IcPec
UGC 4107	SA(rs)c	3504	$0^m.183$	Sano (1997)	Filippenko and Martin (1997)
1997eg	December 4	$13^h11^m36^s.71$	$22°55'28''.9$	$4''.1$ W $33''.1$ N $15^m.6$	IIn
NGC 5012	SAB(rs)c	2619	$0^m.059$	Aoki (1997b)	Filippenko and Barth (1997)
1997ei	December 23	$11^h54^m59^s.98$	$58°29'26''.4$	10″ E 10″ S $16^m.5$	Ic
NGC 3963	SAB(rs)bc	3188	$0^m.100$	Aoki (1997c)	Wang *et al.* (1998)
1998D	January 28	$14^h02^m59^s.28$	$34°44'54''.3$	$26''.1$ W $7''.4$ S $15^m.6$	Ia
NGC 5440	Sa	3689	$0^m.064$	Qiu *et al.* (1998)	Qiu *et al.* (1998)
1998aq	April 13	$11^h56^m25^s.81$	$55°07'41''.6$	18″ W 7″ N $14^m.9$	Ia
NGC 3982	SAB(r)b	1109	$0^m.061$	Armstrong (1998)	Ayani and Yamaoka (1998a)
1998dh	July 20	$23^h14^m40^s.31$	$4°32'14''.1$	$53''.5$ W $10''.4$ N $16^m.8$	Ia
NGC 7541	SB(rs)bc	2678	$0^m.293$	Li *et al.* (1998a)	Garnavich *et al.* (1998)
1998ef	October 18	$1^h03^m26^s.87$	$32°14'12''.4$	$6''.1$ E $2''.1$ S $15^m.2$	Ia
UGC 646	SBb	5319	$0^m.317$	Li *et al.* (1998b)	Filippenko and De Breuck (1998)
1998es	November 13	$1^h37^m17^s.51$	$5°52'50''.4$	$0''.4$ W $10''.8$ N $14^m.6$	IaPec
NGC 632	SO	3168	$0^m.139$	Halderson *et al.* (1998)	Jha *et al.* (1998)
1999D	January 16	$11^h28^m28^s.39$	$58°33'38''.9$	$18''.9$ W $4''.8$ S $15^m.6$	II
NGC 3690	SBm	3064	$0^m.072$	Qiu *et al.* (1999)	Jha *et al.* (1999)
1999X	January 23	$8^h54^m32^s.23$	$36°30'41''.1$	$4''.1$ E $5''.5$ N $16^m.1$	Ia
PGC 25005		7503	$0^m.138$	Schwartz (1999)	Garnavich *et al.* (1999)
1999aa	February 11	$8^h27^m42^s.12$	$21°29'15''.5$	$1''.6$ E $30''.8$ N $15^m.5$	IaPec
NGC 2595	SAB(rs)c	4330	$0^m.172$	Arbour (1999)	Filippenko *et al.* (1999)

bands. Based on the observations of standards from Landolt (1992) and the standard region in the cluster M 67 (Chevalier, and Ilovaisky 1991), we determined (separately for different seasons of observations and different telescope–filter–detector combinations) the coefficients of the equations for the transformation of instrumental magnitudes to standard ones. The equation for the V band is $v = V + K_v(B-V) + C_v$; for the remaining filters, the equations have the same form. For the B, R, and I bands, we used the $B-V$, $V-R$, and $R-I$ color indices, respectively. For the coefficients K_b, K_v, K_r, and K_i, we obtained values from -0.09 to -0.16, from -0.04 to -0.06, from -0.68 to -0.77, and from -0.44 to -0.68, respectively. Despite the large coefficients K_r and K_i, the transformation errors were mainly much smaller than the photometric errors, and the agreement between our results and the data of other authors is satisfactory.

We made photometric measurements of the supernovae relative to one or two comparison stars that were within the CCD field of view together with the SN. We used the aperture photometry subroutine from the IRAF software package; the aperture diameters for measuring the object and the background for each star were chosen individually by analyzing

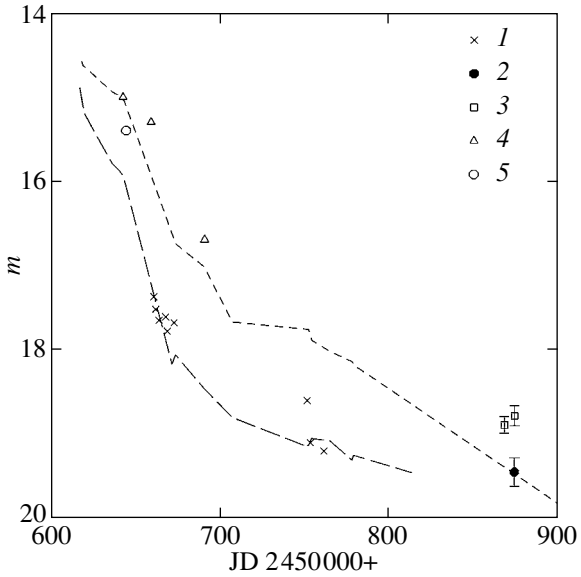

Fig. 1. Light curves for SN 1997cx: *1*, *2*, *3* are our B, V, R magnitude estimates; *4*, *5* are the CCD magnitude estimates without a filter and with the R filter published in IAU Circulars. The dashed lines represent the B (long dashes) and R (short dashes) light curves for SN 1990K.

the brightness distribution in the image. The galactic background was strong and nonuniform for many supernovae; for them, we had to subtract the image of the galaxy that was obtained when the supernova was no longer visible from the image of the galaxy with the SN. The image matching, normalization, and subtraction were performed by using subroutines from the IRAF package.

The results of our CCD observations of the supernovae are presented in Tables 4 and 5. The errors of the CCD magnitudes were determined with the aperture photometry subroutine from IRAF. The errors of the transformation of instrumental magnitudes to standard ones and the errors of the magnitudes for the comparison stars were negligible compared to the measurement errors of the supernovae in almost all cases and were disregarded.

We observed the comparison stars with the 60-cm and 38-cm Crimean reflectors and with the 70-cm and 30-cm Moscow telescopes mainly in 2000–2002. During this period, we also obtained images of the galaxies, which were subtracted from the images with the supernovae. We used SBIG ST-6, ST-7, and ST-8 CCD cameras with various sets of filters that more closely corresponded to the standard R_c, I_c system than those used in 1998–1999. On photometric nights, we observed standards from Landolt (1992) and standards near the stars under study from Mermilliod (1996) together with the comparison stars. The transformation coefficients from the instrumental system to the standard one were determined from the observations of the clusters NGC 7790 (Stetson 2000) and M 67. The magnitudes of the comparison stars were estimated by averaging three to six observations on different nights.

The magnitudes of the comparison stars are given in Table 2. The designations of the stars consist of the galaxy designation and the number of the star near the galaxy in order of decreasing brightness; the errors were calculated as the rms errors of the mean when averaging three to six measurements.

RESULTS

SN 1997cx. Despite the high brightness of this supernova, only four CCD magnitude estimates without a filter and in the R band were published for it in IAU Circulars. One spectrogram is shown at the site of the Supernova Research Group of the Harvard–Smithsonian Astrophysical Center (below referred to as CfA SN, http://cfa-www.harvard.edu/cfa/oir/Research/supernova/RecentSN.html) and was described by Jha *et al.* (1997a). It was taken two days after the discovery and shows that SN 1997cx is a normal type II supernova discovered shortly after its brightness maximum. The photometry is presented in Fig. 1. Clearly, SN 1997cx belongs to type II-L supernovae with a linear brightness decline. Of all the type II-L supernovae studied in detail, the light curves of SN 1990K show the best agreement with the observations of SN 1997cx (Cappellaro *et al.* 1995). The spectrum of SN 1990K taken five to seven days after its discovery is very similar to the published spectrum of SN 1997cx. Unfortunately, SN 1990K was discovered after its brightness maximum, which was not observed. Cappellaro *et al.* (1995) showed that the supernova was most likely discovered 15 days after its maximum. If the light curves of SN 1997cx were similar to those of SN 1990K, then we obtain an estimate for the probable date of maximum brightness of SN 1997cx, JD 2450597 (May 29, 1997, more than fourty days before its discovery). Extrapolation of the light curves yields an estimate $B_{max} \approx R_{max} \approx 14\overset{m}{.}2$. The extinction toward SN 1990K was high, $E(B-V) = 0\overset{m}{.}5$; the relative shift between the B and R light curves for the best match with the observations of SN 1997cx indicates that the extinction is negligible for this supernova. Taking the distance modulus $\mu = 32.05$ (Tully 1988), we obtain an estimate of the absolute magnitude at maximum, $M_{B_{max}} \approx M_{R_{max}} \approx -17\overset{m}{.}9$. This value is slightly higher than the mean absolute magnitude of type II-L supernovae, as inferred from the data by Richardson *et al.* (2002) recalculated to our adopted Hubble constant $H_0 = 75$ km s^{-1} Mpc^{-1}.

SN 1997dn. The spectrum of this supernova taken one day after its discovery was published at

the CfA SN site; its description was given by Jha *et al.* (1997b). It is very similar to the spectrum of SN 1997cx. However, the light curves of SN 1997dn differ greatly from those of SN 1997cx. According to the CCD magnitude estimates without a filter obtained by Moretti and Tomaselli (1997), the brightness of the supernova was almost constant, $\sim 16\overset{m}{.}6$, during December 1997. Our data indicate that the B brightness of the supernova rapidly declined in early November 1997; in late February 1998, its R brightness was approximately equal to $17\overset{m}{.}7$, while its V brightness rapidly decreased, from $18\overset{m}{.}0$ to $18\overset{m}{.}6$, in eight days. It may be concluded that SN 1997dn is a type II supernova with a plateau, and a rapid decline in brightness was observed after the plateau stage in late February 1998. A comparison of the spectrogram for SN 1997dn with the spectra for SN II-P 1999em and 1999gi (Leonard *et al.* 2002a; 2002b) shows that SN 1997dn was discovered at least 25 to 30 days after its brightness maximum. The plateau stage must then have lasted from early October 1997 until mid-February 1998, i.e., $\sim$130 days. This period is significantly longer than that for SN 1999em and 1999gi, for which the plateau stage lasted $\sim$100 days. Unfortunately, the shape of the light curves and the brightness at maximum cannot be determined more accurately because of the lack of observations near the maximum and the low accuracy of the estimates obtained at the plateau stage. We assume the distance modulus for NGC 3451 to be $\mu = 32.1$ (below, the distance to the galaxies that were not included in the catalog by Tully (1988) is determined from the radial velocity corrected for the local velocity field (Bottinelli *et al.* 1986) with $H_0 = 75$ km s^{-1} Mpc^{-1}). If the R brightness on the plateau was about $16\overset{m}{.}6$, then the absolute magnitude is $M_R \approx -15\overset{m}{.}5$. This magnitude is slightly fainter than the absolute magnitudes of SN 1999em and 1999gi on the plateau, $-16\overset{m}{.}1$ and $-16\overset{m}{.}4$, respectively. Strong extinction toward the supernova in NGC 3451 is unlikely, because SN 1997dn exploded in the outer region of the galaxy, no strong interstellar absorption lines were observed in its spectrum, and the $V-R$ color index at the stage of rapid brightness decline after the plateau was approximately the same as that for SN 1999em with negligible extinction.

SN 1997do. A spectrum of this supernova was taken one day after its discovery and proved to be similar to the spectrum of SN Ia1990N one week before its brightness maximum (Qiu *et al.* 1997). Our photographic observations were begun four days after the discovery; they allow the point of maximum brightness to be reliably established. As we see from Fig. 2, our estimates agree well with the light curve of SN Ia1994D (Richmond *et al.* 1995); the maximum brightness was $B_{\max} = 14\overset{m}{.}2$ at JD 2450765 (November 12, 1997). The R light curve for SN 1994D also agrees well with the estimates by Qiu *et al.* (1997) and our data; the relative shift between the B and R light curves for the best match leads us to conclude that the extinction toward SN 1997do is low. Taking the distance modulus $\mu = 33.3$ and the extinction in the Galaxy from Table 1, we find an absolute magnitude, $M_B = -19\overset{m}{.}4$, close to the mean absolute magnitude for SN Ia.

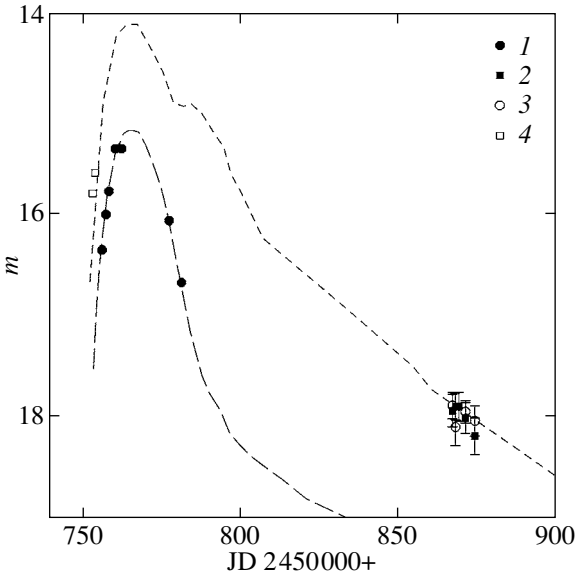

Fig. 2. Light curves for SN 1997do: *1*, *2*, *3* are our B, V, R magnitude estimates; *4* are the R magnitudes published in IAU Circulars. The dashed lines represent the B (long dashes) and R (short dashes) light curves for SN 1994D.

SN 1997dq. Jha *et al.* (1997c) reported that the spectrum of this supernova taken on November 5, 1997, showed that it is a type Ib near its brightness maximum. Matheson *et al.* (2001) obtained a series of spectra for SN 1997dq. They point out that the He I lines are moderately strong, and the impression is that this is an atypical type Ib supernova; there is a similarity to the peculiar type Ib/c SN 1997ef. Six CCD magnitude estimates without a filter were published in IAU Circulars. These estimates show a slow, almost uniform brightness decline from 15^m to $17\overset{m}{.}6$ between early November 1997 and late March 1998. However, our R magnitude estimates in late February 1998 indicate that the supernova is almost 1^m brighter than its published magnitude. Definite conclusions about the shape of the light curves for this supernova cannot be drawn from the available data.

SN 1997ef. This supernova has attracted particular attention in recent years because it has proven to be the first discovered hypernova, a supernova whose explosion energy may far exceed the typical value of $\sim 10^{51}$ erg. Spectroscopic observations, the V light

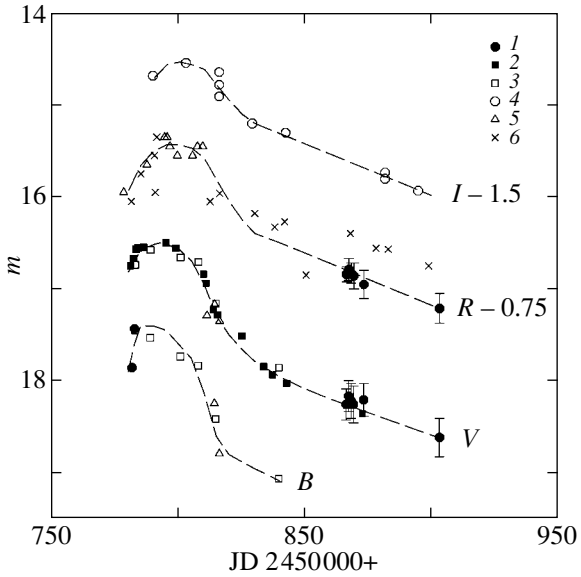

Fig. 3. Light curves for SN 1997ef: *1* are our data; *2* are the data from Garnavich *et al.* (1997a); *3* are the estimates by Mazzali *et al.* (2000); *4* are the I magnitudes from Li *et al.* (2002); *5* are the B, V, R magnitude estimates from the VSNET database and IAU Circulars; *6* are the CCD magnitude estimates without a filter from VSNET and IAU Circulars. The shift between the R and I light curves is indicated.

curve, and simulations of the supernova explosion were presented by Iwamoto *et al.* (2000). The V light curve from Garnavich *et al.* (1997a) is usually given in all the papers devoted to this supernova. The I light curve obtained with the KAIT automatic telescope and one I magnitude estimate obtained with the Hubble Space Telescope (HST) were published by Li *et al.* (2002). These authors point out that the brightness of SN 1997ef at the late stage declined very slowly, by only $2\overset{m}{.}5$ in 1100 days. Several magnitude estimates in the R band and without a filter were published in IAU Circulars, mainly by Wei *et al.* (1997). The VSNET database (http://vsnet.kusastro.kyoto-u.ac.jp/vsnet/index.html) includes two B and three V estimates and several CCD magnitude estimates without a filter. Several B and V magnitude estimates obtained by analyzing the spectra were presented by Mazzali *et al.* (2000). Using all these data and our results, we can construct the light curves for SN 1997ef in four bands (Fig. 3). The most characteristic feature that has not been observed for other SN Ib/c, including other possible hypernovae, is the segment of almost constant brightness at maximum that lasted ~15 days in all bands. Our B magnitude estimates obtained immediately after the discovery indicate that the brightness of the supernova rose rapidly, and that its $B-V$ color index was about 1^m even at this early stage. At the brightness maximum, whose middle point in V occurred near JD 2450792 (December 9, 1997), the V magnitude reached $16\overset{m}{.}5$, while the color indices were $B-V \sim 1^m$, $V-R \approx 0\overset{m}{.}3$, and $R-I \approx 0\overset{m}{.}2$. The rapid brightness decline began near JD 2450800 and lasted approximately 20 days; over this period, the brightness declined by $1\overset{m}{.}2$ in V and slightly less in R and I. Thereafter, the brightness declined linearly at a rate of about $1^m/100^{\rm d}$, which was approximately the same in all bands. Subsequently, the rate of brightness decline decreased further, because, according to Li *et al.* (2002), this rate at the late stage was about $0\overset{m}{.}2/100^{\rm d}$. The spectrum of SN 1997ef and its position in the parent galaxy suggest the absence of significant extinction; we obtained an estimate of the absolute magnitude at maximum, $M_V = -17\overset{m}{.}1$. According to Richardson *et al.* (2002), this magnitude is slightly fainter than the mean absolute magnitude for all SN Ib/c, but is equal to the mean luminosity of normal SN Ib/c.

SN 1997eg. Filippenko and Barth (1997) took a spectrum of this supernova 15 days after its discovery. It proved to be similar to the spectrum of SN 1988Z with characteristic signatures of type IIn SN—strong emission lines, particularly in Hα and Hβ, in a blue continuum. The spectrum taken slightly later is shown at the CfA SN site. Salamanka *et al.* (2002) carried out spectroscopic observations of SN 1997eg in June and July 1998. They detected narrow P Cyg profiles at the tops of the Hα and Hβ emission features and estimated the density of the interstellar medium surrounding the supernova, $n \geq 5 \times 10^7$ cm^{-3}. Radio emission was also detected from the supernova (Lacey *et al.* 1998). Unfortunately, as yet no photometric observations of SN 1997eg have been published. Our observations performed from February 21 through March 1, 1998, indicate that the brightness of the supernova was almost constant over this period. The mean magnitudes were $B = 16\overset{m}{.}18$, $V = 15\overset{m}{.}73$, $R = 15\overset{m}{.}27$, and $I = 14\overset{m}{.}95$. Taking the distance modulus $\mu = 33.0$ (Tully 1988), we obtain the absolute magnitude $M_V = -17\overset{m}{.}3$ about 80 days after the discovery. It may be concluded that at its brightness maximum, SN 1997eg could have had an absolute magnitude between -18^m and -19^m characteristic of the SN IIn.

SN 1997ei. This supernovae was initially classified as SN Ia (Garnavich *et al.* 1997b). However, subsequent observations showed that it is SN Ic (Wang *et al.* 1998; Matheson *et al.* 2001) and was discovered near its brightness maximum. Apart from the magnitude estimated when the supernova was discovered, there is one V magnitude estimate for it in the VSNET database. Our observations were carried out 60 to 70 days after its discovery. They indicate that the brightness of SN 1997ei at this time

was $V \approx 18^m.8$ and $R \approx 18^m.3$. The shape of the light curve cannot be established from these data.

SN 1998D. Only three CCD magnitude estimates without a filter were published for this supernova in IAU Circulars. Qiu *et al.* (1998) pointed out that the spectrum of SN 1998D is similar to the spectrum of SN 1994D two days after its brightness maximum. Our R-band observations and published magnitude estimates agree well with the R light curve for SN 1994D (Richmond *et al.* 1995). The maximum R brightness was $15^m.5$ at JD 2450845 (January 31, 1998). A comparison of the $V-R$ color curve for SN 1994D with our color estimates for SN 1998D shows a color excess $E(V-R) \approx 0^m.12$. Taking the distance modulus $\mu = 33.7$, we then obtain an estimate of the absolute magnitude at maximum, $M_R = -18^m.6$.

SN 1998aq. This is one of the brightest type Ia supernovae in recent years, but its multicolor photometric observations have not yet been published. V-band observations are given at the CfA SN site (mainly before the brightness maximum); an extended series of V magnitude estimates was published by Hanzl (1998). According to these data, the V light curve for SN 1998aq has the shape characteristic of SN Ia, but the rate of brightness decline after maximum is slightly lower than the mean rate, $4^m.6/100^d$. The maximum brightness was $V_{\max} = 12^m.40$ at JD 2450933 (April 29, 1998). The extinction toward SN 1998aq was most likely very low: no interstellar absorption lines can be seen in the spectra taken by Vinko *et al.* (1999) and the CfA SN group. Our B magnitude estimates about 120 days after maximum indicate that the color index is $B-V \approx 0^m.3$. This value is close to the corresponding value for SN Ia1972E without extinction in its parent galaxy. The distance modulus for NGC 3982 was determined from the HST observations of Cepheids by Saha *et al.* (2001) and Stetson and Gibson (2001). These authors obtained slightly differing results, 31.72 and 31.56, respectively. Taking the mean of these values, we find the absolute magnitude of SN 1998aq to be $M_V = -19^m.24$, which is close to the mean absolute magnitude for SN Ia.

SN 1998dh. The spectrogram of this supernova taken six days after its discovery is shown at the CfA SN site and was described by Garnavich *et al.* (1998). The spectrum exhibited interstellar Na I absorption lines that originated in the Galaxy and in NGC 7451 with equivalent widths of 0.1 and 0.04 nm, respectively. Many CCD magnitude estimates in V, R, and without a filter have been collected in IAU Circulars and the VSNET database. All these data agree well with the light curves of SN Ia 1990N (Lira *et al.* 1998); the maximum brightness was $V_{\max} = 13^m.95$ at JD 2451032 (August 6, 1998). If we apply the relation established by Barbon *et al.* (1990) to the intensities of interstellar absorption lines, then we will obtain a large color excess $E(B-V)$ $0^m.25$ for the Galaxy and $0^m.1$ for NGC 7451. This color excess is in conflict with the extinction in the Galaxy estimated from NED data, $A_B = 0^m.29$, and with the reddening estimate for the supernova, $E(B-V) \approx 0^m.1$, that can be obtained by comparing the relative shifts between the light curves of SN 1990N for the best match with the data for SN 1998dh. In this case, the relation by Barbon *et al.* (1990) is probably inapplicable. Taking the distance modulus $\mu = 32.6$ (Tully 1988) and $E(B-V) \approx 0^m.1$, we obtain the absolute magnitude at maximum $M_V = -19^m.0$, which is equal to the mean value for SN Ia.

SN 1998ef. A spectrogram of this supernova was taken by the CfA SN group on October 23, 1998, five days after its discovery. The appearance of the spectrum is typical of SN Ia near the brightness maximum. Several magnitude estimates in R and with CCD cameras without a filter were published in IAU Circulars and the VSNET database. Our R-band observations and most of the published magnitude estimates agree well with the R light curve of SN Ia1998bu (Suntzeff *et al.* 1999). The brightness maximum $R_{\max} = 15^m.0$ occurred near JD 2451112 (October 25, 1998). A comparison of our $V-R$ color estimates with the corresponding data for SN 1998bu indicates that the color excess of SN 1998ef is $E(V-R) \approx 0^m.12$, although the accuracy of this estimate is low. The extinction in the Galaxy corresponds to $E(V-R) = 0^m.06$; thus, extinction most likely also exists in the parent galaxy. Taking the distance modulus $\mu = 34.35$ and $A_R = 0^m.35$, we obtain the absolute magnitude at maximum $M_R = -19^m.7$.

SN 1998es. A spectrum of SN 1998es was taken by Jha *et al.* (1998) on the day after its discovery; it is shown at the CfA SN site and turned out to be similar to the spectrum of the peculiar SN Ia 1991T seven days before its brightness maximum. Ayani and Yamaoka (1998b) took a spectrum slightly later; they also pointed out its similarity to the spectrum of SN 1991T and detected narrow interstellar Na I absorption lines that originated in NGC 632. CCD magnitude estimates in V, R, and without a filter were published in IAU Circulars and the VSNET database. The $BVRI$ photometry for stars near NGC 632 and the light curve in a band close to R obtained by Krisciunas are presented at http://www.astro.washington.edu/kevin/apo.html. We used these magnitudes of the comparison stars to reduce our observations. The photometric data for SN 1998es are shown in Fig. 4. We see that the light curves for SN 1991T (Lira *et al.* 1998) agree well with the observational data. The date of

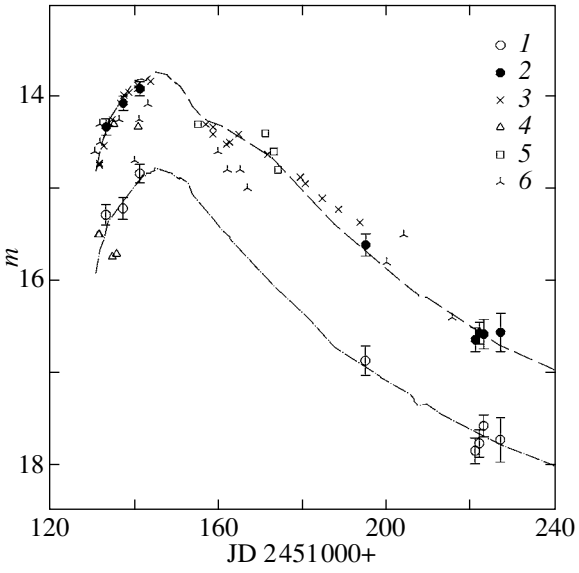

Fig. 4. Light curves for SN 1998es: *1*, *2* are our V and R estimates; *3* are the data from Krisciunas *et al.* (2000); *4*, *5*, *6* are the magnitude estimates in V, R, and without a filter from the VSNET database and IAU Circulars. The dashed and dash–dotted lines represent the R and V light curves for SN 1991T, respectively. The V light curve was shifted downward by 1^m.

maximum brightness is JD 2451146 (November 28, 1998); $V_{\max} = 13^m.8$, $R_{\max} = 13^m.7$. The relative shift between the light curves of SN 1991T for the best match with the data for SN 1998es indicates that the reddening of these supernovae is almost the same. For SN 1991T, we take $E(B-V) = 0^m.16$ estimated by Gibson and Stetson (2001). Taking the same extinction for SN 1998es and the distance modulus $\mu = 33.1$, we obtain the absolute magnitude at maximum $M_V = M_R = -19^m.8$. Thus, SN 1998es is even slightly brighter than SN 1991T, for which $M_V = -19^m.55$ at the distance modulus $\mu = 30.56$ (Gibson and Stetson 2001).

SN 1999D. The spectrogram of this supernova taken two days after its discovery is shown at the CfA SN site; it was described by Jha *et al.* (1999). The spectrum is characteristic of type II supernovae at the early stage—strong Balmer hydrogen lines with P Cyg profiles in a blue continuum. Several magnitude estimates in V and R and with CCD cameras without a filter were published for SN 1999D in IAU Circulars. However, a comparison with our data indicates that most of these estimates have errors that reach 1^m. Our first magnitude estimate was obtained on January 20, four days after the discovery; we performed nine more observations from February 11 through April 26. All V and R magnitude estimates in February and March show an approximately constant brightness with mean values of $V = 17^m.36$ and $R = 17^m.01$. The magnitudes were slightly brighter in V and R on January 20 and slightly fainter in R on April 26 than these values. SN 1999D is undoubtedly SN II-P, and the plateau stage lasted at least 70 days. Since the $V-R$ color index on the plateau is approximately the same as that for SN 1999em, SN 1999D suffered no significant extinction. Taking the distance modulus $\mu = 33.4$ (Tullu 1988), we obtain absolute magnitudes on the plateau, $M_V = -16^m.1$ and $M_R = -16^m.4$, close to the corresponding data for SN 1999em.

SN 1999X. Garnavich *et al.* (1999) took a spectrum of the supernova on February 6, 1999, 14 days after its discovery, and pointed out that it was typical of SN Ia and was most likely obtained seven to ten days after the brightness maximum. Four magnitude estimates with CCD cameras without a filter and one V estimate were published in IAU Circulars. The VSNET database gives a series of B, V, R, I observations obtained from March 3 through April 11 at the Apache Point Observatory (APO). These observations are shown in Fig. 5. The light curves for SN 1990N (Lira *et al.* 1998) are in satisfactory agreement with our and APO observations; the estimates with CCD cameras without a filter show a large deviation from these light curves. We can roughly estimate the magnitudes at maximum: $V_{\max} \approx R_{\max} \approx 16^m.3$; the brightness maximum occurred near JD 2451206 (January 28, 1999), which agrees with the estimate by Garnavich *et al.* (1999). A comparison of the $B-V$ and $V-R$ color indices for SN 1999X with the corresponding data for SN 1990N indicates that the extinction toward SN 1999X is low. At $\mu = 35.0$, we obtain $M_V = -18^m.8$.

SN 1999aa. Filippenko *et al.* (1999) took a spectrum of this supernova one day after its discovery. It was similar to the spectrum of the peculiar type Ia supernova SN1991T about six days before its brightness maximum. The spectrum obtained on the same night is shown at the CfA SN site. Photometric B, V, R, and I observations were carried out by Krisciunas *et al.* (2000). We used the magnitudes of the comparison stars from this paper to reduce our observations. Although many magnitude estimates are available for this supernova in IAU Circulars and the VSNET database, they are much less accurate than the data from Krisciunas *et al.* (2000) and our data; we did not consider them when constructing the light curves shown in Fig. 6. The points of maximum brightness in all bands are determined reliably. The maximum brightness occurred almost simultaneously in B, V, and R at JD 2451235 (February 25, 1999) and slightly earlier in I at JD 2451230. The brightness at maximum was $B_{\max} = 14^m.90$, $V_{\max} = 14^m.85$, $R_{\max} = 14^m.90$, and $I_{\max} = 15^m.2$. The rate of brightness decline after the maximum was about $11^m/100^{\rm d}$ in B and $5^m.1/100^{\rm d}$

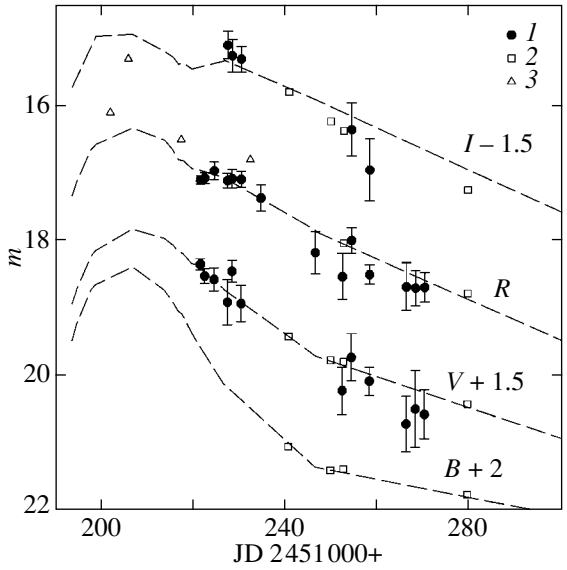

Fig. 5. Light curves for SN 1999X: *1* are our data; *2* are the APO data from the VSNET database; *3* are the CCD estimates without a filter from IAU Circulars. The dashed lines represent the light curves for SN 1990N. The shifts between the curves are indicated.

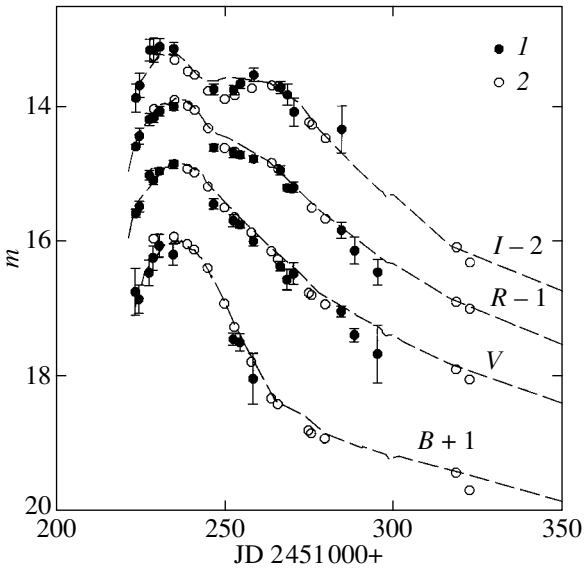

Fig. 6. Light curves for SN 1999aa: *1* are our data; *2* are the data from Krisciunas *et al.* (2000). The dashed lines represent the light curves for SN 1991T. The shifts between the curves are indicated.

in V. A comparison of the light curves for SN 1999aa and SN 1991T in Fig. 6 shows a generally close similarity, although the rate of brightness decline in B and V is slightly higher and the step in the R light curve and the minimum at $20^{\rm d}$ in the I light curve are deeper for SN 1999aa. A comparison of the $B-V$ and $V-R$ color curves indicates that SN 1991T is slightly redder than SN 1999aa at all phases; the color difference roughly corresponds to the color excess $E(B-V) = 0\overset{m}{.}16$ adopted for SN 1991T. It may be concluded that there is virtually no extinction toward SN 1999aa in the parent galaxy; taking $\mu = 33.9$ and the extinction in the Galaxy from Table 1, we obtain the absolute magnitudes at maximum brightness: $M_B = M_V = -19\overset{m}{.}2$, $M_R = -19\overset{m}{.}1$, and $M_I = -18\overset{m}{.}8$. Thus, judging by its luminosity at maximum, SN 1999aa is a normal SN Ia, despite the peculiarities of its spectrum.

CONCLUSIONS

The photometric parameters for most of the supernovae studied are close to the mean parameters for their types. Thus, for five of the six SN Ia, the deviations of the absolute magnitude at maximum from its mean value do not exceed $0\overset{m}{.}4$, while, according to Richardson *et al.* (2002), the dispersion of absolute magnitudes for SN Ia is about $0\overset{m}{.}6$. The deviation is slightly larger than the dispersion only for SN 1998ef. The light curves of these supernovae have also proven to be similar in shape to those for the typical SN Ia1994D, 1990N, and 1998bu. The parameters of the light curves for SN II-L 1997cx and SN II-P 1997dn and 1999D are characteristic of their types. Unfortunately, the data obtained are too scarce to construct the light curves for SN Ib 1997dq and SN Ic 1997ei; there are few objects with well-studied light curves for the supernovae of these types. The unusual shape of the light curve for SN Ic Pec 1997ef with a long period of constant brightness at maximum established previously from V-band observations is confirmed by the B, R, and I data. However, this supernova does not stand out in absolute magnitude among other objects of its type. The most interesting conclusion is that of a normal luminosity for SN 1999aa at maximum; based on their analysis of the light curves and on the similarity between its spectrum and the spectrum of SN 1991T, Krisciunas *et al.* (2000) assumed that it has an enhanced luminosity.

ACKNOWLEDGMENTS

We used the NASA/IPAC Extragalactic Database (NED), supported by the Jet Propulsion Laboratory of the California Institute of Technology under a contract with NASA. We also used the VSNET database. We wish to thank V.P. Goransky and S.Yu. Shugarov, who took part in the observations. P.V. Baklanov participated in the reduction of our observations. This work was supported in part by ISTC grant no. 370.

REFERENCES

1. M. Aoki, IAU Circ. No. 6770 (1997a).
2. M. Aoki, IAU Circ. No. 6790 (1997b).
3. M. Aoki, IAU Circ. No. 6795 (1997c).
4. R. Arbour, IAU Circ. No. 7108 (1999).
5. M. Armstrong, IAU Circ. No. 6875 (1998).
6. K. Ayani and H. Yamaoka, IAU Circ. No. 6878 (1998a).
7. K. Ayani and H. Yamaoka, IAU Circ. No. 7059 (1998b).
8. R. Barbon, S. Benetti, L. Rosino, *et al.*, Astron. Astrophys. **237**, 79 (1990).
9. L. Bottinelli, L. Gouguenheim, G. Paturel, and P. Teerikorpi, Astron. Astrophys. **156**, 157 (1986).
10. T. Boles, IAU Circ. No. 6763 (1997).
11. E. Cappellaro, I. J. Danziger, M. Della Valle, *et al.*, Astron. Astrophys. **293**, 723 (1995).
12. C. Chevalier and S. A. Ilovaisky, Astron. Astrophys., Suppl. Ser. **90**, 225 (1991).
13. A. V. Filippenko and A. J. Barth, IAU Circ. No. 6794 (1997).
14. A. V. Filippenko and C. De Breuck, IAU Circ. No. 7032 (1998).
15. A. V. Filippenko, W. D. Li, and D. C. Leonard, IAU Circ. No. 7108 (1999).
16. A. V. Filippenko and E. L. Martin, IAU Circ. No. 6783 (1997).
17. P. Garnavich, S. Jha, R. Kirshner, *et al.*, IAU Circ. No. 6786 (1997).
18. P. Garnavich, S. Jha, R. Kirshner, and P. Challis, IAU Circ. No. 6796 (1997).
19. P. Garnavich, S. Jha, and R. Kirshner, IAU Circ. No. 6980 (1998).
20. P. Garnavich, S. Jha, and R. Kirshner, IAU Circ. No. 7105 (1999).
21. B. K. Gibson and P. B. Stetson, Astrophys. J. **547**, 103 (2001).
22. E. Halderson, M. Modjaz, T. Shefler, *et al.*, IAU Circ. No. 7050 (1998).
23. D. Hanzl, IAU Circ. No. 6876 (1998); IAU Circ. No. 6898 (1998); IAU Circ. No. 6909 (1998); IAU Circ. No. 6937 (1998); IAU Circ. No. 6978 (1998).
24. K. Iwamoto, T. Nakamura, K. Nomoto, *et al.*, Astrophys. J. **534**, 660 (2000).
25. S. Jha, P. Garnavich, P. Challis, and R. Kirshner, IAU Circ. No. 6700 (1997a).
26. S. Jha, P. Garnavich, P. Challis, and R. Kirshner, IAU Circ. No. 6763 (1997b).
27. S. Jha, P. Garnavich, P. Challis, and R. Kirshner, IAU Circ. No. 6770 (1997c).
28. S. Jha, P. Garnavich, P. Challis, and R. Kirshner, IAU Circ. No. 7054 (1998).
29. S. Jha, P. Garnavich, P. Challis, and R. Kirshner, IAU Circ. No. 7089 (1999).
30. K. Krisciunas, A. Diercks, N. C. Hastings, *et al.*, Astrophys. J. **539**, 658 (2000).
31. C. K. Lacey, K. W. Weiler, R. A. Sramek, and S. D. Van Dyk, IAU Circ. No. 7068 (1998).
32. A. Landolt, Astron. J. **104**, 340 (1992).
33. D. C. Leonard, A. V. Filippenko, E. Gates, *et al.*, Publ. Astron. Soc. Pac. **114**, 35 (2002).
34. D. C. Leonard, A. V. Filippenko, W. D. Li, *et al.*, Astron. J. **124**, 2490 (2002).
35. W. D. Li, M. Modjaz, E. Halderson, *et al.*, IAU Circ. No. 6978 (1998).
36. W. D. Li, M. Modjaz, E. Halderson, *et al.*, IAU Circ. No. 7032 (1998).
37. W. D. Li, A. V. Filippenko, S. D. Van Dyk, *et al.*, Publ. Astron. Soc. Pac. **114**, 403 (2002).
38. P. Lira, N. B. Suntzeff, M. M. Phillips, *et al.*, Astron. J. **116**, 1006 (1998).
39. T. Matheson, A. V. Filippenko, W. D. Li, *et al.*, Astron. J. **121**, 1648 (2001).
40. P. A. Mazzali, K. Iwamoto, K. Nomoto, *et al.*, Astrophys. J. **545**, 407 (2000).
41. J.-C. Mermilliod, *The General Catalogue of Photometric Data*, http://obswww.unige.ch/gcpd (1996).
42. S. Moretti and S. Tomaselli, IAU Circ. No. 6785 (1997).
43. Y. L. Qiu, Q. Y. Qiao, W. D. Li, J. Y. Hu, and A. Esamdin, IAU Circ. No. 6766 (1997).
44. Y. L. Qiu, Q. Y. Qiao, W. D. Li, *et al.*, IAU Circ. No. 6815 (1998).
45. Y. L. Qiu, Q. Y. Qiao, and J. Y. Hu, IAU Circ. No. 7088 (1999).
46. D. Richardson, D. Branch, D. Casebeer, *et al.*, Astron. J. **123**, 745 (2002).
47. M. W. Richmond, R. R. Treffers, A. V. Filippenko, *et al.*, Astron. J. **109**, 2121 (1995).
48. A. Saha, A. Sandage, G. A. Tammann, *et al.*, Astrophys. J. **562**, 314 (2001).
49. I. Salamanka, R. J. Terlevich, and G. Tenorio-Tagle, Mon. Not. R. Astron. Soc. **330**, 844 (2002).
50. Y. Sano, IAU Circ. No. 6778 (1997).
51. P. B. Stetson, Publ. Astron. Soc. Pac. **112**, 925 (2000).
52. P. B. Stetson and B. K. Gibson, Mon. Not. R. Astron. Soc. **328**, L1 (2001).
53. N. B. Suntzeff, M. M. Phillips, R. Covarrubias, *et al.*, Astron. J. **117**, 1175 (1999).
54. R. B. Tully, *Nearby Galaxies Catalog* (Cambridge Univ. Press, Cambridge, 1988).
55. M. Schwartz, IAU Circ. No. 6700 (1997).
56. M. Schwartz, IAU Circ. No. 7105 (1999).
57. J. Vinko, L. L. Kiss, J. Thompson, *et al.*, Astron. Astrophys. **345**, 592 (1999).
58. L. Wang, D. A. Howell, and J. C. Wheeler, IAU Circ. No. 6802 (1998).
59. J. Y. Wei, J. Y. Hu, Y. L. Qiu, *et al.*, IAU Circ. No. 6797 (1997).

Translated by V. Astakhov

Astronomy Letters, Vol. 30, No. 1, 2004, pp. 41–49. Translated from Pis'ma v Astronomicheskiĭ Zhurnal, Vol. 30, No. 1, 2004, pp. 47–57.

Dependence of the Position of the Knee in the Galactic Cosmic Ray Spectrum on the Explosion Energy Distribution of Supernovae

L. G. Sveshnikova*

Institute of Nuclear Physics, Moscow State University, Vorob'evy gory, Moscow, 119992 Russia

Received April 2, 2003

Abstract—The position of the knee in the Galactic cosmic ray (GCR) spectrum is shown to depend on the explosion energy distribution function of supernovae (SN). The position of the knee in the GCR spectrum can be quantitatively explained by the dominating contribution of hypernovae with explosion energies of $(\sim 30-50)\times 10^{51}$ erg, the fraction of which must be no less than 1% of all SN. The model reproduces the main features in the spectrum of all particles measured in extensive air shower (EAS) experiments: the knee in the spectrum of all particles at energy of about 3 PeV, the change in slope by $\delta\gamma \sim 0.3-0.5$ after the knee point, and the steepening of the spectrum near 10^{18} eV. The model predicts a smooth knee if the SN explosion energy distribution is universal and a sharp knee if the hypernovae represent a separate class of events. The suggested model of the GCR spectrum is essentially based on the assumption that a spread in explosion energies exists and that the assumptions of the standard model for the CR acceleration in supernova remnants are valid. © *2004 MAIK "Nauka/Interperiodica"*.

Key words: *supernovae, cosmic rays, particle acceleration.*

INTRODUCTION

Cosmic radiation—the flux of nuclei with various charges from $Z = 1$ to $Z > 80$ observed near the Earth—accounts for a significant fraction of the energy balance in the Galaxy. Its mean energy density, 10^{-12} erg cm^{-3}, is comparable to the energy density of starlight, the magnetic fields of the Galaxy, and its interstellar gas (Berezinsky *et al.* 1990). Cosmic radiation, if it is considered as a Galaxy-filling gas, has an essentially nonthermal, power-law distribution that spans an enormous energy range, from MeV to $> 10^{20}$ eV, with a change in spectral index from -2.7 to -3.1 at energy $\sim 3\times 10^{15}$ eV. This knee was revealed in the 1950s by intensity measurements of extensive air showers (EAS) (Kulikov and Christiantsen 1959).

In the last few decades, intensive studies of the various EAS components have significantly refined the anatomy of the cosmic-ray (CR) spectrum: the spectrum exhibits a steepening at energy 10^{18} eV and then a flattening, which was called an ankle. The CR spectra are assumed to have Galactic and extragalactic origins before and after the ankle, respectively.

The mechanical energy of supernova (SN) explosions in our Galaxy, $\sim 10^{51}$ erg for a medium SN explosion at a SN rate of 0.01–0.03 yr^{-1}, is known to be capable of providing the total CR energy (Berezinsky *et al.* 1990). It has been convincingly shown that there is a mechanism of CR acceleration through diffusion at the shock fronts generated during the propagation of a supernova remnant (SNR) through the interstellar medium. Through this acceleration mechanism, $\sim 10\%$ (or even more; see Berezhko and Volk 2000) of the explosion kinetic energy is transferred to relativistic particles. Substantial theoretical progress in investigating this phenomenon is attributable to the development of a nonlinear kinetic theory for the diffusive particle acceleration at the shock fronts of SNRs (Berezhko *et al.* 1996; Berezhko and Volk 1997, 2000; Berezhko and Ellison 1999; Ellison *et al.* 1997, 2000; Drury *et al.* 2001; Malkov and Drury 2001) and to the understanding of the nonlinear effects of the CR back reaction on the shock structure. Ellison *et al.* (1997) were able to explain not only the main parameters of the CR spectrum up to energy 100–400 TeV but also the relative abundance of heavy elements in cosmic rays with respect to the Solar System precisely due to the study of the nonlinear effects.

The most difficult problem is the origin of the knee in the CR spectrum (Drury *et al.* 2001). A popular

*E-mail: sws@dec1.sinp.msu.ru

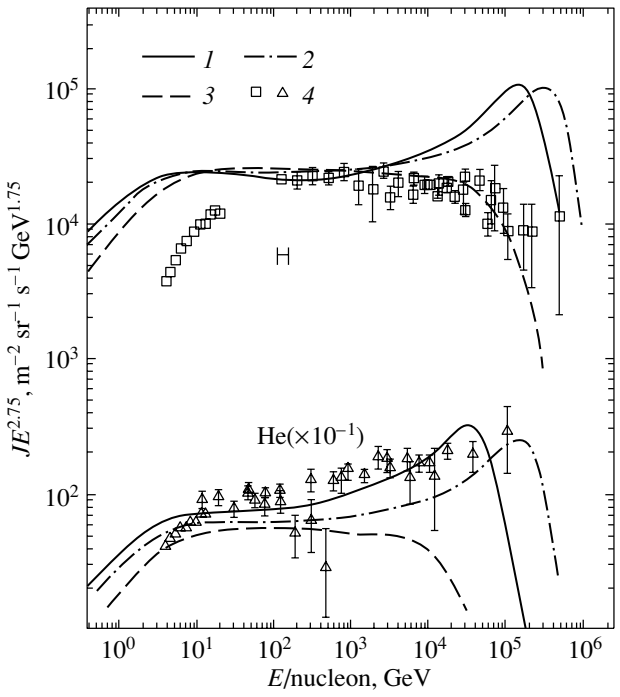

Fig. 1. The CR spectrum from Berezhko *et al.* (1997) for various parameters of the medium: *1*—$T = 10^4$ K, $\eta = 10^{-3}$; *2*—$T = 10^6$ K, $\eta = 10^{-3}$; *3*—$T = 10^4$ K, $\eta = 10^{-5}$; *4*—experimental data from Swordy (1994).

view is that the knee is related to the maximum energy of the accelerated CRs ($E_{\max}$). However, the problem is that the standard acceleration model predicts that during a standard explosion in the interstellar medium, the CR proton spectrum must be cut off at an energy of 100–300 TeV or lower. Only a certain class of supernovae can produce particles with the knee energy (a few PeV), while most SN generate particles of much lower energies (Reynolds and Keohane 1999).

The evolution of a SNR and the CR diffusion at a shock front are difficult to describe. This problem includes the diffusive transport equations for the CR distribution function self-consistently with the gas-dynamic equations that describe the supersonic propagation of the SNR through the interstellar medium and the formation of a shock wave not only at the Sedov phase, when appreciable deceleration begins, but also at the phase of free expansion—the kinetic nonlinear theory (Berezhko *et al.* 1996, 1997; Berezhko and Volk 1997, 2000). Figure 1 shows the computed and experimentally observed spectra of protons and helium nuclei (Berezhko *et al.* 1997) for various densities $n_{\rm H}$, temperatures T, and magnetic fields B of the medium: for the warm phase of a medium with $n_{\rm H} \sim 0.3$ cm^{-3} and $T = 10^4$ K where the maximum proton energy is $E_{\max} \sim 100$ TeV and for a rarefied medium corresponding to the hot phase ($T = 10^6$ K, $n_{\rm H} = 0.003$ cm^{-3}, $B = 3$ μG) where $E_{\max}$ is appreciably higher than 300–400 TeV.

A characteristic feature of the spectra is their flattening before the maximum acceleration energy attributable to the CR back reaction on the shock structure. The larger the injection coefficient of interstellar gas particles η into acceleration, the stronger this effect. Berezhko *et al.* (1997b) believe that the expected value of η lies within the range 10^{-3}–10^{-4}.

Figure 1 shows the observed spectrum, which differs from the CR spectrum generated in SNRs by $\delta\gamma$ due to the CR outflow from the Galaxy (Berezinsky *et al.* 1990). Berezhko *et al.* (1997) chose a $\delta\gamma = 0.75$; i.e., the spectrum generated in the sources has a slope $\gamma \sim 2.0$ and slightly flattens before the maximum acceleration energy.

On the other hand, the maximum acceleration energy can be estimated using the simple formulas from Ellison *et al.* (1997) if only the CR generation at the Sedov phase is considered:

$$E_{\max} \cong 3 \times 10^{14} Z \left(\frac{0.3B}{3\mu\ \mathrm{G}}\right) \left(\frac{n_{\rm H}}{\mathrm{cm}^3}\right)^{-1/3} \times \left(\frac{E_{\rm snr}}{10^{51}\ \mathrm{erg}}\right)^{2/5} \left(\frac{T_{\rm snr}}{10^3\ \mathrm{yr}}\right)^{-1/5} \quad (1)$$

or

$$E_{\max} \cong 2 \times 10^{14} Z \left(\frac{0.3B}{3\ \mu\mathrm{G}}\right) \left(\frac{n_{\rm H}}{\mathrm{cm}^3}\right)^{-1/3} \times \left(\frac{E_{\rm snr}}{10^{51}\ \mathrm{erg}}\right)^{1/3} \left(\frac{V_{\rm sk}}{10^3\ \mathrm{km\ s}^{-1}}\right)^{1/3} \mathrm{eV},$$

where Z is the nuclear charge, $E_{\rm snr}$ is the kinetic energy of the expanding SN shell in 10^{51} erg (below, we denote $E_{51} = E_{\rm snr}/10^{51}$), $V_{\rm sk}$ is the shock velocity (commonly expressed in 1000 km s^{-1}), and $T_{\rm snr}$ is the age of the SNR.

Formula (1) yields $E_{\max} \sim 100$ TeV for the warm phase and $E_{\max} \sim 300$–400 TeV for the hot phase at $E_{51} = 1$ and $V_{\rm sk} = 1$. This result is in satisfactory agreement (with a coefficient of 2) with the complete simulation that includes the total CR spectrum generated at all phases of the time evolution of the SNR (see Fig. 1) and computed by Berezhko *et al.* (1997).

The standard way of increasing the maximum particle acceleration energy to much higher values is to assume that the explosions of some supernovae occur in a medium with a strong magnetic field, for example, the explosions in the winds from Wolf–Rayet stars or the explosions in the superbubbles produced by a cluster of supernovae (Bykov and Toptygin 1997; see also the review by Drury *et al.* 2001;

Ptuskin 2000; Biermann 2000). An increase in magnetic field strength causes the Larmor particle radius to decrease, and, hence, the particle crosses the shock front many times and gains a high level of energy. However, when CRs are accelerated in superbubbles, the additional acceleration by multiple SNRs also has an effect (Bykov and Toptygin 1997).

However, if the contributions from various supernovae to the formation of the CR flux are equivalent, then the region of the knee will be determined not by rare explosions, but by the majority of the most probable explosions in the interstellar medium. Hence, it will be near 300 TeV.

On the other hand, a weak dependence of the maximum acceleration energy on the explosion energy follows from formula (1). Since a large amount of observational data indicative of a wide variety of supernova explosions has been obtained in recent years (Hamuy 2003; Richardson *et al.* 2002; Turatto 2003), it would be of interest to explore the question of how this variety can affect the CR spectrum, because the dependence of the maximum acceleration energy on the explosion energy clearly follows from formula (1).

The significant increase in the number of detected SN explosions has advanced our understanding of the variety and complexity of SN explosions (Turatto 2003). An enormous spread in luminosities (Richardson *et al.* 2002), photospheric expansion velocities, chemical compositions, etc. has been found; this is indicative of an enormous spread in explosion energies and in properties of the explosion-triggering projenitors (Hamuy 2003). A large spread in explosion energies, from $E_{51} = 0.6$ to 5.5 (Hamuy 2003) or at least up to $E_{51} = 3$ (Nadyozhin 2003), has been found even in the subclass of normal type II supernovae, SN IIP (with a plateau in the light curves). In addition, three supernovae (1997ef, 1998bw, 2002ap) that exhibit very smeared spectra without distinct features (which is interpreted as the result of the huge expansion velocities of the ejected shells (Hamuy 2003)), have been discovered in recent years. This fact suggests that these are hyper-energy objects, which have been called hypernovae (Iwamoto *et al.* 1998). The estimated explosion energies of these SN were dozens of times higher than the energies of medium explosions: 7×10^{51} for 2002ap (Mazzali *et al.* 2002), 8×10^{51} for 1997ef (Nomoto *et al.* 2000), and 60×10^{51} for 1998bw (Nomoto *et al.* 2000). The shell expansion velocity for the latter event was estimated to be $>30\,000$ km s^{-1} (Turatto *et al.* 2002). SN 1998bw is distinguished not only by its shell expansion velocity and high energy, but also by the fact that it is associated in time and place of explosion with GRB 980425 (Galama *et al.* 1998). In his review of the properties for supernovae, Hamuy (2003) concludes that, despite the wide variety of SN II and SN Ib/c, certain regularities that are indicative of the existence of a continuum in the properties of these objects with the presupernova mass as a control parameter can be found. This suggests that the explosion mechanism for this class of objects is not fundamentally different. Hamuy (2003) points out that hypernovae may represent a separate class in explosion physics.

On the other hand, there exists the opposite hypothesis that the common phenomenon in the Universe is most likely the standard, fixed energy release in fixed-mass astrophysical sources. The hypothesis of standard energy release ($E_0 = 5 \times 10^{51}$ erg) can probably explain even the enormous spread in observed GRB energies under certain assumptions (Postnov *et al.* 1999). When the CR fluxes are calculated, this is the main hypothesis; all supernovae are assumed to have fixed energy release into shell kinetic energy $\sim 10^{51}$ erg.

The main goal of this study is to try to estimate the average CR flux by taking into account not only the place of supernovae explosions but also the distributions of supernovae in explosion energy and SNR expansion velocity on which the maximum acceleration energy (1) depends. In this case, the explosion energy distribution may be considered either as a continuum of properties or as the contribution from different classes of events. We analyze the dependence of the position of the knee in the CR spectrum and its distinctness on these assumptions and on the supernova rate. Here, it should be emphasized that we are going to apply a formal approach in which only the standard assumptions about CR acceleration will be used without the development of any new approaches. We then present the main features of the model and analyze the dependence of the CR spectrum on the assumptions about the energy distribution function.

THE MODEL FOR CALCULATING THE GCR SPECTRUM

We assume that the CR flux $F(E)$ can be expressed by the formula

$$F(E) = \sum_{i=1}^{N_z} \sum_{j=1}^{N_{tp}} \int_{E_{51}^{min}}^{E_{51}^{max}} \Psi_j(E_{51}) G(E, E_{max}) dE_{51}, \quad (2)$$

where $\sum_i$ denotes the summation over N_z different groups of CR nuclei, and $\sum_j$ denotes the summation over N_{tp} different types of supernova explosions; $\Psi_j(E_{51})$ is the E_{51} distribution function within each class of SN. The upper limit of the integration over the explosion energy in the main calculation was chosen to be $E_{51}^{max} = 80$, because the maximum recorded energy is $E_{51} = 60$ (Nomoto *et al.* 2000). $G(E, E_{max})$

is the average CR spectrum generated in a single explosion at fixed energy E_{51} and at a fixed state of the medium. This spectrum can be fitted by a power law with different slopes in different energy ranges:

$$G(E, E_{\max}) = I_0 E^{-\gamma}; \quad (3)$$
$$\gamma = 2.0, \quad 10\ \mathrm{GeV} < E < E_{\max}/5;$$
$$\gamma = 1.70, \quad E_{\max}/5 < E < E_{\max};$$
$$\gamma = 5, \quad E > E_{\max}.$$

This shape of the spectrum takes into account the CR back reaction on the shock structure (Berezhko and Volk 1997, 2000; Ellison *et al.* 1997): a flattening of the spectrum before the maximum acceleration energy. The chosen slopes are close to the intermediate value of the injection coefficient $\eta = 10^{-4}$ on which the spectral shape depends (see Fig. 1), and the possible variation in η was disregarded.

The value of $E_{\max}$ is related to B, n_{H}, and $(E_{51}V_{\mathrm{sk}})^{1/3}$ by formula (1). Formally, the dependence on the medium in formula (1) can be separated into a cofactor: $E_{\max} = ZE^0_{\max}(E_{51}V_{\mathrm{sk}})^{1/3}$ or $E_{\max} = ZE^0_{\max}E_{51}^{2/5}T_{\mathrm{sk}}^{-1/5}$. This cofactor will depend only on the properties of the medium and, by definition, is equal to the maximum acceleration energy for protons at $E_{51} = 1$ and $V_{\mathrm{sk}} = 1$. The maximum energy decreases with decreasing shock velocity and increasing SNR age (1). Formally, according to these estimates, CRs of maximum energies are produced at the beginning of the Sedov phase T_0. Substituting T_{snr} for T_0, we can obtain a minimum dependence on the explosion energy, $E_{\max} \sim E^0_{\max}E_{51}^{0.4}$. However, since T_0 also depends weakly on E_{51}, we will use the dependence

$$E_{\max} = ZE^0_{\max}E_{51}^{0.5}, \quad (4)$$

which gives $E_{\max} = E^0_{\max}$ for protons at $E_{51} = 1$. Formula (4) is the key estimation dependence that is discussed in detail in the Appendix. Here, we only note that calculations which include the CR flux at all phases of the SNR life in a given explosion (Berezhko *et al.* 1997) show that the highest-energy and intermediate-energy CRs are generated at the end of the free expansion phase and at the Sedov phase, respectively. Dependence (4) was derived under the above assumption.

The intensity of the CRs accelerated in a SNR, I_0, can be determined from the condition

$$\int I_0 E^{-\gamma} E dE = 0.1E_{51}. \quad (5)$$

As was shown by Berezhko and Volk (1997, 2000), the fraction of the SNR kinetic energy transferred to CRs reaches even a larger value, 30%.

For our calculations with formula (2), it remains to choose the most probable values of the magnetic-field strength and the density of the medium in which supernovae explode. For SN II, SN Ib/c, and SN Ia, we chose a hot phase with $E^0_{\max} = 300$ TeV. This phase corresponds to the rarefied and hot halo gas that occupies ~50% of the Galactic spiral arms where the medium is heated precisely by supernova explosions (Kononovich and Moroz 2001).

In addition, the SN IIn (whose remnants, by definition, actively interact with the surrounding material) were separated into an isolated class (Hamuy 2003; Turatto 2003), and a much higher maximum energy may be assumed for them, $E^0_{\max} = 5 \times 10^{16}$–$10^{17}$ eV (see the review by Drury *et al.* 2001; Ptuskin 2000; Biermann 2000).

To simplify our calculations, we divided all CR nuclei into five groups: p, He, (C, N, O), (Mg, Si, Ne), and Fe with mass fractions of 0.36, 0.25, 0.15, 0.13, and 0.15, respectively. This chemical composition takes into account the fact that the measured spectra of the heavy elements are slightly flatter than the proton spectra at energy above 1 TeV (Shibata 1995), which leads to a heavier chemical composition near the knee than the chemical composition at 1 TeV (Erlykin and Wolfendale 2001). For the sake of simplicity, the shape of the spectrum for all elements is described by the same law (3).

We can now turn to the quantitative calculations with formula (2).

It should be noted that we disregarded the distortion of the CR spectrum due to the CR propagation in the Galaxy. As a result of this propagation, the spectral index of the CRs in the sources γ_{sour} differs from the observed spectral index γ_{obs} by $\delta\gamma$: $\gamma_{\mathrm{sour}} = \gamma_{\mathrm{obs}} - \Delta\gamma$, where $\Delta\gamma = 0.3$–0.8, depending on the propagation model (Jones *et al.* 2001).

THE DEPENDENCE OF THE CR SPECTRUM ON THE EXPLOSION ENERGY DISTRIBUTION FUNCTION

To analyze the dependence of the CR spectrum on the explosion energy distribution function at the first stage, we assumed that all supernovae had a universal Gaussian energy distribution:

$$\frac{dN}{d\log(E_{51})} = \frac{1}{\sqrt{2\pi\sigma^2}} \times \exp\left(-\frac{(\log E_{51} - \langle \log E_{51}\rangle)^2}{2\sigma^2}\right), \quad (6)$$

where $\sigma(\log E_{51})$ is the dispersion of the distribution. The choice of this form of function follows from Richardson *et al.* (2002). According to these authors, the distribution of all supernovae in absolute

magnitude M_b can be fitted by the sum of Gaussian distributions. Since $\log E_{51}$ is generally a linear function of M_b, it can be fitted in the first approximation, by a Gaussian distribution (Sveshnikova 2003). $dN/d\log E_{51}$ can then be transformed into $dN/dE_{51} = \Psi(E_{51})$, which is an asymmetric distribution with a long tail.

Figure 2 shows the spectra for all particles and separately for different groups of nuclei for three calculations using formula (2) with the dependence $E_{max} = 300E_{51}^{0.5}$ TeV. In all three calculations, the mean $\langle \log E_{51} \rangle$ was chosen to be -0.3, while the dispersion of the distributions differed in different calculations: $\sigma(\log E_{51}) = 0.1$ (Fig. 2a), 0.5 (Fig. 2b), and 1.0 (Fig. 2c). The first calculation corresponds to SN Ia with a narrow energy distribution; the second calculation roughly corresponds to SN II-P with a spread in energies E_{51} from 0.6 to 2.7 (Nadyozhin 2003); this spread in explosion energies could be even larger, from 0.6 to 5.5 (Hamuy 2003). The third calculation corresponds to SN Ib/c, among which both ordinary explosions and hypernovae with energies reaching 60×10^{51} erg are observed. In Figs. 2–4, the CR intensity was multiplied by a factor of E^2 for clarity of perception and is given in arbitrary units.

We see the following from Fig. 2.

(1) For a small dispersion, the knee point in the spectrum occurs at $E_{knee} = 300$ TeV, which corresponds to the maximum proton acceleration energy for the hot phase of the medium. In this case, the combined spectrum virtually follows the spectrum for a single supernova presented by formula (3), with a flattening before the knee. The spectrum after the knee in the range E_{knee}–$26 \times E_{knee}$ is determined by the gradual extinction of various nuclei with a maximum energy that is a factor of Z higher than the proton energy (see (1)). In the first calculation, this region is irregular in shape. The spectrum is cut off after $26E_{knee}$; for the CR spectrum after this point to be explained, we must assume that some of the SN explode in a medium with a strong magnetic field.

(2) As the dispersion of the energy distribution increases, the contribution of the most energetic explosions is emphasized due to condition (5) in our calculations (the total energy of the accelerated CRs is proportional to the explosion energy), while the maximum energy is shifted to higher energies due to dependence (4). In this case, the shape of the knee becomes smoother, although the change in spectral slope is still determined by the contribution from iron nuclei w(Fe). To a first approximation, this change can be estimated as follows:

$$\delta\gamma = \frac{\log(1/w(\mathrm{Fe}))}{\log 26}.$$

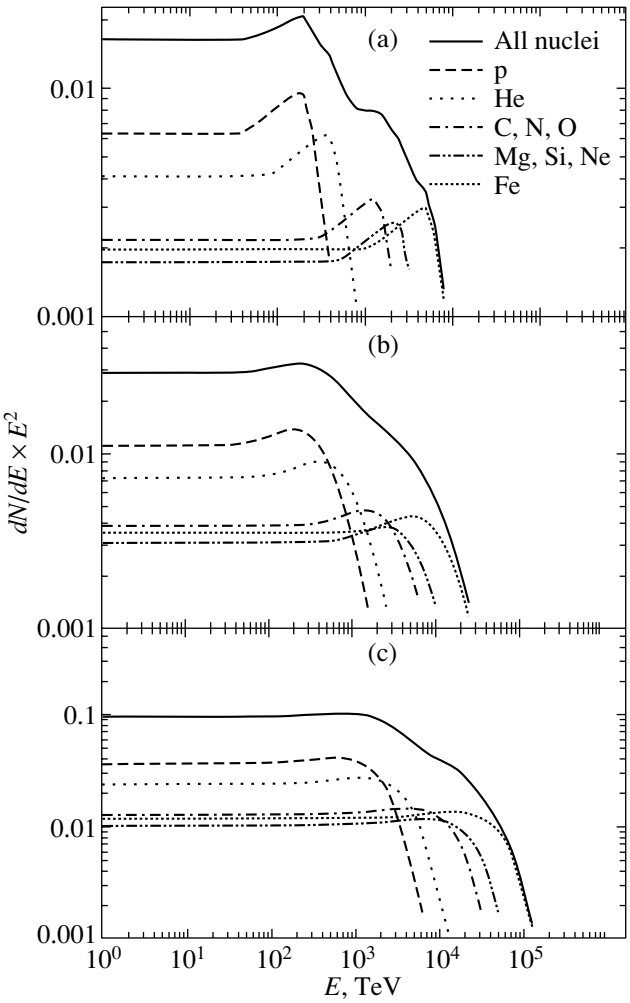

Fig. 2. The total GCR spectrum and the contributions from different groups of nuclei for various SN energy distribution functions: (a) $\sigma(\log E_{51}) = 0.2$; (b) $\sigma(\log E_{51}) = 0.5$; (c) $\sigma(\log E_{51}) = 1.0$. For all SN, $\langle \log E_{51} \rangle = -0.3$.

At w(Fe) $\sim$ 0.15–0.20, $\delta\gamma \sim 0.5$.

(3) In the third calculation, the position of the knee becomes close to the experimental value of 3 PeV, because events with hypernova parameters ($E_{51} \sim$ 30–50) appear in the distribution. They determine the knee point in the GCR spectrum.

In the next, more realistic calculation shown in Fig. 3, we assumed that different groups of supernovae have different properties (Hamuy 2003; Richardson *et al.* 2002). We chose the following parameters in the distribution function (6) for the four groups of supernovae (with relative fractions given in parentheses) SN Ia (0.25), SN II (0.45), SN Ib/c (0.20), and SN IIn (0.1): $\langle \log E_{51} \rangle = -0.3$, -0.3, 0, 0, and dispersions 0.2, 0.5, 1.2, 0.5. This reflects the

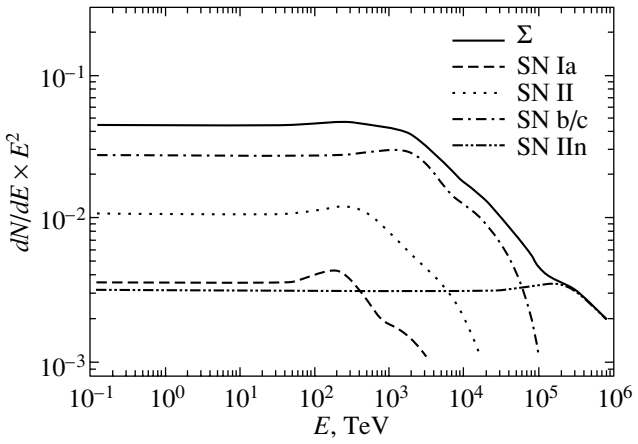

Fig. 3. Calculation of the total GCR spectrum when different groups of supernovae have different dispersion in energy $E^0_{\max} = 300$ TeV; $E^0_{\max} = 10^{17}$ eV only for SN IIn.

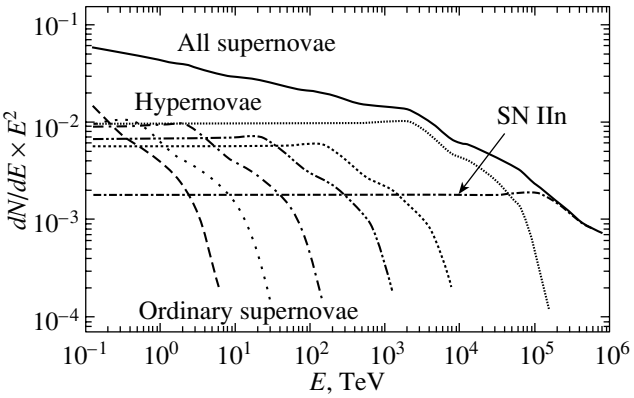

Fig. 4. Calculation where the ordinary supernovae have a narrow energy distribution and 1% of hypernovae are separated into a class also with a narrow energy distribution. $E^0_{\max} = 0.1$–300 TeV for ordinary supernovae and $E^0_{\max} = 10^{17}$ eV for SN IIn.

fact that hypernovae are observed precisely among SN Ib/c. We chose $E^0_{\max} = 300$ TeV for all SN and $E^0_{\max} = 10^{17}$ eV for SN IIn.

The contribution of SN Ia (although they account for 25% of the original sample) to the total CR flux is significantly suppressed, because they have a narrow energy distribution. The knee in the spectrum is determined by the maximum energy for the protons accelerated in the most energetic SN Ib/c with energy $E_{51} = 30$–50, the fraction of which in the given distribution is $\sim$2%. As we see from Fig. 3, if the fraction of such events decreases by a factor of 2 to 3, then the contribution of CRs from SN IIP will begin to dominate, and the knee will be shifted to lower energies. The contribution of the hypernovae required to form the knee can also be estimated from general considerations. Clearly, if the total power of 100% of the supernovae with a mean explosion energy $E_{51} = 1$ in our Galaxy is enough to provide the total CR power in the Galaxy, $\sim 10^{-12}$ erg cm^{-3} (Berezinsky *et al.* 1990), then 2% of the supernovae with $E_{51} = 50$ or 3% of the supernovae with $E_{51} = 30$ can also provide the total CR power in our Galaxy.

The required fraction of hypernovae can be slightly decreased by assuming that the explosion energy distribution function is not continuous and that the hypernovae represent a separate class of events with a small dispersion but a much larger mean energy: $\langle \log E_{51} \rangle = 1.7$, $\sigma(\log E_{51}) = 0.2$. Their contribution is $\sim$1%. The rest of the supernovae have a universal explosion energy distribution with a small dispersion: $\langle \log E_{51} \rangle = 0$, $\sigma(\log E_{51}) = 0.2$. SN IIn are identical in energy to ordinary SN and account for 10% of all SN; for them, $E^0_{\max} = 10^{17}$ eV. We also took into account the fact that the maximum CR acceleration energy among ordinary supernovae can be much lower than 100 TeV (Reynolds and Keohane 1999; Drury *et al.* 2001; Ptuskin and Zirakashvily 2003) and introduced a uniform distribution in $E^0_{\max}$ for ordinary supernovae in a wide energy range, $E_{\max}(E_{51}) = (0.1$–$300) E_{51}^{0.5}$ TeV.

Figures 4 and 5 show the CR spectra obtained in the calculation with a 1% fraction of hypernovae. The contributions from various types of SN and various groups of nuclei are indicated in Figs. 4 and 5, respectively.

We see first that the knee point remains at 3 PeV and is much more pronounced than that in Fig. 3, although we chose a smaller flattening of the spectrum before $E_{\max}$ in this calculation—$\gamma = 1.9$, in contrast to fit (3). Second, the $E_{\max}$ distribution from 0.1 to 300 TeV in this case leads to a steepening of the spectrum (by 0.15 in Fig. 4) in the range of 0.1 to 1000 TeV; this steepening depends on the fraction of hypernovae. As we see from Fig. 4, the combined CR spectrum is determined by the power of ordinary sources at low energies and by the power of hypernovae near the knee. SN IIn (conditionally speaking) determine the behavior of the GCR spectrum at $E > 26 E_{\text{knee}}$, i.e., in the range $E \gtrsim 5 \times 10^{16}$–$10^{18}$. Two steps will be observed in each nuclear CR component (Fig. 5); the second step arises from supernovae with a high $E^0_{\max}$ (conditionally SN IIn). The combined spectrum at $E > 3$ PeV is the sum of such double steps shifted in groups with different Z. The maximum CR energy is determined by the iron nuclei generated in SN IIn and is close to 10^{18} eV.

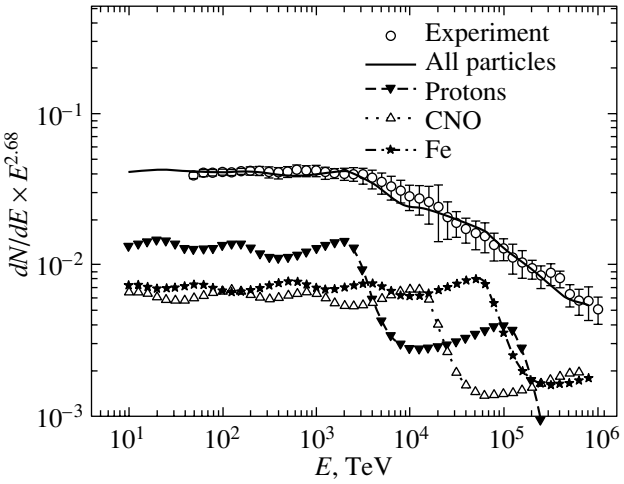

Fig. 5. Same as Fig. 4, but the CR spectrum observed near the Earth rather than in the sources is shown. The contribution from various groups of nuclei is shown separately, and the experimental spectrum for all particles obtained by averaging over different EAS experiments (Hoerandel 2002) is presented.

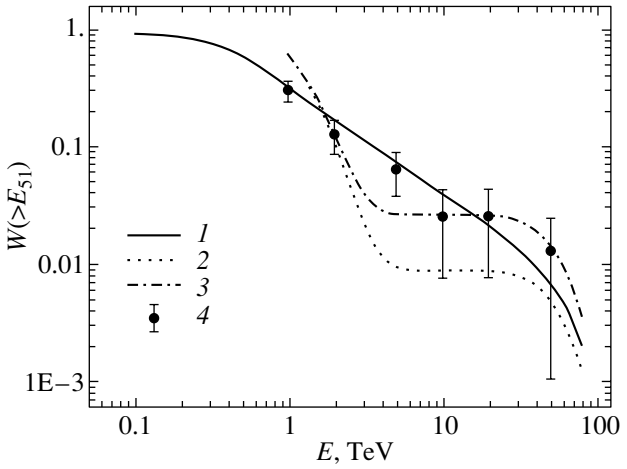

Fig. 6. Cumulative explosion energy distribution functions $W(>E_{51})$ for the various calculations shown in Fig. 3 (*1*), Fig. 4 for 1% of hypernovae (*2*), and for 3% of hypernovae (*3*); *4* represent the data from Hamuy (2002) for real supernovae.

Figure 5 shows the experimental spectrum obtained by Hoerandel (2002) by averaging various experimental EAS data. The computed spectra obtained under the same assumptions as those in Fig. 4 were reduced to the observed spectra by taking into account the CR outflow from the Galaxy

$$\gamma_{\rm obs} = \gamma_{\rm sour} + \Delta\gamma,$$

where $\Delta\gamma = 0.54$ was chosen in accordance with predictions of a simple diffusion model (Jones *et al.* 2001). As we see, this calculation describes the experimental data excellently.

To summarize, we may say that, in general, our calculations reproduce the main features of the spectrum for all particles measured in EAS experiments (Hoerandel 2003): the knee in the spectrum at $\sim$3 PeV, the change in slope by $\delta\gamma \sim 0.3$–0.5 after the knee, and the steepening of the spectrum near 10^{18} eV. In the opinion of some authors, for example, Erlykin and Wolfendale (1997), the shape of the knee measured in EAS experiments is sharp, and even peaks can be detected after the knee. In our model, this behavior can also be explained by assuming that hypernovae represent a separate class of events and that the CR back reaction on the shock structure is strong (as in Fig. 1, where the spectral index before the knee is $\gamma = -1.7$). Our model clearly predicts that the chemical composition becomes heavier sharply, from $\langle \ln A \rangle = 1.5$ at $E \sim 3$ PeV to $\langle \ln A \rangle = 3.5$ at $E \sim 3 \times 26$ PeV, then the mass number decreases to $\langle \ln A \rangle = 1.5$ at $E \sim 10^{17}$ eV, because only the contribution from SN IIn remains in this region, and then again the chemical composition becomes heavier. Here, we do not consider the possible explanation of the spectrum in a region higher by several units at 10^{18} eV (the ankle region), because the contribution of extragalactic CRs in this region can be significant. In addition, the CR outflow from the Galaxy ceases to have an effect and $\gamma_{\rm obs} \sim \gamma_{\rm sour}$.

The cumulative energy distribution functions for all supernovae $W(>E_{51})$ for which the spectra in Figs. 3 and 4 were obtained are shown in Fig. 6. For comparison, this figure also shows the E_{51} distribution constructed using tables from Hamuy (2003), where the physical parameters for real SN II, SN Ibc, and SN IIdw are presented. This distribution is designated in Fig. 6 as an experimental one, although it clearly depends on the theoretical assumptions made when determining the explosion energy and may be distorted by the sample of events. The distribution is a power law with a slope of -0.75, implying that the differential distribution is $\sim E^{-1.75}$. Since Hamuy (2003) considered only supernovae with $E_{51} > 1$ and did not specify their fraction of all SN, we normalized this fraction to 0.3 to reconcile it with our calculations. In this case, within the error limits, all our calculations of $W(>E_{51})$ presented in Figs. 3, 4, and 5 are consistent with the experimental function.

Thus, at an explosion rate of all supernovae of $\sim$0.01 yr^{-1}, hypernovae must explode at a rate $(2 \pm 1) \times 10^{-4}$ yr^{-1}.

How many SN provide the CR flux? If we consider the calculation presented in Fig. 3, where the contribution of hypernovae prevails even at low energies, then we obtain the following estimates: If the CR lifetime in the Galaxy is $\sim 3 \times 10^7$ yr and the hypernovae rate is $(2 \pm 1) \times 10^{-4}$ yr^{-1}, then this implies that $\sim 6 \times 10^3$ provide the CR intensity in the Galaxy. However, for high-energy ($\sim$1 PeV) CRs, the lifetime $T_{\rm esc}$ is much shorter, because the mean free path in the Galaxy $\lambda_{\rm esc}$ decreases as $E^{-\alpha}$ ($\alpha = 0.54$) at energies above 5 GeV (Jones *et al.* 2001). The number of the explosions that mainly contribute to CRs at $E \sim 1$ PeV can be small in the entire Galaxy ($\sim$10–15), and only a few supernovae may provide the CR flux after the knee near the Solar system.

CONCLUSIONS

(1) We have suggested a model for the formation of the GCR flux that includes a hypothetical explosion energy distribution of various types of supernovae and that is based on standard assumptions of the existing theory for the CR acceleration in SNRs. The position and shape of the knee are shown to depend on the assumed supernova energy distributions.

(2)The position of the knee in the GCR spectrum can be explained by the quantitatively dominating contribution of hypernovae with explosion energies of $(\sim 30\text{–}50) \times 10^{51}$ erg, the fraction of which must be no less than 1% of all supernovae. The SN rate of 1 to 3 in 10^4 yr is high enough to provide the total CR flux in the Galaxy. Several thousand SN produce the CR flux at low energies, but only a few explosions can give the dominating contribution to the CR flux in the knee region near the Solar system.

(3) In general, the model reproduces the main features of the spectrum for all particles measured in EAS experiments: the knee in the spectrum at $\sim$3 PeV, the change in slope by $\delta\gamma \sim 0.3\text{–}0.5$ after the knee, the sharp change in CR chemical composition after the knee point, and the steepening of the spectrum near 10^{18} eV. The model predicts a sharp knee if the explosion energy distribution is not universal and if the hypernovae represent a separate class of events.

ACKNOWLEDGMENTS

I wish to thank K.A. Postnov, V.S. Ptuskin, A.D. Erlykin, G.T. Zatsepin, O.G. Ryazhskaya, M.I. Panasyuk, N.N. Kalmykov, T.M. Roganova, L.A. Kuzmichev, N.V. Sokolskaya, and A.K. Managadze for their numerous and helpful discussions. I am grateful to the referee for their remarks, which allowed the paper to be significantly corrected. I am also grateful to all colleagues of the RUNJOB and NUKLON Collaborations, of which I am a member, for their support and discussions. This work was supported in part by the Russian Foundation for Basic Research (project no. 03-02-16272).

APPENDIX

The Derivation of the Estimation Dependence $E_{\max}(E_{51})$. Formula (1) was derived by Ellison *et al.* (1997) from simple considerations: the mean free path for scattering by magnetic inhomogeneities, which increases linearly with particle energy (because it is related to the Larmor particle radius), should not be more than 30% of the shock radius $R_{\rm sk}$; otherwise, the particle will escape from the acceleration region. The following estimate arises from this assumption:

$$E_{\max} \sim V_{\rm sk} R_{\rm sk}. \qquad (7)$$

The relations of the shock radius and velocity to the explosion energy and the SNR age $T_{\rm snr}$ are given by the standard Sedov formulas

$$R_{\rm sk} \sim E_{51}^{1/5} T_{\rm snr}^{2/5}, \quad V_{\rm sk} \sim E_{51}^{1/5} T_{\rm snr}^{-3/5}.$$

Substituted into formula (7), they yield estimates (1) $E_{\max} \sim (V_{\rm sk} E_{51})^{1/3}$ or $E_{\max} \sim E_{51}^{0.4} T_{\rm snr}^{-0.2}$. The maximum energy decreases with decreasing shock velocity and increasing SNR age. Formally, according to these estimates, CRs of maximum energies are produced at the onset of the Sedov phase with the parameters T_0, R_0, and V_0, which begins when the mass of the swept-up gas exceeds the mass of the ejected shell. Before this phase, we may assume that the SNR velocity and kinetic energy do not change greatly: $T_0 V_0 = R_0$ and $E_{51} \sim M_{\rm ej} V_0^2/2$ (such simplified estimates are given in several papers (Ellison *et al.* 2007; Ptuskin and Zirakashvily 2003), i.e., $\frac{4\pi}{3} R_0^3 \rho = \text{const} \times M_{\rm ej}$. Hence,

$$T_0^{-0.2} \sim M_{\rm ej}^{-1/6} \rho^{1/15} E_{51}^{0.1}.$$

Substituting $T_0^{-0.2}$ into (1) and disregarding the weak dependence of this additional factor on $M_{\rm ej}$ and on the density of the medium ρ, we obtain formula (4) for the dependence on E_{51}, $E_{\max} = E_{\max}^0 E_{51}^{0.5}$ for protons, which is used in our calculations.

The calculations that take into account the formation of the CR flux at all phases of the SNR life in a given explosion (Berezhko *et al.* 1997) show that the highest-energy and intermediate-energy CRs are generated at the end of the free expansion phase and at the Sedov phase, respectively. Dependence (4) was derived precisely under this assumption.

The same estimation dependence can be derived if we formally substitute const $\times V_0$ for $V_{\rm sk}$ into formula (1). In this case, the postshock flow velocity

$u2(\text{l.f.}) \sim V_0$ is close to the velocity of the outer part of the expanding supernova shell. In the frame of the shock front, the preshock velocity is $u1 = -V_{\rm sk}$, and the postshock velocity is $u2 = -V_{\rm sk}/r$, where r is the compression ratio (Ellison *et al.* 1997). In the laboratory frame, the postshock flow velocity is then $V_0 \sim u2(\text{l.f.}) = V_{\rm sk}(1 - 1/r)$. At $r = 4$–7 commonly obtained in calculations (Ellison *et al.* 1997), $V_{\rm sk} \sim V_0$ with a 30% accuracy. Then, $E_{\rm max} = E^0_{\rm max} A E^{0.5}_{51}$, and assuming that $A = 1$ to obtain $E_{\rm max} = E^0_{\rm max}$ at $E_{51} = 1$, we derive (4). The dependence of $E_{\rm max}$ on the SNR velocity may be even stronger (Ptuskin and Zirakashvily 2003).

REFERENCES

1. E. G. Berezhko and D. C. Ellison, Astrophys. J. **526**, 385 (1999).
2. E. G. Berezhko, V, K. Elshin, and L. T. Ksenofontov, Zh. Éksp. Teor. Fiz. **82**, 1 (1996).
3. E. G. Berezhko, G. F. Krymsky, V. K. Yelshin, *et al.*, astro-ph/9706209 (1997).
4. E. G. Berezhko and H. J. Volk, Astropart. Phys. **7**, 183 (1997).
5. E. G. Berezhko and H. J. Volk, Astron. Astrophys. **357**, 283 (2000).
6. V. S. Berezinsky, S. V. Bulanov, V. L. Ginzburg, *et al.*, *Astropysics of Cosmic Rays* (North-Holland, Amsterdam, 1990).
7. P. L. Biermann, *Astrophysical Sources of High Energy Particles and Radiation, 12 CISCRA, Erice, Italy,* Ed. by M. M. Shapiro, T. Stanev, and J. P. Wefel (Kluwer, Dordrecht, 2000), Ser. II, Vol. 44, p. 115.
8. A. M. Bykov and I. N. Toptygin, *Proc. 25th ICRC, 1997,* p. 365.
9. D. C. Ellison, E. G. Berezhko, and M. G. Baring, Astrophys. J. **540**, 292 (2000).
10. D. C. Ellison, L. O'C Drury, and J.-P. Mayer, Astrophys. J. **487**, 197 (1997).
11. A. D. Erlykin and A. W. Wolfendale, J. Phys. G **23**, 979 (1997).
12. A. D. Erlykin and A. W. Wolfendale, Phys. Scripta **63**, 504 (2001).
13. T. J. Galama, P. M. Vreeswijk, J. Paradijs, *et al.*, Nature **395**, 670 (1998).
14. M. Hamuy, astro-ph/0301006 (2003).
15. J. Hoerandel, Astropart. Phys. **19**, 193 (2003).
16. K. Iwamoto, P. A. Mazzali, K. Nomoto, *et al.*, Nature **395**, 672 (1998).
17. F. C. Jones, A. Lukasiak, V. Ptuskin, and W. Webber, Astrophys. J. **547**, 264 (2001).
18. É. V. Kononovich and V. I. Moroz, *A General Course on Astronomy* (URSS, Moscow, 2001) [in Russian].
19. G. V. Kulikov and G. B. Christiansen, Zh. Éksp. Teor. Fiz. **35**, 441 (1959).
20. M. A. Malkov and L. Drury, Rep. Prog. Phys. **64**, 429 (2001).
21. P. A. Mazzali, J. Deng, K. Maeda, *et al.*, Astrophys. J. **572**, L61 (2002).
22. D. K. Nadyozhin, Astron. Astrophys. (2003, in press).
23. K. Nomoto, K. Maeda, H. Umeda, *et al.*, astro-ph/0209064 (2002).
24. K. Nomoto, T. Mazzali, T. Nakamura, *et al.*, astro-ph/0003077 (2000).
25. L. O'C Drury, D. C. Ellison, F. A. Aharonian, *et al.*, astro-ph/0106046 (2001).
26. K. A. Postnov, M. E. Prokhorov, and V. M. Lipunov, Astron. Zh. **45**, 276 (2001) [Astron. Rep. **45**, 236 (2001)].
27. V. S. Ptuskin, *Astrophysical Sources of High Energy Particles and Radiation,* Ed. by M. M. Shapiro, T. Stanev, and J. P. Wefel (Kluwer, Dordrecht, 2000), Ser. II, Vol. 44, p. 251.
28. V. S. Ptuskin and V. N. Zirakashvily, astro-ph/0302053 (2003).
29. S. R. Reynolds and J. W. Keohane, Astrophys. J. **525**, 368 (1999).
30. D. Richardson, D. Branch, D. Casebeer, *et al.*, Astron. J. **123**, 745 (2002).
31. T. Shibata, *Proc. 24th ICRC, 1995,* p. 713.
32. S. Swordy, *Proc. 23rd ICRC, Invited, Rapporteur and Highlight Papers,* Ed. by D. A. Leahy and R. B. Hicks (World Sci., 1994), p. 243.
33. L. G. Sveshnikova, astro-ph/0303159 (2003).
34. M. Turatto, Astrophys. J. **534**, L57 (2000).
35. M. Turatto, *Supernovae and Gamma-Ray Bursts,* Ed. by K. W. Weiler (Springer, New York, 2003).
36. M. Turatto, S. Benetti, and E. Cappelaro, astro-ph/0211219 (2002).

Translated by V. Astakhov

Astronomy Letters, Vol. 30, No. 1, 2004, pp. 50–57. Translated from Pis'ma v Astronomicheskiĭ Zhurnal, Vol. 30, No. 1, 2004, pp. 58–66.

Two Years of Observations of the X-ray Pulsar SMC X-1 with the ART-P Telescope onboard the Granat Observatory

A. A. Lutovinov[1,2*], S. S. Tsygankov[1], S. A. Grebenev[1], M. N. Pavlinsky[1], and R. A. Sunyaev[1,2]

[1] *Space Research Institute, Russian Academy of Sciences, Profsoyuznaya ul. 84/32, Moscow, 117810 Russia*

[2] *Max-Plank-Institut für Astrophysik, Karl Schwarzschild Straße 1, 86740 Garching bei München, Germany*

Received June 15, 2003

Abstract—We present the observations of the pulsar SMC X-1 with the ART-P telescope onboard the Granat observatory. We investigate the variability of the flux from the source on time scales of several tens of days. The intensity variation of the pulsar are shown to be consistent with the presence of a periodicity in the system with a characteristic time scale of ∼61 days. The precession of an inclined accretion disk, as indirectly confirmed by the absence of low-state pulsations, may be responsible for the observed variability. The spectrum of the source is well described by a power-law energy dependence of the photon flux density with a slope of ∼1.5 and an exponential cutoff at energies above ∼14–18 keV. We estimated the inclinations between the planes of the orbit and the accretion disk and the magnetic field of the neutron star. © *2004 MAIK "Nauka/Interperiodica".*

Key words: *pulsars, neutron stars, X-ray sources.*

INTRODUCTION

The X-ray pulsar SMC X-1 located in one the nearest galaxies, the Small Magellanic Cloud (SMC), is one of the most intense and rapidly rotating accreting X-ray pulsars. The source, which was first discovered in X-rays in 1971 (Price *et al.* 1971), is a member of a high-mass binary together with the companion star Sk160, a B0-type supergiant with a mass of $17.2M_\odot$ and a radius of $18R_\odot$ (Reynolds *et al.* 1993). On short time scales, its flux pulsates with a period of about 0.71 s, while the neutron star itself is eclipsed by its companion for ∼15 h (the duration of the X-ray eclipse) with a period $P_{\rm orb} \simeq 3.892$ days. Analyzing the results obtained over the entire preceding history of observations of this source, Levine *et al.* (1993) determined the orbital parameters of the binary and established that its orbital period is decreasing at a rate $\dot{P}_{\rm orb}/P_{\rm orb} = -3.35 \times 10^{-6}$ yr^{-1}.

Apart from the rotation period of the neutron star and the orbital period, the observations are indicative of a 50–60-day cycle in the binary (Wojdowski *et al.* 1998), during which the X-ray luminosity of the source varies between 10^{37} erg s^{-1} and several units of $\times 10^{38}$ erg s^{-1}. The latter value is close to or even higher than the Eddington limit for a spherically accreting neutron star with a mass of $1.4M_\odot$. This fact as well as the observed steady spinup of the neutron star for the more than 30 years since the discovery of the pulsar (see, e.g., Wojdowski *et al.* 1998; Bildsten *et al.* 1997; Lutovinov *et al.* 1994; and references therein) suggest that a disk accretion model is most likely realized in the Sk160/SMCX-1 system; the accretion disk itself can be formed either from stellar wind or during mass transfer through the inner Lagrangian point.

Analyzing the EXOSAT light curves for the pulsar SMC X-1, Angelini *et al.* (1991) found a sharp (by a factor of ∼3), short-time increase in the flux from this source with a duration of ∼80 s, which they interpreted as a type-II X-ray burst. Recent RXTE observations of the pulsar have revealed more than a hundred such events with time scales of several tens of seconds (Moon *et al.* 2003), suggesting that the radiation and accretion mechanisms in the source SMC X-1 under study and the pulsar/burster GRO J1744–28 are similar.

In this paper, we analyze the archival data obtained with the ART-P telescope onboard the Granat observatory to study the long-term flux variations of the source as well as its temporal and spectral parameters.

*E-mail: aal@hea.iki.rssi.ru

1063-7737/04/3001-0050$26.00

Table 1. ART-P observations of the pulsar SMC X-1 in 1990–1992

Date	Duration, s	Orbital phase	Pulsation period, s[a]	Pulse fraction, %[b]	Flux,[c] mCrab	Luminosity,[b] 10^{38} erg s^{-1}
Apr. 5, 1990	30750	0.33–0.46	–	5.1[e]	5.36 ± 0.47	0.24 ± 0.02
Apr. 22, 1990	34490	0.65–0.77	$0.70957531 \pm 0.00000006$	40.5 ± 1.9	64.0 ± 1.0	2.90 ± 0.04
Apr. 24, 1990	12750	0.19–0.23	$0.70957326 \pm 0.00000012$	41.1 ± 2.3	63.0 ± 1.2	2.86 ± 0.06
Apr. 25, 1990	8300	0.42–0.45	$0.70957451 \pm 0.00000054$	37.1 ± 2.9	63.3 ± 1.4	2.87 ± 0.06
May 11, 1990	17040	0.52–0.59	$0.70955929 \pm 0.00000027$	36.1 ± 3.3	58.9 ± 1.3	2.67 ± 0.06
May 12, 1990	44230	0.75–0.91	$0.70955668 \pm 0.00000015$	38.4 ± 5.8	27.2 ± 0.7	1.23 ± 0.03
Jan. 25, 1991	8240	0.08–0.11	$0.70932134 \pm 0.00000057$	27.8 ± 5.5	18.8 ± 3.5	0.85 ± 0.16
Apr. 13, 1991[d]	12060	0.09–0.14	$0.70925884 \pm 0.00000223$	16.0 ± 7.2	12.8 ± 2.4	0.58 ± 0.11
Apr. 14, 1991[d]	28340	0.38–0.46	$0.70926034 \pm 0.00000087$	11.7 ± 2.1	33.9 ± 2.0	1.53 ± 0.09
Apr. 21, 1991[d]	6250	0.13–0.16	$0.70925315 \pm 0.00000140$	18.7 ± 3.5	47.1 ± 4.7	2.13 ± 0.21
Apr. 22, 1991[d]	34320	0.43–0.56	$0.70925311 \pm 0.00000014$	18.1 ± 2.0	62.2 ± 2.2	2.82 ± 0.10
May 17, 1992	15110	0.86–0.92	–	1.9[e]	12.9[e]	0.58[e]
May 18, 1992	19200	0.17–0.26	$0.70899141 \pm 0.00000623$	4.2[e]	11.6[e]	0.52[e]

[a] After correction for the motion of the Solar-System barycenter and the orbital motion in the binary.
[b] In the energy range 6–20 keV.
[c] In the energy range 6–20 keV for the assumed distance of $d = 50$ kpc to the source.
[d] For technical reasons, the spectrum of the source cannot be restored.
[e] The 3σ upper limit for the pulse fraction is given in mCrab.

OBSERVATIONS

The ART-P X-ray telescope onboard the Granat international orbital astrophysical observatory consists of four coaxial, completely independent units, each of which includes a position-sensitive detector with a geometric area of 625 cm^2 and an URA-based coded mask. The telescope can image a selected region of the sky by a coded-aperture technique in a $3.^\circ4 \times 3.^\circ6$ field of view (the full beam width) with a nominal resolution of ~5 arcmin in the energy range 3–60 keV. It has an energy resolution of ~22% in the calibration 5.9-keV iron line. The observations were carried out in the photon-flux mode. In this mode, for each photon, its coordinates on the detector, the energy (1024 channels), and the arrival time (the accuracy of the photon arrival time is 3.9 ms, and the dead time is 580 μs) were written to buffer memory. This mode allows one to perform both timing and spectral analyses of the radiation from each X-ray source within the field of view of the telescope. A detailed description of the telescope was given by Sunyaev *et al.* (1990).

The Granat observatory observed the region of the SMC that contained the pulsar SMC X-1 in series once a year (Table 1). A total of three series of observations with a total exposure time of ~271 000 s were carried out for the source, which allowed us to study in detail the radiation from the pulsar as well as its spectrum and variability on various time scales. Preliminary results of our timing analysis of the ART-P/Granat observations of the pulsar SMC X-1 were presented previously (Lutovinov *et al.* 1994). The typical pulse profile for the source in the energy ranges 3–6, 6–10, 10–20, and 20–30 keV (Fig. 1) exhibits two symmetric peaks located in the phase ranges 0.1–0.4 and 0.5–1.0, with the width of the second peak decreasing with increasing photon energy.

It should be noted that during the first series of observations (in the spring of 1990), we used the first module of the telescope. The subsequent observations were performed with the third module, which had

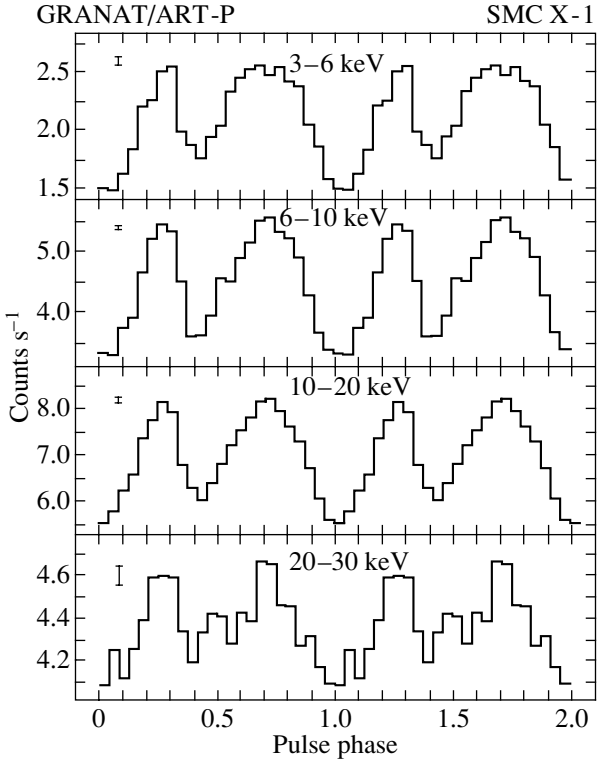

Fig. 1. Energy dependence of the pulse profile for SMC X-1, as derived from the ART-P data of April 24, 1990. The errors correspond to one standard deviation.

a lower sensitivity at soft energies; therefore, all of the results presented here refer to the energy range 6–20 keV. In addition, the high-voltage level of the detector of this module varied significantly over time, and it was not always possible to carry out calibration observations of the Crab Nebula. As a result, we ran into considerable difficulties in constructing the response matrix for some of the observing sessions, making it difficult or, in several cases, even impossible to carry out a spectral analysis of the X-ray radiation recorded with this module.

LONG-TERM INTENSITY VARIATIONS OF THE SOURCE AND BURSTS

As was noted above, the long-term observations of SMC X-1 showed that, apart from the proper rotation of the neutron star and its orbital motion, the system has another, nearly periodic component—intensity variability of the source on a time scale of several days, with the recorded X-ray flux decreasing by more than an order of magnitude. A similar pattern is also observed in the other two well-known X-ray pulsars Her X-1 and LMC X-4, where it is attributable to periodic eclipses of the emitting regions of the neutron star by a precessing accretion disk (Lutovinov *et al.* 2000; La Barbera *et al.* 2001; and references

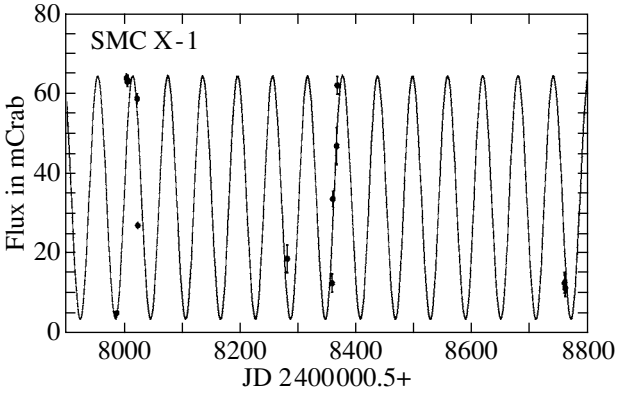

Fig. 2. The 6–20-keV light curve for SMC X-1 constructed over two years of ART-P observations. The dots indicate the measured fluxes during an individual observation, and the solid line represents the best sinusoidal fit with a 61-day period.

therein). It is assumed that the same mechanism may also be responsible for the observed intensity variations in the pulsar SMC X-1.

To determine the precession period $P_{\rm prec}$ of the accretion disk, we fitted the ART-P data by a sinusoidal signal with a trial period varying in the range of 40–80 days. The deviations of the measured fluxes from their predicted values were determined by the least-squares method. The best value was obtained for a period $P_{\rm prec} \simeq 61$ days. This period agrees with the results by Wojdowski *et al.* (1998), who found long-term variations in the X-ray flux from SMC X-1 with a period of 50–60 days when simultaneously analyzing the ASM/RXTE and BATSE/CGRO data. The limited set of data (observing sessions) makes it impossible to completely cover the entire presumed period. Therefore, our period estimate is not an accurate and statistically significant measurement of the possible precession period $P_{\rm prec}$ (the statistical significance of the peak on the periodogram is $\sim 1.5\sigma$). It most likely gives circumstantial evidence for the presence of a third type of periodicity in the system and the possible mechanism of its formation (see below).

The analysis of the light curve for the source by Clarkson *et al.* (2003) shows that the presumed precession period is not constant in itself, but varies smoothly over an interval of 40–60 days with a characteristic time scale of $\sim$1600 days.

Figure 2 shows the light curve for SMC X-1 constructed over two years of ART-P observations in the energy range 6–20 keV. The dots with (1σ) error bars indicate the measured fluxes from the source in mCrab during individual observing sessions, and the solid line represents their best sinusoidal fit with a period of $\sim$61 days. It is undoubtedly of considerable

interest to compare the phases of the light curves obtained simultaneously with the ART-P telescope and the BATSE observatory. However, the quality of the latter in this period was too low to make such a comparison (see Fig.1 from Wojdowski *et al.* 1998). A comparison with more recent RXTE observations of the pulsar has revealed no correlation with our results, which is most likely attributable to the variability of the precession period (see above).

When analyzing the light curves for the presence of X-ray bursts, we found several events that were similar to those recorded by the RXTE observatory (Moon *et al.* 2003) and that could be interpreted as weak type-II bursts. Note that the statistical significance of the recorded events is low, 3–5σ. However, their roughly triangular shapes and HWHM of $\simeq$13 s obtained by Gaussian fitting are similar to those observed previously. Figure 3 shows the profile of one of such bursts.

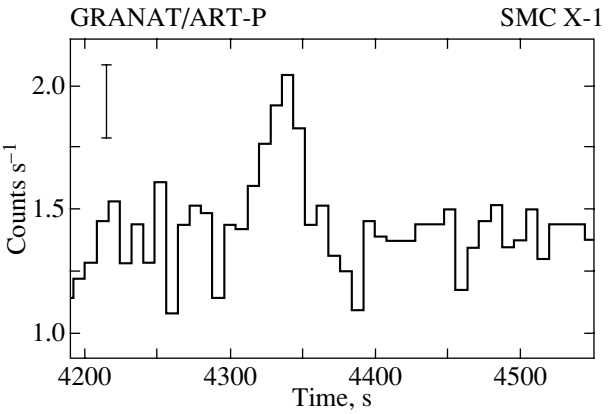

Fig. 3. The profile of a typical X-ray burst detected by ART-P from SMC X-1 during the observing session of April 22, 1990. Time in seconds from the beginning of the observing session is along the horizontal axis. The time bin is 8 s.

SPECTRAL ANALYSIS

The spectrum of the X-ray pulsar SMC X-1 is typical of this class of objects and can be described by a simple power law. In general, depending on the specific source, this model is modified by an exponential cutoff at high energies, absorption at soft energies, and emission or absorption lines. In the case of SMC X-1, we did not detect any significant features in emission or absorption. In addition, as our study shows, the interstellar absorption estimated by different authors to be in a wide range, 5.9×10^{20}–3.2×10^{22} atoms cm^{-2} (Wojdowski *et al.* 1998; Moon *et al.* 2003), plays no important role in our analysis of the radiation from the X-ray source in the energy range 6–20 keV. Thus, the ultimate formula that we used in our spectral analysis of the radiation from SMC X-1 is

$$I(E) = I_{10}\left(\frac{E}{10\ \mathrm{keV}}\right)^{-\alpha} \times \begin{cases} 1, & \text{if } E < E_\mathrm{c} \\ \exp\left[-(E-E_\mathrm{c})/E_\mathrm{f}\right], & \text{if } E \geq E_\mathrm{c}. \end{cases} \quad (1)$$

Here, E is the photon energy in keV, I_{10} is the normalization of the power-law component to 10 keV, α is the photon spectral index, E_c is the cutoff energy, and E_f is the characteristic e-folding energy in the spectrum of the source (although this is a purely empirical formula with a cutoff at E_c, it is widely used to fit the spectra of X-ray pulsars; see White *et al.* (1983)).

Figure 4 shows the photon spectra for the pulsar (in photons cm^{-2} s^{-1} keV^{-1}) measured during several observing sessions with different intensity levels. The curves represent the best-fit model spectra for the source based on a simple power law or formula (1); the best-fit parameters are given Table 2. In choosing between a simple power law and its modification by a cutoff at high energies, we used the $\Delta\chi^2$-test. Based on this test, we determined the probability that it was no accident that the χ^2 value improved when passing to a more complex model. The statistical significance of this passage is higher than 95% in most cases.

If we assume that the low state is observed when the source is hidden behind the outer edge of a warped or inclined (to the orbital plane) accretion disk and that we see the flux attenuated by absorption and scattering in the cold material on the disk periphery or scattered in the hot corona above the disk (as is the case in the system Her X-1 (Lutovinov *et al.* 2000)), then, to a first approximation, the spectra of the high and low states may be considered to differ only by normalization and additional absorption. Fitting the low-state spectrum of the pulsar (April 5, 1990) by formula (1) with the parameters fixed at their high-state values does not give a positive answer to the above assumption (an appreciable increase in χ^2). However, it cannot be completely rejected either, because the data are statistically limited. In this case, an important criterion could be an increase in absorption at low energies. However, we cannot be certain about this, because the energy range is limited: the measured absorption in the low state is estimated to be $(31.5 \pm 12.0) \times 10^{22}$ atoms cm^{-2}, while the upper limit for the absorption is 20×10^{22} atoms cm^{-2} (1σ).

To investigate the spectral evolution of the source on a scale of one pulse period, we performed phase-resolved spectroscopy of the pulsar radiation in the high state for two observing sessions, April 24 and

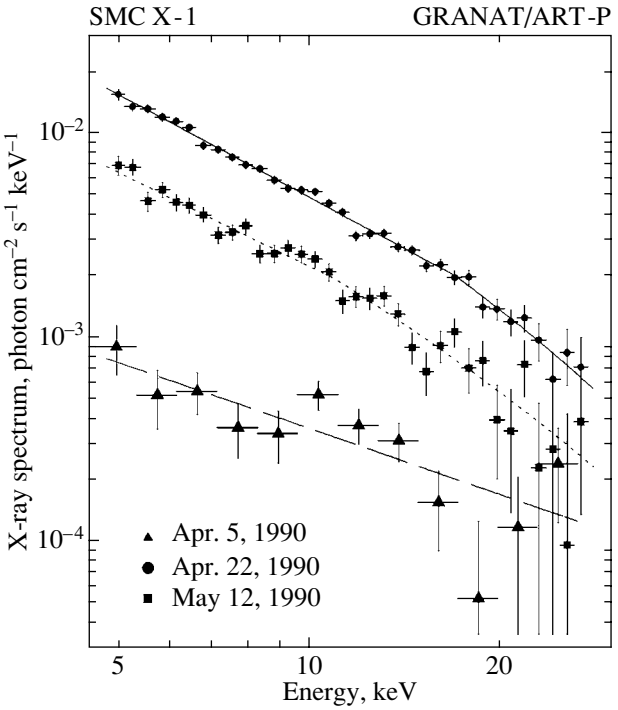

Fig. 4. The photon spectra for SMC X-1 measured with the ART-P telescope during the first series of observations (the spring of 1990). Different symbols (circles, squares, and triangles) indicate the photon spectra for the source in states with different intensity levels; the curves represent their best fits by a power-law decrease in photon flux density or formula (1).

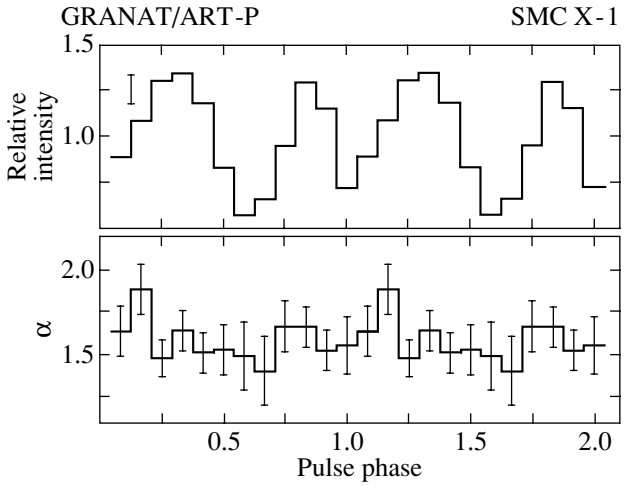

Fig. 5. Photon spectral index versus pulse phase. The errors correspond to one standard deviation (σ).

May 11, 1990. To this end, the data obtained during each observing session were folded with the pulsation period and divided into 12 time bins (the arrival time of each photon was first corrected for the barycenter of the Solar System and the motion of the neutron star in the binary). The total accumulation time of the signal for each of the 12 spectra was 1137 and 1568 s for the sessions of of April 24 and May 11, respectively. The subsequent analysis indicated that the spectra obtained in this way are well described by a simple power law in the energy range 6–20 keV; the spectral slope is virtually independent of the pulse phase. This conclusion is illustrated by Fig. 5, which shows a plot of the photon spectral index against the pulse phase for the observing session of April 24.

DISCUSSION

High and Low States

It follows from the observations of SMC X-1 by different observatories that the recorded X-ray flux from this pulsar is not constant but undergoes large, nearly periodic variations on a time scale of 50–60 days. By analogy with the well-known binaries SS 433, Her X-1, and LMC X-4, which exhibit a similar pattern, the precession of an inclined accretion disk is considered to be one of the main causes of the observed variability. The normal companion Sk160 in the binary under consideration is a supergiant with an intense stellar wind that provides the bulk of the accreting material forming the accretion disk. The mechanism of its formation is not yet completely understood, because, in general, supergiants are close to filling their Roche lobes and material can be transferred to the compact object through the inner Lagrangian point. Both mechanisms may operate in the system simultaneously. It should be noted, however, that, according to Clarkson *et al.* (2003), even if the stellar wind plays a major role in the formation of the disk, it is a collimated wind, and, thus, the two cases are characterized by similar patterns of mass transfer to the accretion disk.

Larwood (1998) showed that a relation exists between the precession period and the binary parameters for a precessing accretion disk:

$$\frac{P_{\rm orb}}{P_{\rm prec}} = (3/7)q(1+q)^{-1/2}(R_{\rm o}/a)^{3/2}\cos\delta, \qquad (2)$$

where q is the mass ratio of the normal component and the compact object; $R_{\rm o}$ is the outer radius of the accretion disk, which may be expressed in fractions β of the Roche lobe size; a is the separation between the binary components; and δ is the angle between the orbital and disk planes. It follows from an analysis of the optical light curves for Sk160/SMC X-1 (Howarth 1982; Khruzina and Cherepashchuk 1987) that the size of the accretion disk is $\beta \simeq 0.7$–1.0. For the mass ratio $q = 10.8$ and periods $P_{\rm orb}/P_{\rm prec} \simeq 0.064$, we can estimate the range of possible inclinations, $\delta \sim 25°$–$58°$. The minimum angle between the orbital and disk planes, $\cos\delta \simeq 1$,

Table 2. Best-fit parameters for the spectra based on different models[a]

Date	PL			PL+HEC				
	$I_{10}^{b}, 10^{-4}$	α	$\chi^2_N(N)^c$	$I_{10}, 10^{-4}$	α	E_c, keV	E_f, keVB	$\chi^2_N(N)$
Apr. 5, 1990	3.6 ± 0.5	1.07 ± 0.23	1.28(11)	4.4 ± 0.9	0.39 ± 0.54	12.9 ± 3.5	6.3 ± 4.4	1.16(9)
Apr. 22, 1990	47.7 ± 0.4	1.75 ± 0.03	1.43(32)	49.2 ± 0.6	1.67 ± 0.04	17.0 ± 2.8	24.9 ± 14.0	1.09(30)
Apr. 24, 1990	45.9 ± 0.6	1.63 ± 0.04	1.35(34)	47.9 ± 0.8	1.52 ± 0.05	18.1 ± 3.0	15.4 ± 10.7	1.09(32)
Apr. 25, 1990	48.8 ± 0.8	1.68 ± 0.05	1.14(26)	50.7 ± 1.1	1.59 ± 0.06	19.7 ± 3.9	13.3 ± 13.3	1.02(24)
May 11, 1990	44.0 ± 0.7	1.74 ± 0.05	1.37(32)	47.8 ± 1.3	1.49 ± 0.09	13.7 ± 1.8	13.2 ± 4.7	0.73(30)
May 12, 1990	20.8 ± 0.4	1.76 ± 0.06	1.27(32)	22.6 ± 1.2	1.53 ± 0.16	10.9 ± 3.2	24.8 ± 10.9	1.15(30)
Jan. 25, 1991	10.5 ± 3.2	0.29 ± 0.50	0.45(7)	–	–	–	–	–

[a] PL—a power-law spectrum, HEC—a high-energy cutoff.
[b] The flux in photons cm^{-2} s^{-1} keV^{-1} measured at 10 keV.
[c] The χ^2 value normalized to the number N of degrees of freedom.

corresponds to an accretion-disk size of $\beta \sim 0.65$, which slightly exceeds the maximum disk radius, $\beta \sim 0.61$, obtained by Paczynski (1977) for accretion only through the inner Lagrangian point. This discrepancy is even larger if we take into account the range of possible precession periods. Thus, mass transfer from the normal companion only through the inner Lagrangian point in the system Sk160/SMC X-1 is unlikely.

As was noted above, no X-ray pulsations were found during the low state of the source, and only upper limits for the pulse fraction were obtained (Table 1). However, since these limits are rather large, we cannot completely rule out the presence of pulsations in the low state. Wojdowski *et al.* (1998) presented ROSAT measurements of the pulsation period in the low state. However, they stipulate that these measurements were made at the very beginning of the low state, when the source may have not yet been completely shielded by the disk. A similar situation was probably observed by the ART-P telescope on May 18, 1992, when the intensity of the source was low, but X-ray pulsations were recorded with low statistical significance ($\sim 4\sigma$).

Magnetic Field

Based on the observed parameters of SMC X-1 obtained over a long observing period, we can try to estimate the magnetic field of the neutron star in the system by using the model of an accretion disk suggested by Li and Wang (1996).

The history of measurements of the pulsation period for SMC X-1 is indicative of a virtually uniform spinup of the neutron star since its discovery. The mean rate of change of the period during our observations in the period 1990–1992 was $\dot{P} = -(32.6 \pm 0.8) \times 10^{-5}$ s yr^{-1}. Subsequent ROSAT, ASCA, and RXTE observations of the source yield a similar value, $\dot{P} = -(32.0 \pm 0.2) \times 10^{-5}$ s yr^{-1} (Wojdowski *et al.* 1998). Thus, assuming that the observed variability of the source is not related to the variations in the intrinsic radiation from the pulsar, but is determined by extraneous effects, we estimated its bolometric luminosity from the observed spectral parameters as $L_x = 47 \times 10^{37}$ erg s^{-1}.

In a situation where the neutron star spins up almost uniformly over a long time interval, the change in its rotation period is related to the binary parameters by the equation

$$\dot{P} = -\frac{\dot{M}(GM_x r_0)^{1/2} n(\omega_s) p^2}{2\pi I}, \qquad (3)$$

where $\dot{M}$ is the accretion rate; I is the moment of inertia of the star; r_0 is the inner edge of the accretion disk, which in our model is assumed to be equal to the Alfvén radius r_A; $n(\omega_s) = 1 + \frac{20(1-1.94\omega_s)}{31(1-\omega_s)}$ is the dimensionless angular momentum; and $\omega_s = \Omega_s/\Omega_k(r_0)$ is the speed parameter. The latter depends on the angular velocities Ω_s and $\Omega_k(r_0)$ of the neutron star and the material at the inner edge of the accretion disk, respectively. We estimated the moment of inertia of the neutron star from the relation $I = 0.4 M_x R^2$

and assumed that its radius is $R = 10^6$ cm, the mass is $M_x = 1.4M_\odot$.

The magnetic moment μ of the neutron star estimated using formula (3) shows that the best agreement with the experimental data is achieved for $\mu \simeq (0.05{-}0.1) \times 10^{30}$ G cm^3, which is equivalent to a neutron-star surface magnetic field of $\sim(1{-}2) \times 10^{11}$ G. This conclusion about the relative weakness of the magnetic field is consistent with the observation of bursts from the source that can be classified as type-II bursts (see Moon *et al.* 2003). Moon *et al.* (2003) also established that these bursts have much in common with the bursts observed previously from another super-Eddington pulsar, GRO J1744–28. They suggested separating out the so-called group of pulsars/bursters with magnetic fields of $\sim 10^{11}$ G. Another important argument for this hypothesis is the absence of cyclotron features in the spectrum of the source in the energy range 3–100 keV, which corresponds to magnetic fields of $\geq 5 \times 10^{11}$ G.

Note that the applicability of the model under consideration at large μ is limited by the fact that the speed parameter reaches the critical value ω_c at which the angular momentum is not transferred to the neutron star. Having reached this level, the pulsar must pass from spinup to spindown, which is not observed for SMC X-1. The fact that μ approaches 10^{30} G cm^3 means that the speed parameter falls within the range of critical values ω_s.

CONCLUSIONS

The X-ray pulsar SMC X-1 was repeatedly observed in 1990–1992 with the ART-P telescope onboard the Granat observatory. Over this period, we accumulated the data that allowed us to investigate the variability of the source on various time scales and its spectrum and to estimate the binary parameters.

We showed that, apart from the periodicities associated with the proper rotation of the neutron star and the orbital motion, the system has yet another, nearly periodic component that may be associated with the precession of the accretion disk. Its period $P_{\rm prec} \sim 61$ days, as inferred from the ART-P data, agrees well with the observations of other observatories.

The spectrum of the source is typical of X-ray pulsars and can be described by a simple power law with a cutoff at high energies. Our analysis showed that the spectral shape depends weakly on the orbital phase and intensity of the source. Phase-resolved spectroscopy of the radiation from the source in the high state revealed no dependence of the spectral slope on the pulse phase either.

The above estimates of the magnetic field for the neutron star show that its strength must be $\sim 10^{11}$ G to be consistent with the observational data (the spinup rate the star, X-ray bursts, and the absence of cyclotron features in the spectrum).

ACKNOWLEDGMENTS

This work was supported by the Russian Foundation for Basic Research (project no. 02-02-17347), the Ministry of Industry and Science (grant no. NSh-2083.2003.2 from the President of Russia), and the Nonstationary Phenomena in Astronomy Program of the Russian Academy of Sciences. We are grateful to M. Revnivtsev for their discussions and valuable remarks. We wish to thank Flight Director K.G. Sukhanov; the staffs of the Lavochkin Research and Production Center, RNIIKP, and the Deep Space Communications Center in Evpatoria; the Evpatoria team of the Space Research Institute (Russian Academy of Sciences); the team of I.D. Tserenin; and B.S. Novikov, S.V. Blagii, A.N. Bogomolov, V.I. Evgenov, N.G. Khavenson, and A.V. D'yachkov from the Space Research Institute who operated the Granat Observatory, provided the scientific planning of the mission, and performed a preliminary processing of telemetry data. We also wish to thank the team of M.N. Pavlinsky (Space Research Institute) and the staff of the former Research and Development Center of the Space Research Institute in Bishkek who designed and manufactured the ART-P telescope.

REFERENCES

1. L. Angelini, L. Stella, and N. White, Astrophys. J. **371**, 332 (1991).
2. A. La Barbera, L. Burderi, T. Di Salvo, *et al.*, Astrophys. J. **553**, 375 (2001).
3. L. Bildsten, D. Chakrabarty, J. Chiu, *et al.*, Astrophys. J., Suppl. Ser. **113**, 367 (1997).
4. I. Howarth, Mon. Not. R. Astron. Soc. **198**, 29 (1982).
5. T. S. Khruzhina and A. M. Cherepashchyuk, Astron. Zh. **64**, 345 (1987) [Sov. Astron. **31**, 180 (1987)].
6. J. Larwood, Mon. Not. R. Astron. Soc. **299**, L32 (1998).
7. A. Levine, S. Rappoport, J. Deeter, *et al.*, Astrophys. J. **410**, 328 (1993).
8. X.-D. Li and Z.-R. Wang, Astron. Astrophys. **307**, L5 (1996).
9. A. A. Lutovinov, S. A. Grebenev, R. A. Sunyaev, and M. N. Pavlinsky, Pis'ma Astron. Zh. **20**, 631 (1994) [Astron. Lett. **20**, 538 (1994)].
10. A. A. Lutovinov, S. A. Grebenev, M. N. Pavlinsky, and R. A. Sunyaev, Pis'ma Astron. Zh. **26**, 803 (2000) [Astron. Lett. **26**, 765 (2000)].
11. D.-S. Moon, S. Eikenberry, and I. Wasserman, Astrophys. J. Lett. **582**, L91 (2003).

12. F. Nagase, Publ. Astron. Soc. Jpn. **41**, 1 (1989).
13. R. Price, D. Groves, R. Rodrigues, *et al.*, Astrophys. J. Lett. **168**, L7 (1971).
14. A. Reynolds, R. Hilditch, W. Bell, and G. Hill, Astron. Astrophys. **261**, 337 (1993).
15. E. Schreier, R. Giacconi, H. Gursky, *et al.*, Astrophys. J. Lett. **178**, L71 (1972).
16. R. A. Sunyaev, S. I. Babichenko, D. A. Goganov, *et al.*, Adv. Space Res. **10** (2), 233 (1990).
17. N. White, J. Swank, and S. Holt, Astrophys. J. **270**, 711 (1983).
18. P. Wojdowski, G. W. Clark, A. M. Levine, *et al.*, Astrophys. J. **502**, 253 (1998).

Translated by A. Dambis

Astronomy Letters, Vol. 30, No. 1, 2004, pp. 58–63. Translated from Pis'ma v Astronomicheskiĭ Zhurnal, Vol. 30, No. 1, 2004, pp. 67–73.

Anomalous Fe II Spectral Effects and High H I Lyα Temperature in Gas Blobs Near η Carinae

S. Johansson[1] and V. S. Letokhov[1,2*]

[1] *Observatory, Lund University, PO Box 43, Lund, SE-221 00 Sweden*

[2] *Institute of Spectroscopy, Russian Academy of Sciences, Troitsk, Moscow oblast, 142190 Russia*

Received June 17, 2003

Abstract—We consider the origin of the anomalously high intensity of the ultraviolet Fe II $\lambda\lambda$2507/2509 Å lines observed with high spatial and spectral resolutions from gas blobs (GBs) near η Carinae. This rare effect in stellar spectra is attributable to a combination of several factors: (1) the high hydrogen density ($>10^8$ cm^{-3}) that ensures the blocking of the Lyman continuum by GBs and, accordingly, the formation of a cold H I region with completely ionized Fe atoms; (2) the small distance between the GBs and the central star that ensures a high (>8000–10 000 K) Lyα H spectral temperature, which photoexcites Fe II selectively; and (3) the population of Fe II levels and, accordingly, the opening of a stimulated emission channel, which together with spontaneous transitions creates a radiative cycle where a single Fe II ion can multiply absorb Lyα emission. © *2004 MAIK "Nauka/Interperiodica".*

Key words: *interstellar medium, gaseous nebulae, η Car, gas blobs, stimulated emission, Fe II.*

INTRODUCTION

The goal of this study is to interpret anomalous spectral effects, in particular, the UV 2507/2509 Å Fe II lines observed with high spatial and spectral resolutions from gas blobs (GBs) near η Carinae, the most massive and luminous star in the Galaxy. These UV Fe II lines are known to arise from the selective photoexcitation of Fe II ions by Lyα emission due to the chance coincidence of the wavelengths (Johansson and Jordan 1984; Johansson and Hamann 1993). Lyα H coincides with the transition that combines a low-lying (1 eV) excited state with two nearby high-lying Fe II states, while the spontaneous decay of these two states yields the above two spectral lines. These anomalously intense lines (2507/2509 Å) attract particular attention, because they are present in the spectra of GBs in the close vicinity of η Car taken with high spatial and spectral resolutions separately from the spectrum of the central star (see the review by Davidson and Humphreys 1997) using the Hubble Space Telescope (HST).

The first direct observations of compact GBs in the vicinity of η Car were made by using speckle interferometry (Weigelt and Ebersberger 1986). They revealed three GBs near the central star (at distances of several hundred AU from the central star). The sharply increased observational capabilities of the HST with a high-spectral-resolution spectrometer (the Space Telescope Imaging Spectrograph, STIS) made it possible to obtain spectra simultaneously with a high spatial resolution (0.″1) and a spectral resolution $\lambda/\Delta\lambda \simeq 10^5$ (Kimble *et al.* 1998). These instruments allowed the GB spectra to be observed separately from the photospheric radiation of the central star. Analysis of the spectra showed that the GBs emit many narrow lines of ionized elements (Zethson 2001). However, the extremely intense fluorescence Fe II $\lambda\lambda$2507/2509 Å lines (Davidson *et al.* 1995) and the most recent HST data (Gull *et al.* 2001) were most surprising.

THE FORMATION MODEL FOR THE Fe II $\lambda\lambda$2507/2509 Å LINES IN GBs

The column density of neutral hydrogen, $n_{\rm H} = N_{\rm H}D$, for GBs (in particular, GB "B") near η Car is estimated to be higher than 4×10^{21} cm^2, where $N_{\rm H}$ is the H I density and D is the GB size. This means that the GB is optically thick for the Lyman continuum ($\lambda < 912$ Å), i.e.,

$$\tau_{\rm c} = \sigma_{\rm ph}(\nu_{\rm c}) N_{\rm H} D \gg 1, \qquad (1)$$

where $\sigma_{\rm ph}(\nu_{\rm c})$ is the photoionization absorption cross section near the ionization limit. Eq. (1) leads us to conclude that two spatially separated but adjacent regions are formed in the GB: a hot H II region to the side of the central star and a cold H I region

*E-mail:~letokhov@isan.troitsk.ru;vladilen.letokhov@astro.lu.se

behind it. These two regions are separated by the Strömgren boundary that passes inside the GB. The cold H I region is responsible for the numerous narrow Fe II lines that can be divided into categories: the fluorescence lines from high-lying levels photoexcited by Lyα and the forbidden lines from low-lying, metastable levels.

Condition (1) ensures the formation of a cold H I region where the Fe atoms are ionized by radiation with $\lambda > 912$ Å that passes through the H II region. This provides the basis for the physical model of the formation of the $\lambda\lambda 2507/2509$ Å lines (Johansson and Letokhov 2001; Klimov *et al.* 2002) in GBs at distances $R_b \simeq (10^2 - 10^3) r_s$ from the central star, where r_s is the radius of η Car. Another critical requirement is that the distance to the star R_b be small enough to ensure a high Lyα spectral temperature at the frequency of the Fe II absorption line.

The Lyα spectral temperature $T\alpha$ in the GB region can be estimated by two methods: (1) by estimating the energy of the radiation from η Car with $\lambda < \lambda_c$ absorbed in the GB; and (2) by estimating the lower limit for $T\alpha$ from the condition for the formation of anomalously intense $\lambda\lambda 2507/2509$ Å lines. Let us consider both approaches.

ESTIMATING $T\alpha$, THE Lyα EFFECTIVE TEMPERATURE

Let us consider a spherical GB with a diameter $D \ll R_b$ (Fig. 1). Condition (1) is satisfied if the hydrogen density N_H exceeds a critical value (Johansson and Letokhov 2001):

$$N_H^{cr} = \left(\frac{I_{ph}}{\alpha_H}\right)^{1/2} = \frac{r_s}{2R_b}\left(\frac{P(\nu_c, T_s)\Delta\nu_{ph}}{\alpha_H D}\right)^{1/2}, \quad (2)$$

where α_H is the rate constant of the H II $\rightarrow$ H I recombination to the 2p state. The integrated intensity of the hydrogen-photoionizing stellar radiation with $\lambda < 912$ Å that reaches the GB surface is

$$I_{ph} = \Omega \int_{\nu_c}^{\infty} P(\nu, T_s) d\nu \simeq \Omega \mathbf{P}(\nu_c, T_s)\Delta\nu_{ph},$$

where $P(\nu, T_s)$ is the spectral Planck intensity distribution (in photons cm^{-2} s^{-1} sr^{-1} Hz^{-1}) for a star with a photospheric temperature T_s. For the estimation, we can use the effective frequency range $\Delta\nu_{ph} \simeq 7$ eV above the ionization limit, where $P(\nu)$ and $\sigma_{ph}(\nu)$ are large enough. At $T_s = 30\,000$ K, $\mathbf{P}(\nu_c, T_s)\Delta\nu_{ph} \simeq 10^{23}$ photons cm^{-2} s^{-1}.

For $N > N_H^{cr}$, the neutral H I component of the GB absorbs almost all of the Lyman continuum radiation from the central star. The absorbed power is

$$P_{abs}(\nu > \nu_c) \simeq \Omega_0 S_{abs} \int_{\nu_c}^{\infty} P(\nu, T_s) d\nu \quad (3)$$
$$= \Omega\pi^2 D^2 \mathbf{P}(\nu_c, T_s)\Delta\nu_{ph},$$

where $\Omega_0 = 4\pi\Omega$ is the solid angle subtended by the GB from the central star and $S_{abs} = (\pi/4)D^2$ is the area of the GB disk. The absorbed energy is reradiated in the hydrogen recombination spectrum, with the largest fraction ($\eta_1 = 0.7$) being emitted in the H I Lyα resonance line. The maximum optical density τ_0(Lyα) in the H II region at the center of the line is

$$\tau_0^m = \sigma_0/\sigma_{ph}(\nu_c) \simeq 5 \times 10^3, \quad (4)$$

where $\sigma_0 = \sigma_{12}(\text{Ly}\alpha) = 1.4 \times 10^{-14}$ cm^{-2} is the resonant scattering cross section at the center of the line, $\sigma_{ph}(\nu_c) = 3 \times 10^{-18}$ cm^2.

Lyα radiation is diffusively confined in the H II region, but the diffusive confinement time is limited by the fact that the number of scatterings is limited. This limitation is attributable to the Doppler frequency redistribution during the scattering of Lyα photons, which ensures relatively fast photon escape from the confinement region through the wings of the Doppler profile (Osterbrock 1989). Since the optical density τ_0 is limited by $\tau_0^m = \sigma_0/\sigma_{ph}$ and the damping factor for Lyα is $\alpha = \Delta\nu_{rad}/\Delta\nu_D$, the optical density in the Lorentz wings is $\alpha\tau_0^m \simeq 1$. Therefore, Lyα photons escape from the H II region through diffusion with the Doppler width increasing by a factor of $\beta \simeq (\ln\tau_0^m)^{1/2} \simeq 3$. Thus, the total power emitted by the GB surface in the Lyα line is

$$P_{em}(\text{Ly}\alpha) \simeq 4\pi S_{em} P(\nu_{\text{Ly}\alpha}, T\alpha)(\Delta\nu_D\beta), \quad (5)$$

where $T\alpha$ is the Lyα effective spectral temperature and $S_{em} = \pi D^2$ is the area of the emitting surface of a spherical GB. In reality, S_{em} can differ slightly from πD^2 because of the peculiar shape of the emitting surface of the H II region (Fig. 1).

The mean Lyα spectral intensity at the GB surface is determined by the Planck distribution at frequency ν_α(Lyα) and by the spectral brightness temperature $T\alpha$, where the spectral broadening during the confinement is taken into account. In the steady state, assuming that the absorption of the confined Lyα radiation in the H II region of the GB is negligible, we obtain

$$\eta P_{abs}(\nu > \nu_c) = P_{em}(\text{Ly}\alpha). \quad (6)$$

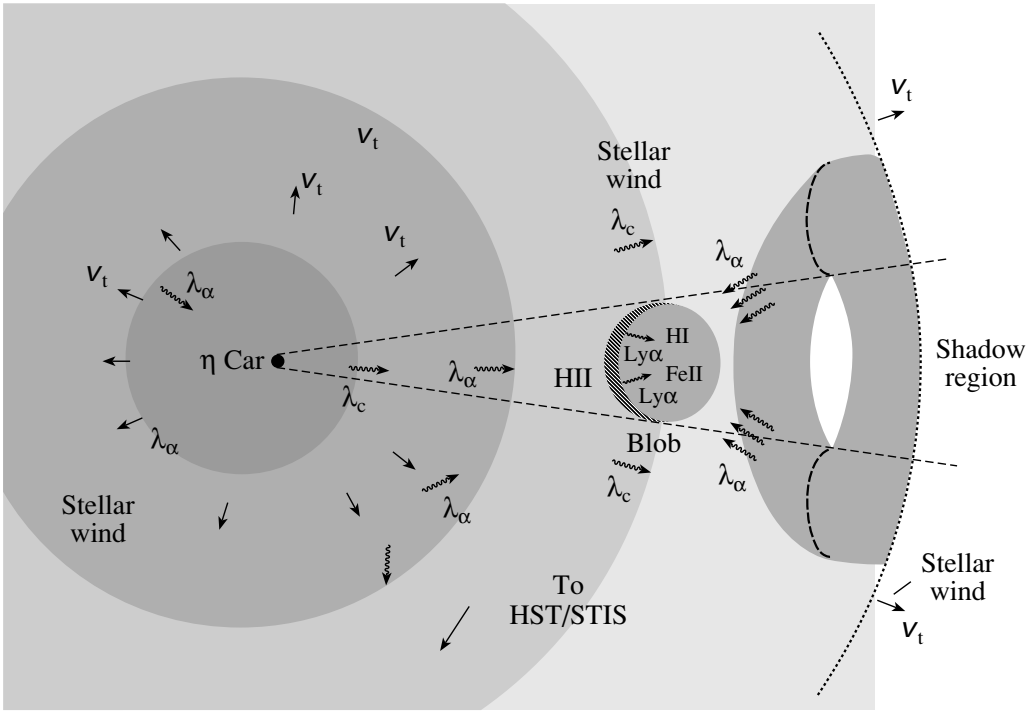

Fig. 1. The arrangement geometry of η Car and the gas blob (GB) that blocks the Lyman continuum radiation so that the front part of H II is completely ionized and the back part of H I contains Fe II ions. Fe II ions in the H I region are selectively photoexcited by Lyα photons that diffuse either from the H I region of the GB or from the nearby torus-shaped region of the stellar wind from η Car, which is also ionized by the Lyman continuum.

Hence, the brightness temperature $T\alpha$ for the Lyα radiation from the GB can be estimated from Eq. (6):

$$P(\nu_{\mathrm{Ly}\alpha}, T\alpha) = \frac{\eta_1}{4}\Omega\frac{\Delta\nu_{\mathrm{ph}}}{\Delta\nu_{\mathrm{D}}\beta}\mathbf{P}(\nu_{\mathrm{c}}, T_{\mathrm{s}}). \qquad (7)$$

The dilution factor for the radiation from the central star is largely offset by the spectral compression of the absorbed Lyman-continuum energy into a relatively narrow recombination Lyα line. The compression factor f is

$$f = \frac{\Delta\nu_{\mathrm{abs}}}{\Delta\nu_{\mathrm{em}}} = \frac{\Delta\nu_{\mathrm{ph}}}{\Delta\nu_{\mathrm{D}}\beta} \simeq 10^3, \qquad (8)$$

where $\Delta\nu_{\mathrm{abs}} \simeq \Delta\nu_{\mathrm{ph}}$ is the effective spectral width of the photoionization absorption, $\Delta\nu_{\mathrm{em}} = \beta\Delta\nu_{\mathrm{D}}$ is the width of the Lyα spectrum, and $\Delta\nu_{\mathrm{D}} = 6\ \mathrm{cm}^{-1}$ is the Doppler width of the Lyα line.

For the closest vicinity of the central star, it is convenient to introduce a spectral brightness conversion parameter Ω_{br}:

$$\Omega_{\mathrm{br}} = \eta_1\Omega\left(\frac{\lambda_{\mathrm{Ly}\alpha}}{\lambda_{\mathrm{c}}}\right)^2\left(\frac{S_{\mathrm{abs}}}{S_{\mathrm{em}}}\right)f. \qquad (9)$$

This parameter includes the absorbed energy conversion ratio η_1, the standard spatial dilution factor Ω, the mode density enhancement factor $(\lambda_{\mathrm{Ly}\alpha}/\lambda)^2$, the ratio of the absorption and emission areas, and the key spectral compression factor $f \gg 1$. The following equation relates the temperatures T_α and T_{s} (for $h\nu_{\mathrm{Ly}\alpha} \gg kT_{\mathrm{s}}, kT_\alpha$):

$$\frac{h\nu_{\mathrm{Ly}\alpha}}{kT\alpha} = -\ln\Omega_{\mathrm{br}} + \frac{h\nu_{\mathrm{c}}}{kT_{\mathrm{s}}}. \qquad (10)$$

This relation is virtually equivalent to the expression for the source function in Lyα in terms of the source function in the Lyman continuum known for a nebula illuminated by a star (Sobolev 1975).

Note that the intensity of the Lyα radiation inside the H II region of the GB is higher that on the GB surface by a factor of δ that includes the diffusive confinement of the radiation:

$$\delta = \beta^2 = \ln\tau_0^{\mathrm{m}} \simeq 8\text{–}10. \qquad (11)$$

According to the calculations by Auer (1968), the intensity of the Lyα radiation can be even a factor of 20 to 25 higher because of the confinement effect. Given this effect, the increase in Lyα intensity described by Eq. (10) can be written in a more accurate form:

$$\frac{h\nu_{\mathrm{Ly}\alpha}}{kT\alpha} = -\ln(\Omega_{\mathrm{br}}\delta) + \frac{h\nu_{\mathrm{c}}}{kT_{\mathrm{s}}}. \qquad (12)$$

For the GB "B" of η Car, $\Omega_{\mathrm{br}}\delta \simeq 10^{-2}$, which corresponds to $T\alpha \simeq (10\text{–}15) \times 10^3$ K inside the GB.

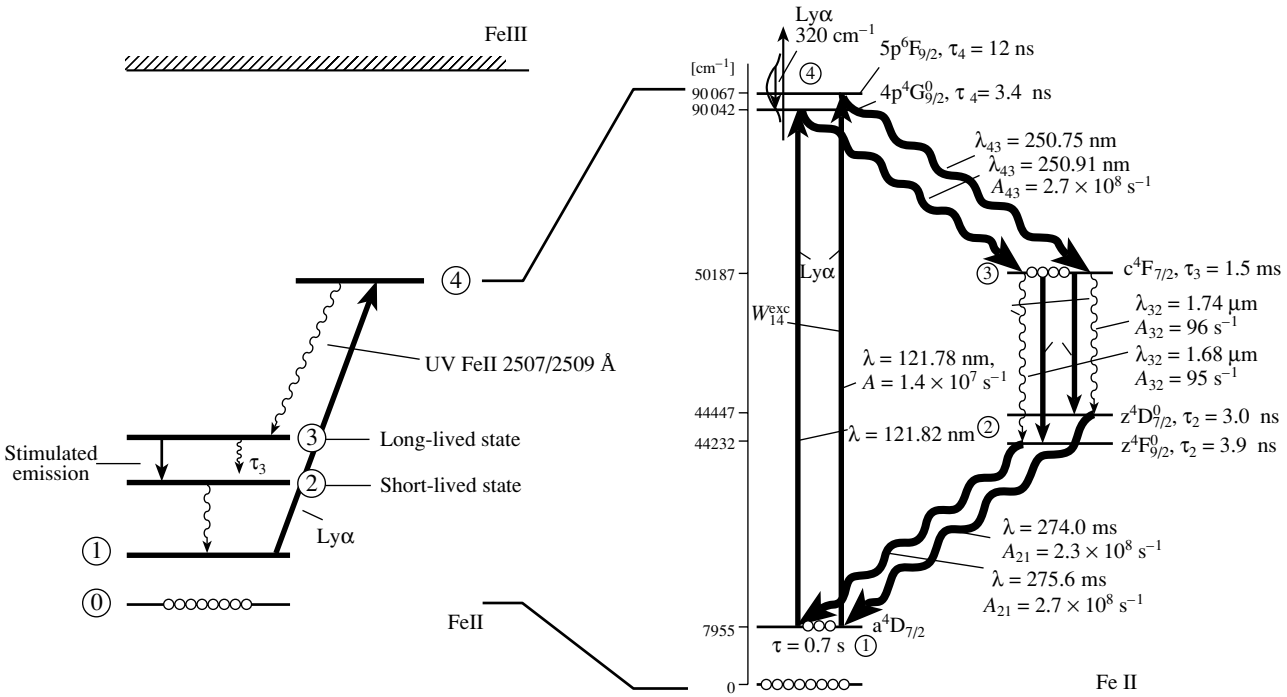

Fig. 2. Simplified and more detailed diagrams for Fe II quantum transitions, showing the quantum transitions of selective photoexcitation $1 \to 4$, rapid spontaneous decays $4 \to 3$, $2 \to 1$, and stimulated emission $3 \to 2$ that form a closed radiative cycle.

This value is comparable to or even higher than the electron temperature, implying a sharp change of the energy balance in the GB compared to a classical planetary nebula. Actually, the ratio μ of the Lyα radiation energy density inside the GB, $E(\mathrm{Ly}\alpha)$, to the free energy density, E_{fr}, stored in charged particles (H II ions and electrons) becomes equal to

$$\mu = \frac{E(\mathrm{Ly}\alpha)}{E_{\mathrm{fr}}} = n_{\mathrm{e}}\alpha_{\mathrm{H}}\frac{D}{c}\delta\frac{\nu_{\mathrm{Ly}\alpha}}{\nu_{\mathrm{c}}}, \qquad (13)$$

where n_{e} is the electron density (or the density N_{H}, $N_{\mathrm{H\,II}}$). This ratio has a simple physical meaning: the ratio of the lifetime of a Lyα photon inside the GB, $\tau_{\mathrm{ph}} = \dfrac{D}{c}\delta$, due to the diffusive escape through the spectral line wings to the ion recombination time, $1/(n_{\mathrm{e}}\alpha_{\mathrm{H}})$. If we assume for the GB "B" of η Car that $n_{\mathrm{e}} \simeq 2 \times 10^8$ cm^{-3} and $D = 10^{15}$ cm, then this ratio will be $\mu = 10$. The ratio of the density of $E(\mathrm{Ly}\alpha)$ to the density of the charged-particle kinetic energy E_{kin} is even higher, because $h\nu_{\mathrm{c}} \gg kT$. The density of the Lyα energy $E(\mathrm{Ly}\alpha)$ is higher than the density of the Lyman continuum energy $E(\mathrm{Ly_c})$ at least by the factor of $\delta \simeq \ln \tau_0^{\mathrm{m}}$ or even more (Auer 1968).Therefore, the following equation is valid for an optically thick (for $\mathrm{Ly_c}$) GB:

$$E(\mathrm{Ly}\alpha) \gg E(\mathrm{Ly_c}), \quad E_{\mathrm{fr}} \gg E_{\mathrm{kin}}. \qquad (14)$$

This equation means that the photoprocesses in the GB are governed by Lyα and Lyman continuum, $\mathrm{Ly_c}$, radiation. Such GBs may be called *radiation-rich* GBs, to distinguish them from standard *thermal* planetary nebulae (Aller 1984).

ESTIMATING $T\alpha$ FROM THE CONDITION OF THE Fe II RADIATIVE CYCLE

We can now independently estimate $T\alpha$ from the observations of intense Fe II $\lambda\lambda$2507/2509 Å spectral lines. Figure 2 shows a simplified diagram of the Fe II energy levels and quantum transitions related to the formation of these lines. The selective photoexcitation by Lyα radiation transfer Fe II ions from the low-lying metastable state 1 to the short-lived odd states 4 ($5\mathrm{p}^6\mathrm{F}^0_{9/2}$, $4\mathrm{p}^4\mathrm{G}^0_{9/2}$). These levels decay to state 3 (predominantly to $\mathrm{c}^4\mathrm{F}_{7/2}$ and, to a lesser extent, to $\mathrm{c}^4\mathrm{F}_{9/2}$), emitting intense $\lambda\lambda$2507/2509 Å lines. For $T(\mathrm{Ly}\alpha) = T\alpha \gtrsim 12\,000$ K, the photoexcitation rate $W_{\mathrm{exc}}(1 \to 4)$ exceeds the radiative decay rate for states 3:

$$W_{\mathrm{exc}} = A_{41}\left[\exp\left(\frac{h\nu_{14}}{kT\alpha}\right) - 1\right]^{-1} \gtrsim \frac{1}{\tau_3} \simeq 10^3\ \mathrm{s}^{-1}, \qquad (15)$$

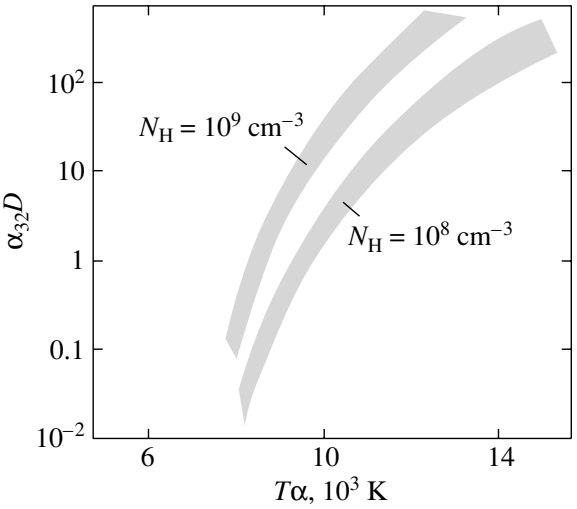

Fig. 3. Exponential $(\alpha_{32}D)$ in the amplification factor $K = \exp(\alpha_{32}D)$ versus effective (spectral) radiation temperature $T\alpha$ for two hydrogen densities N_H.

where $A_{41} = 1.4 \times 10^7$ s^{-1} is the Einstein coefficient for the $4 \rightarrow 1$ transition. Thus, if condition (15) is satisfied, then Fe^+ ions will be accumulated in the "pseudo-metastable" $c^4F_{9/2,7/2}$ states. The lifetimes of these levels are on the order of a millisecond, because they are associated with the truly metastable Fe II levels, but they lie above the next, higher configuration of opposite parity in the complex atomic structure (state 2 in Fig. 2). This accumulation of ions in pseudo-metastable states is unusual and is an important ingredient of our model for the origin of the anomalous $\lambda\lambda$2507/2509 Å lines. It should be emphasized that at densities $N_H \ll 10^{13}$ cm^{-3}, collisions give no contribution to the relaxation of the long-lived Fe II states.

Previously, it has been shown (Johansson and Letokhov 2003) that the accumulation of Fe II in the "pseudo-metastable" state 3 automatically leads to the population inversion of the ΔN_{32} levels with respect to the low-lying short-lived states 2 ($z^4D^0_{7/2}$ and $z^4F^0_{9/2}$). For a sufficiently large GB and high Fe II density, the arising amplification increases the intensity of the spontaneous radiation due to *stimulated* transitions whose rate is much higher than the spontaneous decay rate. Note that the inverse population of $\Delta N_{32} = N_3 - N_2$ emerges always, irrespective of W_{exc}, because the lifetime of the lower level 2 is very short (3–4 ns). Under condition (15), the inverse population is at a maximum, whereas for $W_{exc} \ll 1/\tau_3$, the amplification factor α_{32} for the $3 \rightarrow 2$ transition is given by

$$\alpha_{32} = \sigma_{32}\Delta N_{32}, \quad \text{where} \quad \Delta N_{32} = W_{14}^{exc}\tau_3 N_3. \tag{16}$$

The stimulated radiation cross section for the $3 \rightarrow 2$ transition is $\sigma_{32} \simeq (1.2–3.7) \times 10^{-16}$ cm^2, and $N_1 = f_0 N_{Fe}$ is the population density of the initial level 1, where f_0 is the fraction of the Fe^+ ions in state 1. Figure 3 shows a plot of the exponential $(\sigma_{32}D)$ in the amplification factor $K = \exp(\alpha_{32}D)$ for the $3 \rightarrow 2$ transition against the spectral temperature $T\alpha$, for two hydrogen densities N_H in the GB. We may take $D = 10^{15}$ cm and $f \simeq 10^{-2}$. The uncertainty in $(\alpha_{32}D)$ is attributable to the temperature uncertainty in the H I region, $T = 100–1000$ K, and the corresponding uncertainty in the Doppler width for the $3 \rightarrow 2$ transition, $\Delta\nu_D \simeq (200–600)$ MHz. As we see from (16), a decrease in N_3 for $W_{exc} \ll 10^3$ s^{-1} at $T\alpha \leq 12\,000$ K may well be offset by an increase in Fe II density to achieve the required amplification factor. For example, at $T\alpha = 10\,000$ K, the excitation rate is $W_{exc} = 10^2$ s^{-1}; to obtain a high amplification factor and, accordingly, the $1 \rightarrow 4 \rightarrow 3 \rightarrow 2 \rightarrow 1$ radiative cycle involving stimulated radiation, the population of the initial state N_1 should be increased by a factor of 10 by increasing the GB density and, accordingly, N_{Fe} by a factor of 10. This condition is milder than that in our previous paper (Johansson and Letokhov 2003). If, however, $T\alpha$ is lower than 8000–9000 K, a large decrease in amplification takes place, which is difficult to offset by increasing N_1. Therefore, an independent estimate of $T\alpha \gtrsim 10\,000$ K follows from the experimental observation of the intense Fe II $\lambda\lambda$2507/2509 Å lines that arise from cyclic transitions mentioned above.

CONCLUSIONS

In conclusion, let us discuss the Lyα radiation sources with the required temperature $T\alpha$ at the Fe II absorption wavelength in accordance with the geometry shown in Fig. 1. The required Lyα radiation can arrive from two regions: (1) the completely ionized front H II region of the GB, where intense Lyα radiation is generated through a photoionization–recombination cycle and (2) from the stellar-wind region of η Car adjacent to the back part of the GB that recedes from the GB with the terminal velocity v_t and, accordingly, has the required Doppler shift to compensate for the detuning between the Lyα and Fe II absorption wavelengths.

The first source is the H II region produced by the absorption of radiation from η Car in the region of the Lyman continuum, which is effectively converted into intense Lyα radiation (much more intense than the Lyα radiation from the central star).

This radiation from the H II region illuminates the immediately adjacent Fe II-containing H I region of the GB. This source has been discussed previously (Klimov *et al.* 2002). Doppler diffusion in the H I medium with a minimum optical depth $\tau_0(\mathrm{Ly}\,\alpha) \simeq 2 \times 10^8$ is required to compensate for the 2.4 Å detuning between the wavelengths of the Lyα line and the Fe II absorption line (Hamann *et al.* 1999). This value agrees with the previous estimate of the H I column density (Davidson and Humphreys 1997). At first glance, the H I region acts as a diffuse reflector of Lyα photons that escape from the H II region with open boundaries. This question was briefly discussed by Auer (1968), but we do not know any detailed calculations of the degree of diffusive penetration of Lyα radiation from the H II region into the H I region.

The second source is the torus-shaped zone of the stellar wind from η Car behind the GB (Fig. 1) that recedes from the GB with the negative Doppler shift sufficient to compensate for the wavelength detuning. This region of the stellar wind is illuminated by the Lyman continuum from the central star and emits Lyα. There are no accurate data on the hydrogen density in the asymmetric stellar wind from η Car near the GB, but, from the viewpoint of compensation for the frequency detuning and the maximum Lyα intensity, the location of the Strömgrem boundary in the stellar wind in the GB region would be optimal.

Further studies with the HST and the STIS camera can yield data on the contribution from each of the possible Lyα radiation sources to the selective photoexcitation of Fe II.

ACKNOWLEDGMENTS

We wish to thank N.N. Chugai for his valuable remarks after reading our manuscript.

REFERENCES

1. L. H. Aller, *Physics of Thermal Gaseous Nebulae* (Reidel, Dordrecht, 1984).
2. L. N. Auer, Astrophys. J. **153**, 783 (1968).
3. K. Davidson and R. M. Humphreys, Ann. Rev. Astron. Astrophys. **35**, 1 (1997).
4. K. Davidson, D. Ebbets, G. Weigelt, *et al.*, Astron. J. **109**, 1784 (1995).
5. T. Gull, K. Ishibashi, K. Davidson, and N. Collins, ASP Conf. Ser. **242**, 391 (2001).
6. F. W. Hamann, K. Davidson, H. Ishibashi, and T. Gull, ASP Conf. Ser. **179**, 116 (1999).
7. S. Johansson and F. W. Hamann, Phys. Scripta **T47**, 157 (1993).
8. S. Johansson and C. Jordan, Mon. Not. R. Astron. Soc. **210**, 239 (1984).
9. S. Johansson and V. S. Letokhov, Astron. Astrophys. **378**, 260 (2001).
10. S. Johansson and V. S. Letokhov, Phys. Rev. Lett. **90**, 011101 (2003).
11. R. I. Kimble *et al.*, Astrophys. J. Lett. **492**, L83 (1998).
12. V. Klimov, S. Johansson, and V. S. Letokhov, Astron. Astrophys. **385**, 313 (2002).
13. D. E. Osterbrock, *Astrophysics of Gaseous Nebulae and Active Galactic Nuclei* (Univ. Sci. Books, Sausalito, California, 1989).
14. V. V. Sobolev, *A Course on Theoretical Astrophysics* (Nauka, Moscow, 1975) [in Russian].
15. G. Weigelt and J. Ebersberger, Astron. Astrophys. **163**, L5 (1986).
16. T. Zethson, PhD Thesis (Lund University, Lund, Sweden, 2001).

Translated by N. Samus'

Astronomy Letters, Vol. 30, No. 1, 2004, p. 64. Translated from Pis'ma v Astronomicheskiĭ Zhurnal, Vol. 30, No. 1, 2004, pp. 74–75.

In Memory of Dr. V. L. Khokhlova (1927–2003)

The astronomical community has suffered a great loss: Vera L'vovna Khokhlova, an eminent astrophysicist, doctor of physical and mathematical sciences, and a member of the Editorial Board of *Pis'ma v Astronomicheskii Zhurnal*, died on September 24, 2003, at the age of 77.

Dr. Khokhlova was born in the town of Babushkin, Moscow Region, on July 25, 1927. After graduating from Moscow State University in 1950, she began research on active solar regions at the Crimean Astrophysical Observatory under the direction of A.B. Severnyi and defended her thesis on this subject. Her development as a scientist took place in an atmosphere of creative cooperation with G.A. Shain, E.R. Mustel, S.B. Pikel'ner, and I.S. Shklovskii.

In 1961, Dr. Khokhlova started working at the Astronomical Council of the Academy of Sciences of the USSR (subsequently called the Institute of Astronomy of the Russian Academy of Sciences), where she continued to investigate the Sun and took part in a comprehensive program of lunar research. In the mid 1960s, her scientific interests shifted to stellar astrophysics, particularly studies of chemically peculiar A stars with evidence of strong magnetic fields. During this period, the concept of a spotted structure of chemical anomalies on the surfaces of peculiar A stars had just begun to emerge. She was enthralled by the possibility of extracting information about the nonuniform distribution of chemical elements on the surfaces of rotating stars from the analysis of changes in the shapes and equivalent widths of absorption line profiles. The limited possibilities of photographic spectra required significant efforts to reach reliable conclusions. Success in this way would have been impossible without the distinctive feature of Dr. Khokhlova's scientific style: suggesting very high-quality criteria for observations and spectrum processing, combined with a critical attitude toward the results obtained. Her persistent studies bore fruit. By the mid 1970s, she and her colleagues managed to establish that the spotted distribution of chemical elements is a characteristic feature of chemically peculiar A stars. These results received general acceptance and brought her to the forefront of research on chemically peculiar stars.

In the late 1970s, Dr. Khokhlova realized that the increased accuracy of spectroscopic measurements due to the appearance of digital signal recording and processing techniques would allow a breakthrough to be achieved in mapping the distribution of chemical elements on stars. Her idea consisted of extracting all the information contained in the variable line profile by solving ill-defined inverse problems. This idea grew into a series of works performed by Dr. Khokhlova together with mathematicians from Moscow State University. These priority studies laid the foundation for the now widely used methods of mapping the chemical abundances, temperatures, and magnetic field strengths of stars by using intensity and polarization spectra.

The exactingness to the reliability of published results characteristic of Dr. Khokhlova's scientific work played a great role in shaping new *Pis'ma v Astronomicheskii Zhurnal*, in the publication of which she took an active part as a deputy of the Editor-in-Chief.

All those who knew Dr. Khokhlova remember her as a very talented woman, an attentive and clever conversationalist, and an inquisitive investigator who selflessly and steadfastly served scientific truth.

1063-7737/04/3001-0064$26.00